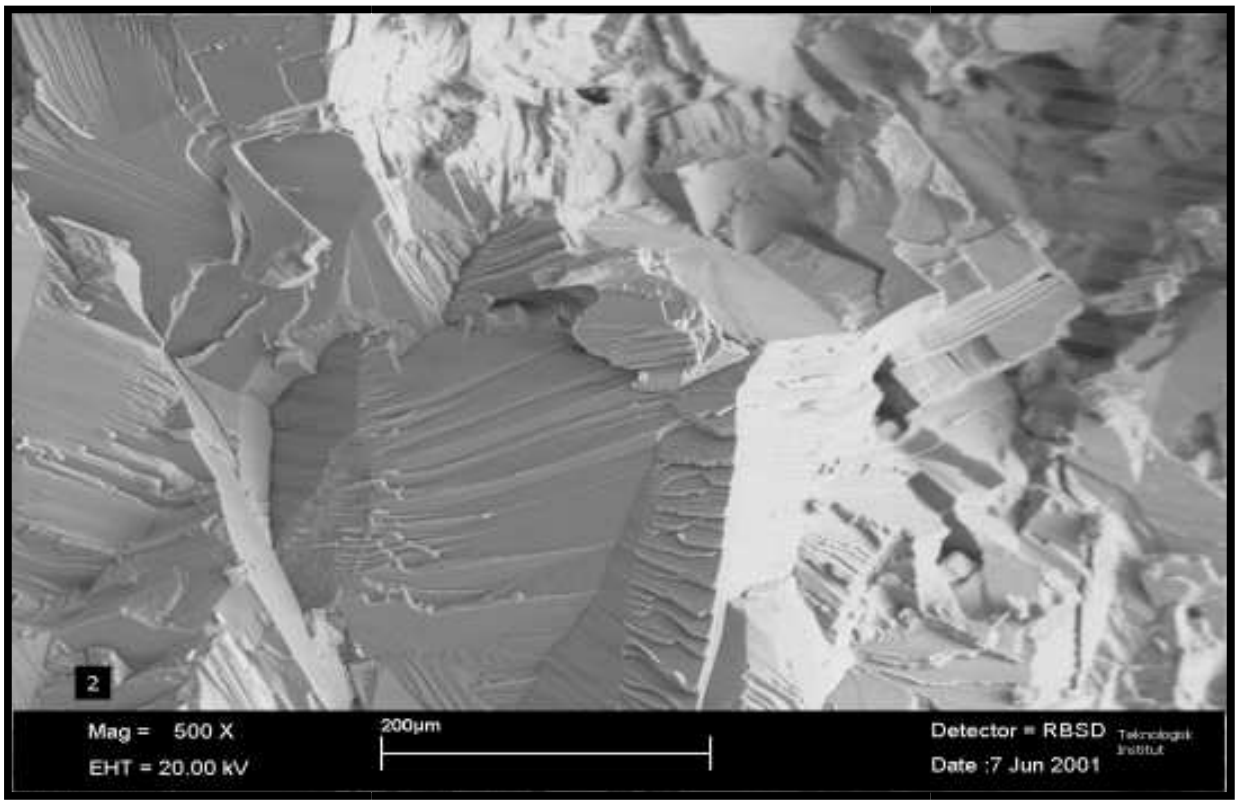

Detailed Investigation of Cl-Corrosion Initiated by Deposits Formed in Biomass-Fired Boilers

FORSKEL-5820, Final Report

Version 4.5

By Flemming J. Frandsen and Simone van Lith,

DTU Chemical and BioChemical Engineering, Technical University of Denmark

CHEC Research Centre, CHEC Report No. 0905, 2009

Final Report, FORSKEL Project No. 5820, October 2009

Foreword:

This is the final report covering the FORSKEL-5820 Project 'Detailed Investigation of Cl-Corrosion Initiated by Deposits Formed in Biomass-Fired Boilers', 2005-2009. It is a joint co-operative research and development project between the CHEC Research Centre, at DTU Chemical Engineering, and IPL, at DTU Mechanical Engineering.

The work has mainly been carried out by, post. doc, Simone C. van Lith at CHEC, but with close guidance and supervision from an Advisory Group, consisting of:

- Søren A. Jensen, DONG Energy
- Tommy Wilhelmsen, Vattenfall AB
- Melanie Montgomery, DTU Mechanical Engineering
- Flemming J. Frandsen, DTU Chemical and Biochemical Engineering

I want to thank you all for a very nice cooperation during the project, and especially Simone for several hours of hard work at the corrosion test-rig, doing SEM analyses, and/or writing papers etc. The content of this report is based on the following peer viewed journal/conference papers;

- S.C. van Lith, F.J. Frandsen, M. Montgomery, T. Vilhelmsen, S.A. Jensen; Lab-Scale Investigation of Deposit Induced Chlorine Corrosion of Superheater Materials under Simulated Biomass-Firing Conditions, Proc. Int. Conf. *EUROCORR 2008*, Edinburgh, UK, September 7-11, 2008
- S.C. van Lith, F.J. Frandsen, M. Montgomery, T- Wilhelmsen, S.A. Jensen; Lab-Scale Investigation of Deposit-Induced Chlorine Corrosion of Superherater Materials under Simulated Biomass-Firing Conditions. Part 1: Exposure at 560 °C; Energy and Fuels, 23, 3457-3468, 2009
- S.C. van Lith, F.J. Frandsen, M. Montgomery, T. Vilhelmsen, S.A. Jensen; Lab-Scale Investigation of Deposit-Induced Chlorine Corrosion of Superheater Materials under Simulated Biomass-Firing Conditions, Proc. Int. Conf. *Impacts of Fuel Quality on Power Production and the Environment*, Banff, Alberta, Canada, September 29 – October 3, 2008

DTU, 07-10-2009, Flemming J. Frandsen

1. Defining the Frame of FORSKEL-5820

The aim of FORSKEL-5820 was to investigate deposit-induced Cl-corrosion under well-controlled laboratory conditions, simulating the conditions in biomass-fired boilers. This has been done by exposing pieces of superheater tubes, covered by synthetic salts, at temperatures and gas mixtures simulating biomass-fired conditions. The corroded specimens have been studied in detail using a Scanning Electron Microscope (SEM), in order to determine the corrosion rate, and to investigate the chemistry and morphology of the corrosive attack.

The project has been divided into four activities:

A1: Relationship between the Cl-concentration in the deposit, and the corrosion rate.

A2: Influence of cation type (K^+ and Na^+) on the mobility of Cl in the deposit.

A3: Influence of metal temperature on the corrosion rate.

A4: Critical evaluation of the existing experience for minimizing corrosion in full-scale boilers firing totally or partly with biomass.

The main parameters controlling high-temperature corrosion in plants (co-)utilizing straw for heat and power production, are;

- Choice of material;
- Temperatures;
  - Gas phase temperature
  - Metal (surface) temperature
  - Gradients in the temperature (from bulk gas to metal surface)
- Flue gas composition;
  - Especially [SO_2], when firing straw on a grate, due to potential sulfation of KCl(cr)
- Exposure time;
- Deposit chemistry;

- Presence of Cl close to the metal surface
- High [Cl] breaks down the protective oxide scale

2. Introduction to High-Temperature Cl-Induced Corrosion

The basic causes of reduction in the boiler tube lifetime in waste and biomass combustors are well known in general terms; being the presence of chlorine, alkali, and heavy metals in the fuel, which combine to form low-melting, highly corrosive deposits on the tubes, as well as the heterogeneous chemical and physical nature of waste and biomass, which makes it difficult to handle, and causes combustion conditions that are often very hard to control [Wright and Krause, 1996].

The poor combustion characteristics of the waste and biomass may cause regions of incomplete combustion, including localized reducing conditions (high CO-levels), high heat flux from flame impingement, and possibly the presence of chemically aggressive species in inner layer deposits. These fuels also introduce Cl-containing species, alkali metal species, and – for waste - heavy metals such as Pb, Sn, and Zn, all of which may combine in the flame to form potential corrodants. Low-melting point metal chlorides, or mixtures of chlorides deposited on the heat transfer surfaces, remove protective oxide scale from the tube surfaces, thereby allowing rapid dissolution into the molten salts, and rapid oxidation [Wright and Krause, 1996].

Tube failures typically occur on the upstream side of the final stage superheater, and near the locations of the soot blowers. Maximum tube thinning is located on the crown of the tube facing the gas flow [Wright and Krause, 1996]. The deposit layers in these zones consist typically of mainly alkali and alkaline-earth sulfates (very low [Cl]), a scale of iron oxide, and an innermost, often laminated layer rich in metal chlorides [Wright and Krause, 1996].

The sequence of events in the corrosion process involving such deposits has been postulated to be the following [Miller et al., 1972a,b];

- Potassium (and other alkali and alkaline-earth), chloride, and, sulphur dioxide in the deposit, react with oxygen, producing K_2SO_4 and HCl or chlorine (Cl_2).
- The liberated HCl/Cl_2 reacts with the underlaying alloy to produce ferrous chloride, which can further react with oxygen, to form iron oxide, and free chlorine, serving to perpetuate the corrosion process [Wright and Krause, 1996].

[Otsuka et al., 1993] used simulated deposits to investigate the relative effects of chlorides and sulfates on the corrosion of austenitic steels and Ni-base alloys. They found that high-Ni alloys such as 825, G3, 625, 690, 600, and pure Ni, exhibited good corrosion resistance to Cl-based deposits at 400 °C, whereas Fe-based alloys such as 304 and 316L were severely corroded. In contrast, predominantly for the sulphate deposits (containing much smaller amounts of Cl) expected to form on superheater tubes, the corrosion behavior at 550 °C appeared to be a function of the alloy Cr-content, with the higher-Cr alloys corroding slowest. For alloys of similar Cr-content, increasing Ni content appeared to degrade the resistance to corrosion. The best-performing alloy in all the environments tested was Alloy 625 [Otsuka et al., 1993].

Straw contain significant amounts of K and Cl, which is being present as KCl in parts of the combustion system. Significant levels of KCl has been detected in fly ash, but particularly in inner layers of deposits formed in straw-fired plants. The flue gas will contain a certain level of SO_2(g) originating from the combustion of straw. It has been suggested in several papers [Krause, 1989; Reid, 1971; Alexander, 1963] that corrosion of superheater tubes is driven by sulfation of alkali chloride to alkali sulfates, eg. KCl to K_2SO_4, causing a relatively high partial pressure of chlorine, close to the metal (heat transfer) surface. Thus, the initiation reaction in the presence of KCl deposits, may be one of the below reactions, depending on the presence of SO_2:

$$2\,KCl + O_2 + SO_2 \rightarrow K_2SO_4 + Cl_2 \qquad (1)$$

$$2\,KCl + SO_2 + H_2O \rightarrow K_2SO_4 + 2\,HCl \qquad (2)$$

$$KCl + Fe_2O_3 + ½\,O_2 \rightarrow K_2Fe_2O_4 + Cl_2 \qquad (3)$$

This role of SO_2 was demonstrated in laboratory experiments [Miller et al., 1972a,b], in which alloys were exposed to sulphate-chloride salt mixtures, in a synthetic flue gas with and without SO_2. Introduction of only 250 ppmv SO_2, a level very common in waste-fired boilers, caused large increases in the corrosion rates. Increasing the SO_2–concentration to 2500 ppmv, a level not uncommon for coal-fired boilers, caused a significant increase on the attack of C-steel, but had only minor effect on T11. Type 321 stainless steel underwent slightly less corrosion at the higher [SO_2]-level. The effect of increasing temperatures was also investigated, increasing the temperature from 427 to 538 °C caused a much higher increase in the corrosion rate than an increase in the amount of NaCl in the deposit did.

These results indicate that only small amounts of alkali chloride in a superheater deposit may cause serious corrosion. It is important to emphasize that without a deposit on the metal, the gas phase attack by the synthetic flue gas containing 250 ppmv SO_2 was slight, showing that formation of HCl in the deposit is the critical factor [Wright and Krause, 1996].

S-bearing compounds play an important role with regard to molten salt attack, over the entire range of temperatures experienced by boiler tubes. For example, the most corrosive salts found in laboratory tests intended to simulate the conditions experienced at the waterwalls of coal-fired boilers [Miller et al., 1972a,b] at 316 °C, were the pyrosulfates and the bisulfates. Since the corrosion reactions, which are electrochemical in nature, will take place more readily in liquids than in solids, the presence of a liquid phase is very critical.

Chlorine is known to be able to penetrate, and destroy, the oxide scale, probably through cracks and pores, and at the metal/scale interface react with Cr and Fe, thereby forming volatile metal chlorides. A detailed study of the disruption of the oxide scale on steel by HCl in flue gas was reported by [Mayer et al., 1980]. Experiments were conducted at a metal temperature of 538 °C, and a flue gas temperature of 1060 °C. Without HCl in the flue gas, a continuous non-porous scale consisting of FeO, Fe_2O_3, and Fe_3O_4 was formed. With 0.1 %(v/v) HCl present in the gas, the inner scale layers were continuous, but the outer Fe_2O_3-layer became blistered and cracked. This Fe_2O_3-layer in turn became porous and discontinuous when [HCl] in the gas was increased to 0.2 %(v/v) [Wright and Krause, 1996]. A further increase of [HCl] to 0.8 %(v/v) caused complete disintegration of the Fe_2O_3-layer, and the Fe_3O_4-layer became irregular and porous. The maximum [HCl] that was investigated was 2 %(v/v), a level which destroyed the continuity of both outer layers, thereby exposing the underlying metal to attack by oxygen and HCl [Wright and Krause, 1996]. A mechanism of scale disruption proposed by [Crolet, 1993a,b], involves direct reaction, between the metal and the Cl, thereby producing a volatile oxychloride.

Both eqn (1) and eqn (3) above, causes release of Cl_2-gas which may then migrate through the oxide, to react with the metal at the metal-oxide scale interface, according to eqn (4);

$$Cr + Cl_2 \rightarrow CrCl_2 \qquad (4)$$

The $CrCl_2$ formed migrates out of the metal due to its high volatility, to areas with a higher oxygen partial pressure, where it is converted to Cr_2O_3 and Cl_2 (eqn (5)).

$$2\,CrCl_2 + 1\tfrac{1}{2}\,O_2 \rightarrow Cr_2O_3 + 2\,Cl_2 \qquad (5)$$

The precipitated Cr_2O_3 is non-protective and is therefore susceptible to spallation. Chlorine then migrates into the corrosion front to form metal chlorides again. A similar reaction can occur for Fe, forming $FeCl_3$, if there is no Cr available for reaction at the metal-scale interface. Iron chloride, $FeCl_3$, will migrate more readily from the corrosion product, as it is more volatile than chromium chloride ($CrCl_2$) and is expected to form an oxide on top of the Cr_2O_3, at higher partial pressures of oxygen. Thus, at lower temperatures which do not encourage evaporation of $CrCl_3$, $FeCl_3$ will still evaporate from the corrosion front [Montgomery et al., 2000a,b].

Temperature also has an important effect on the corrosion in combustors. Early tests by [Vaughan et al, 1974, 1977] showed that both the metal, and the gas temperature, influenced the corrosion rates. At gas temperatures of 460 and 593 °, the corrosion rates and the temperature-dependence of corrosion were significantly lower than at the higher gas temperatures, an effect especially pronounced at metal temperatures above 371 °C [Vaughan et al., 1974, 1977].

Laboratory studies of simulated deposits [Otsuka et al., 1993] have shown that, for both sulphate- and chlorine-based deposits, corrosion was only slight to negligible, at temperatures below the melting point of the deposit. As soon as constituents of the deposit melted, rapid corrosion was observed. Also, in the absence of a deposit, corrosion from a simulated flue gas containing 1500 ppmv HCl was minimal, at temperatures up to 550 °C [Wright and Krause, 1996].

Several other corrosion mechanisms may be responsible for a corrosive attack of the nature observed in grate-fired units. [Spiegel and Grabke, 1991] suggests that chlorine may be liberated close to the metal surface, by NaCl reacting with the oxide scale, forming Na_2CrO_4 and $Na_2Fe_2O_4$. [Fujikawa and Maruyama, 1986] and [Hiramutsu et al., 1989] proposed that NaCl reacts with chromium carbide, preferably found at the grain boundaries, in order to form Na_2CrO_4 and Cl_2. And, finally, [Shinata et al., 1986, 1987] studied the effect of NaCl on chromium, Cr-Ni alloys, and stainless steels. They suggested a mechanism where NaCl reacts with Cr_2O_3 to form Na_2CrO_4 in an initiation step, followed by the formation of a eutectic melt between NaCl and Na_2CrO_4. The oxidation reaction is going on in the melt, and it is considered difficult to form a protective scale in such a melt. The eutectic temperature in the system NaCl and Na_2CrO_4 is 577 °C.

Several field investigations of corrosion have been conducted at straw-fired CHP-boilers in Denmark, over the past two decades [Larsen and Henriksen, 1996; Henriksen and Larsen, 1997; Montgomery and Karlsson, 1999; Montgomery et al., 2002a,b; Nielsen, 1998; Frandsen et al., 2006], providing basic data on corrosion rates of different materials at different temperatures and exposure times. In order to supply these data, laboratory tests under well-controlled conditions have shown that KCl contribute significantly to the increased corrosion rates observed in real-scale [Nielsen et al., 1999], while the flue gas composition seems to be of a somewhat lesser importance [Montgomery and Larsen, 2002].

Below is an outline of Danish experiences with and investigations on corrosion, in thermal fuel conversion systems fired solely or partly with straw.

3. Corrosion when Firing Straw on a Grate

A series of field campaigns have been carried out at straw-fired grate-boilers in Denmark; including the Rudkøbing, the Masnedø, and the Ensted CHP-plants. These campaigns have typically consisted of; [a)] exposure of metal rings on water/air-cooled cylindrical probes, [b)] investigation of a number of materials built into a test superheater section, and/or, [c)] removal of sections of the actual superheater section in a plant, for specific deposit chemistry, and corrosive potential, analysis. Both austenitic steels and ferritic steels have been exposed, at steam temperatures typically in the range: [450-570 °C]. The aim of the corrosion investigations has been to accurately quantify corrosion rates and mechanisms in existing superheaters, as a function of material choice, exposure time or steam temperatures (i.e. increased efficiency).

3.1. Corrosion at the Rudkøbing CHP Plant

Only negligible corrosion was observed on existing, superheater tubes, operated at a steam temperature of 450 °C ($T_{surface}$ ~ 480 °C), at the Rudkøbing CHP [Montgomery et al., 2000a]. Corrosion tests by an air-cooled cylindrical probe were conducted in which ferritic and high-alloyed austenitic steels were exposed to metal temperatures in the range [520-600 °C]. The corrosion probes were exposed for 450-3000 hours in a position in the top of the furnace. Both the metal wastage and the depth of the selective corrosion were measured, and those two thicknesses were added to provide a measure of the total corrosion depth [Montgomery et al., 2000a].

The corrosion rate was found to be strongly dependent on the metal temperature; below 480 °C, the corrosion rate was minimal, however, from 520-550 °C, increased corrosion rates were observed. At temperatures above 550°C corrosion rates increased catastrophically [Montgomery et al., 2000a].

Selective corrosion was observed for the austenitic steels tested at Rudkøbing (AISI 347H and Sanicro 31 HT), at metal temperatures above 520 °C [Larsen and Henriksen, 1996].

Chromium, and to a lesser extent Fe, were removed from the alloy, leaving back a degraded alloy phase, enriched in Ni. The ferritic steel (X20) showed no signs of selective corrosion.

No signs of flue gas components other than Cl-species were observed in the degraded metal zone. The corrosion rate at elevated temperature was found to be 2-20 times higher than what has been observed in PC- and CFB-boilers [Larsen and Henriksen, 1996].

The nature of the corrosive attacks observed at the Rudkøbing CHP-plant, indicated that the corrosion was caused by either HCl or Cl_2 in the gas phase, a mechanism quite well described in the literature [Nielsen, 1998; Fielder et al., 1984; Iisa et al., 1999; Boonsongsup et al., 1997; Harlow, 1944, 1949].

3.2. Corrosion at the Masnedø CHP Plant

At the Masnedø CHP, another corrosion investigation was performed using an air/water-cooled probe, located in the boiler positions shown in Figure 1. It was found that with metal temperature fluctuating in the range [450-600 °C], the corrosion was very high, and that the low- and high-Cr-alloyed steels had the highest corrosion rates [Montgomery and Karlsson, 1999]. In line with the Rudkøbing corrosion data, relatively high corrosion rates were observed at metal temperatures of 550°C, where no protective oxide scale was formed, while modest - almost parabolic type - corrosion (associated with formation of a more protective oxide scale), was observed at temperatures below 500°C [Montgomery et al., 2000a]. For the austenitic steels, Cr was preferentially attacked at the grain boundaries, anyhow, selective corrosion of Cr within grains was also observed [Montgomery and Karlsson, 1999]. Based on corrosion rates from the test superheater, it was deduced that a Cr-content of 15-18 %(w/w) gives the lowest corrosion rates [Montgomery and Karlsson, 1999].

The observed, relatively low corrosion rates at the in-boiler superheater section of the Masnedø CHP plant, may be explained by the presence of a K_2SO_4-layer, acting as a protective layer (film) [Montgomery et al., 2000a; Hansen et al., 2000]. This is consistent with experimental studies [Alexander, 1963] showing that a layer of K_2SO_4 on top of a metal sample, may slow down/inhibit selective Cl-corrosion, at temperatures below 700 °C,

while a layer of KCl can significantly enhanced corrosion down to temperatures of 400 °C. These data are consistent with the corrosion data from the Rudkøbing CHP, where the inner layer consisted of KCl, and corrosion problems were experienced above 490 °C [Michelsen et al., 1998].

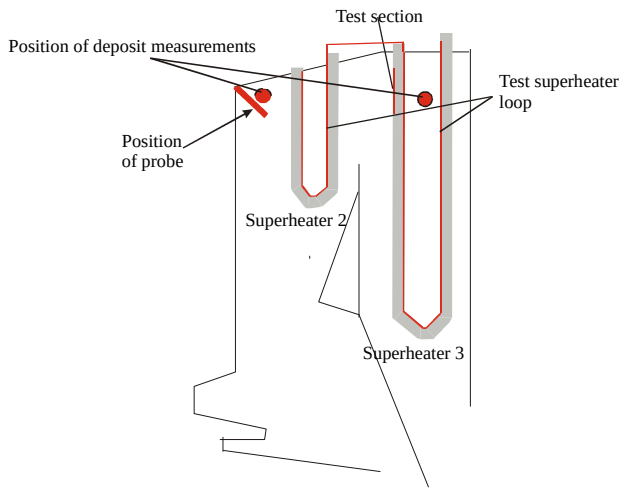

Figure 1: Schematic diagram of Masnedø CHP plant showing positions of corrosion and deposit investigations. Source: [Montgomery et al., 2000a]

3.3. Corrosion at the Ensted CHP Plant

At the Ensted CHP, test sections were welded into the superheater 2 and 3, see Figure 2. The specimens investigated were exposed for 2500 respectively 5000 hours, at conditions corresponding to steam temperatures in the range [447 – 470 °C], see Table 1.

The corrosion rates at the Ensted CHP were found to be rather low, as would also be expected at such low temperatures. Another series of experiments was performed with exposure for 10,000 hours, in order to quantify the corrosion over time, and establish whether the corrosion kinetics at these low temperatures as parabolic, linear (as at high temperatures), or paralinear. The deposits from these corrosion studies were found by SEM-EDX to consist mainly of K, S and O, although there was also sign of Cl-corrosion, since Cl was found on the outside of the metal-oxide interface. It should be emphasized that the ratio of K, S and O did not in the majority of cases correspond to K_2SO_4. There was a large surplus of K, compared to S [Montgomery et al., 2000a].

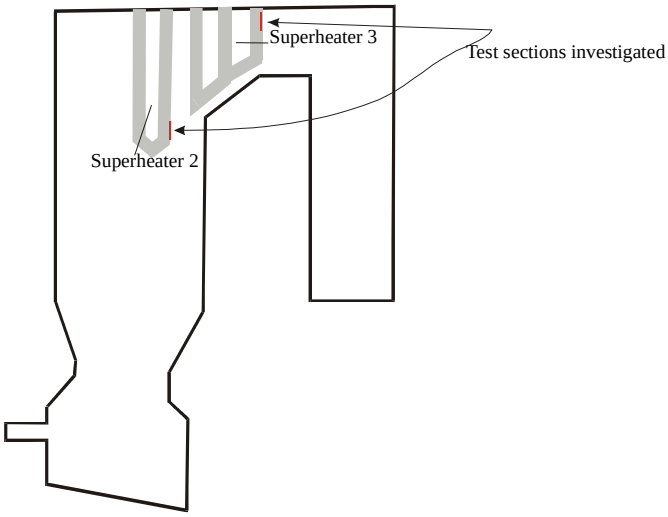

For the Rudkøbing, Masnedø and Ensted CHP-plants, the observations with respect to corrosion, and deposit morphology, are summarised in Table 1.

Figure 2: Schematic diagram from Ensted CHP plant showing positions of test sections. Source: [Montgomery et al., 2000a].

4. EFP-96 Lab-Scale Study of Corrosion in Straw-Fired Boilers

Corrosion measurements were performed in lab-scale, in order to investigate the high-temperature corrosion of superheater tubes in straw-fired boilers, under relatively well-defined and controlled experimental conditions [Nielsen, 1998; Nielsen et al., 1999]. Boat-shaped metal test elements covered with deposits were exposed to a synthetic flue gas, in an electrically heated oven. The experiments were divided into two series according to their objectives;

1. to quantify the corrosion rate for metal test elements covered by a KCl-rich deposit
2. to test the influence of different deposit compositions on the metal test elements.

Plant	T_{steam}	T_{metal}	Corrosion morphology	Deposit formation
Mas-nedø	520°C		Protective oxide formation with grain boundary attack – oxide has tendency to spallation	KCl with K_2SO_4 adjacent to the surface oxide. Iron oxide dendrites in both.
	450-570	460-615°C	Selective corrosion and grain boundary attack at the higher temperatures. Protective oxide at the lower temperatures	
		~ 580°C	Selective corrosion and grain boundary attack	KCl
Rud-købing	450°C		Formation of a protective oxide.	Predominantly KCl, minor amounts of sulphates and silicates or K_2SO_4 with some KCl. Iron oxide dendrites in both.
		520-650°C	Selective corrosion	
Ensted	470°C, 447°C		Protective oxide prone to spallation	K_2SO_4 with minor amounts of KCl. Iron oxide dendrites.

Table 1: Summary of findings correlating corrosion morphology and deposit chemistry to each other at the Rudkøbing, Masnedø respectively Ensted CHPs. Source: [Montgomery et al., 2000a].

The experimental equipment consisted of a gas mixing panel and two electrically heated ovens, see Figure 3. The deposits were placed on top of metal test elements, initially. The metal test elements were placed on specially designed quartz sledge, see Figure 4, and inserted into a quartz reactor in the horizontal oven. The metal test elements had boat-shape, and were approximately 20 mm long, 10 mm wide, and, with a thickness of 3 mm, see Figure 4. Two commercial superheater alloys were tested in the experiments, the ferritic X20CRMOV121 (X20) and the austenitic AISI 347HG (AISI 347). The test elements were not oxidized prior to exposure. The compositions of the two alloys are shown in Table 3. The samples were exposed to a synthetic flue gas, simulating the flue gas composition of a straw-fired boiler [Nielsen, 1998]. The ovens were kept at a constant temperature of 550 °C.

An overview of the two test series is shown in Table 2.

Parameter:	Test of rate law:	Test of different deposits:
Deposit	KCl	KCl, K_2SO_4, eutectic mixture of KCl-K_2SO_4[1], real deposit from Rudkøbing CHP, no deposit
Exposure time	1 week, 1, 2, 3, 5 months	3 months
Temperature	550 °C	550 °C
Metals	X20, AISI 347	X20, AISI 347
Flue gas	Simulated straw combustion: 6 %(v/v) O_2, 12 %(v/v) CO_2, 400 pmmv HCl, 60 pmmv SO_2, N_2 saturated with water at room temperature to balance.	

Table 2: Experimental conditions for lab-scale corrosion experiments. Note: [1] – 47 %(mol/mol) KCl. Source: [Nielsen, 1998].

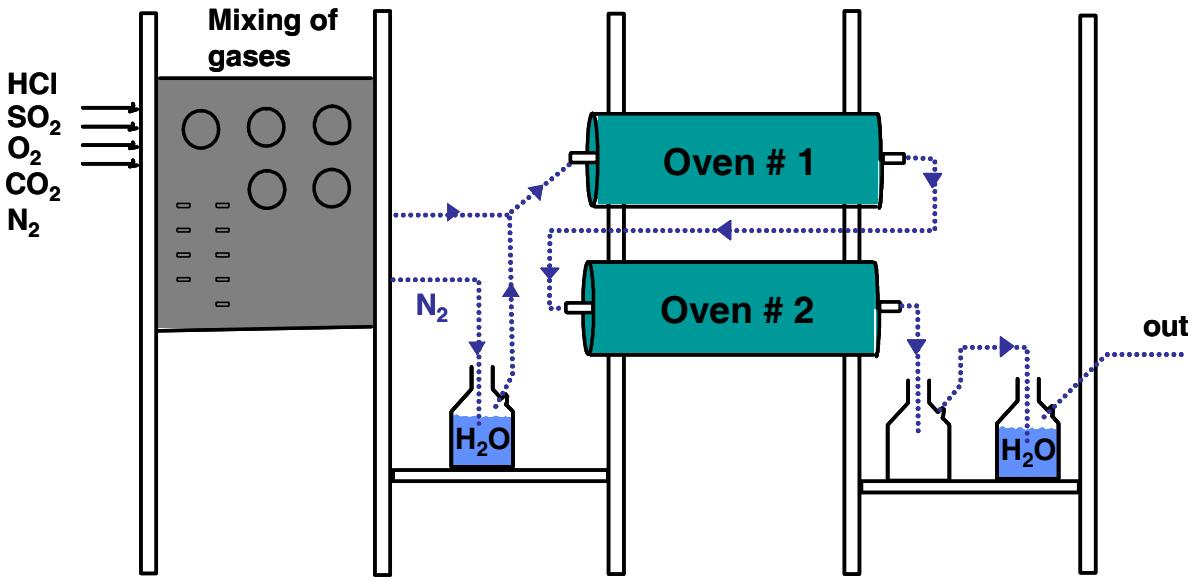

Figure 3: Experimental set-up for lab-scale corrosion experiments. Source: [Nielsen, 1998].

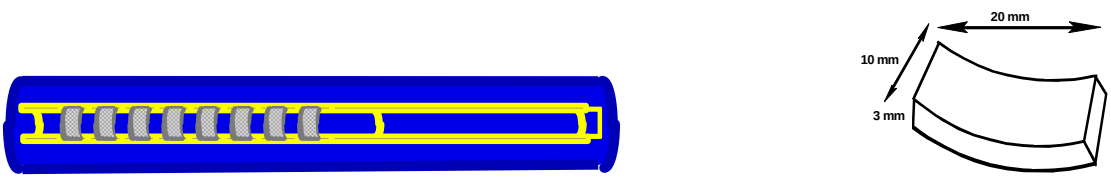

Figure 4: Reactor with quartz sledge for metal test elements. To the right, the dimensions of a test element. Source: [Nielsen, 1998, Nielsen et al., 1999].

The corrosion attack observed in the lab-scale experiments was, in general, quite uniform, and the corrosion products consisted mainly of oxides of Fe and Cr. The inner oxide scale contained both Fe and Cr oxides whereas the outer part consisted primarily of Fe-oxides. Thin layers of sulfide (chromium sulphide, Cr_2S_3) were observed on some of the elements right next to the base metal [Nielsen, 1998, Nielsen et al., 1999].

Traces of Fe and Cr chlorides were detected at the corrosion front, between the base metal and the inner oxide scale in several of the samples.

Metal	Abr.	Fe	C	Cr	Ni	Mo	Si	Mn	Other
X20CRMOV121	X20	Bal	0.20	12	0.5	1.0	<0.5	<1.0	0.5V
AISI 347HG	AISI 347	Bal	0.07	18	12	-	<0.75	2.0	<1.2Nb+Ta

Table 3: Composition (%(w/w)) of iron-based alloys used in lab-scale corrosion experiments. Source: [Nielsen, 1998; Nielsen et al., 1999].

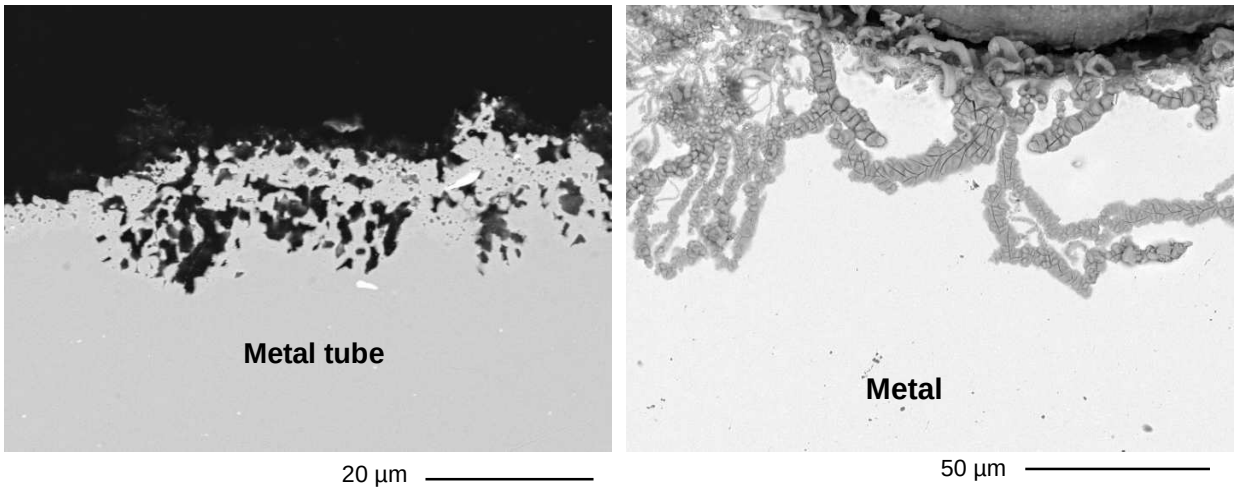

Figure 5: SEM micrographs showing examples of internal corrosion on test elements exposed to a synthetic flue gas in the laboratory. Source: [Nielsen, 1998].

Internal corrosion attack was generally limited, but an internal attack of 10-50 µm was found in some areas. The nature of the internal attack varied and occurred as cracks, voids, and internal attack through the grain boundaries. Figure 5 show examples of internal corrosion. Some test elements showed severe pits or areas of internal corrosion with depths up to 200 µm (Figure 6, right image). Chlorine was found in the pits, and the metal was

depleted in Cr and Fe, but not in Ni. This indicates the partitioning of chlorine in the localized pitting attack.

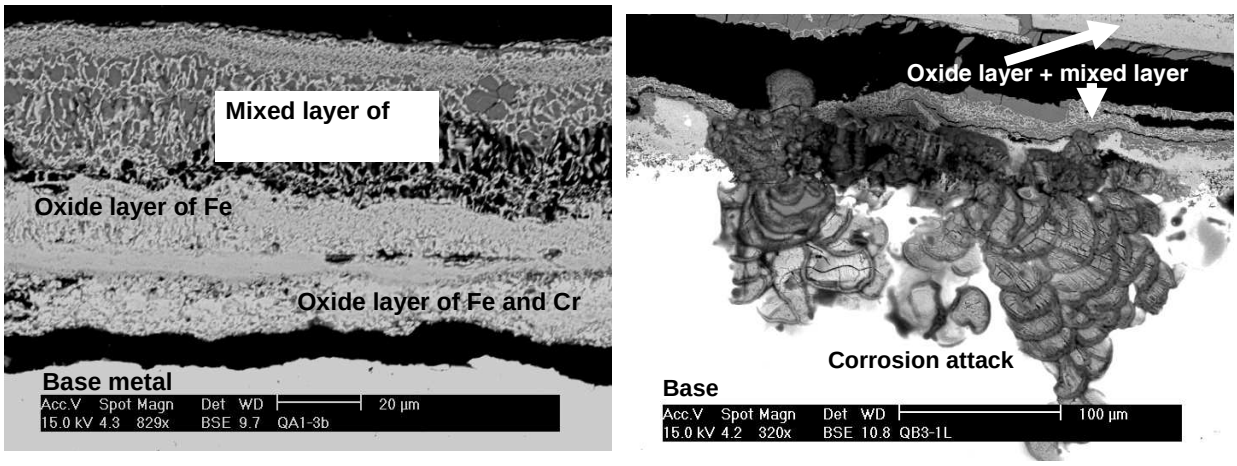

Figure 6: SEM micrographs, showing the scale structure on top of a corroded metal test element (left image), and internal attack of a test element covered by KCl-deposit. Source: [Nielsen, 1998].

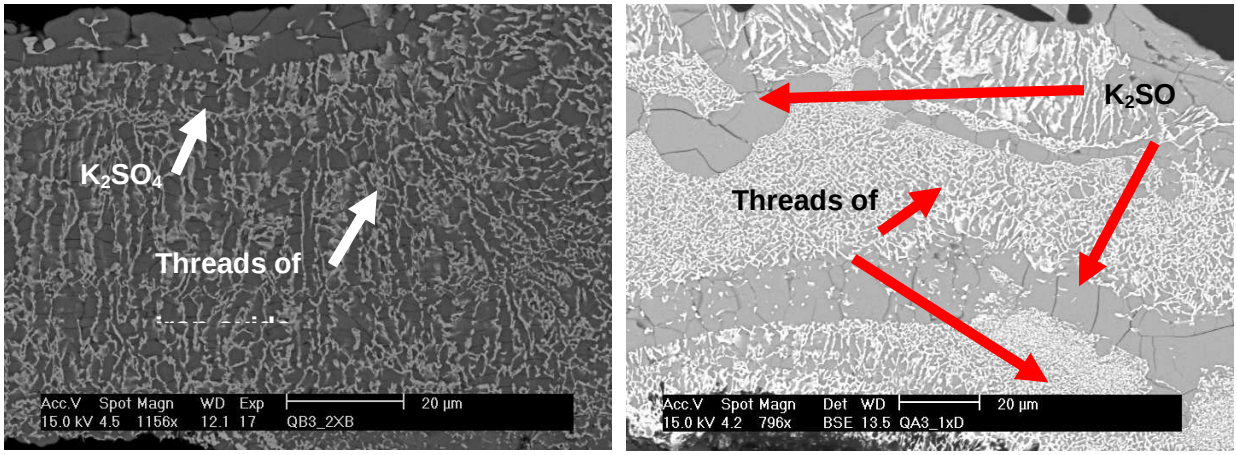

Figure 7: SEM micrograph of the inner layer of K_2SO_4 and iron oxide (left image), respectively of the inner layer of K_2SO_4 and iron oxide (right image). Source: [Nielsen, 1998].

On top of the oxide layers, a dense and very distinct 'mixed layer' of K_2SO_4 and iron oxide (Fe_XO_Y) was present on all the 20 samples analyzed (see Figures 6 and 7, left image). The structure of this layer was very characteristic, with threads of iron oxides (white) making up a framework in a matrix of K_2SO_4 (grey) (Figure 7). In the quite uniformly structured matrix, certain layers and areas of pure K_2SO_4 could be found (Figure 7).

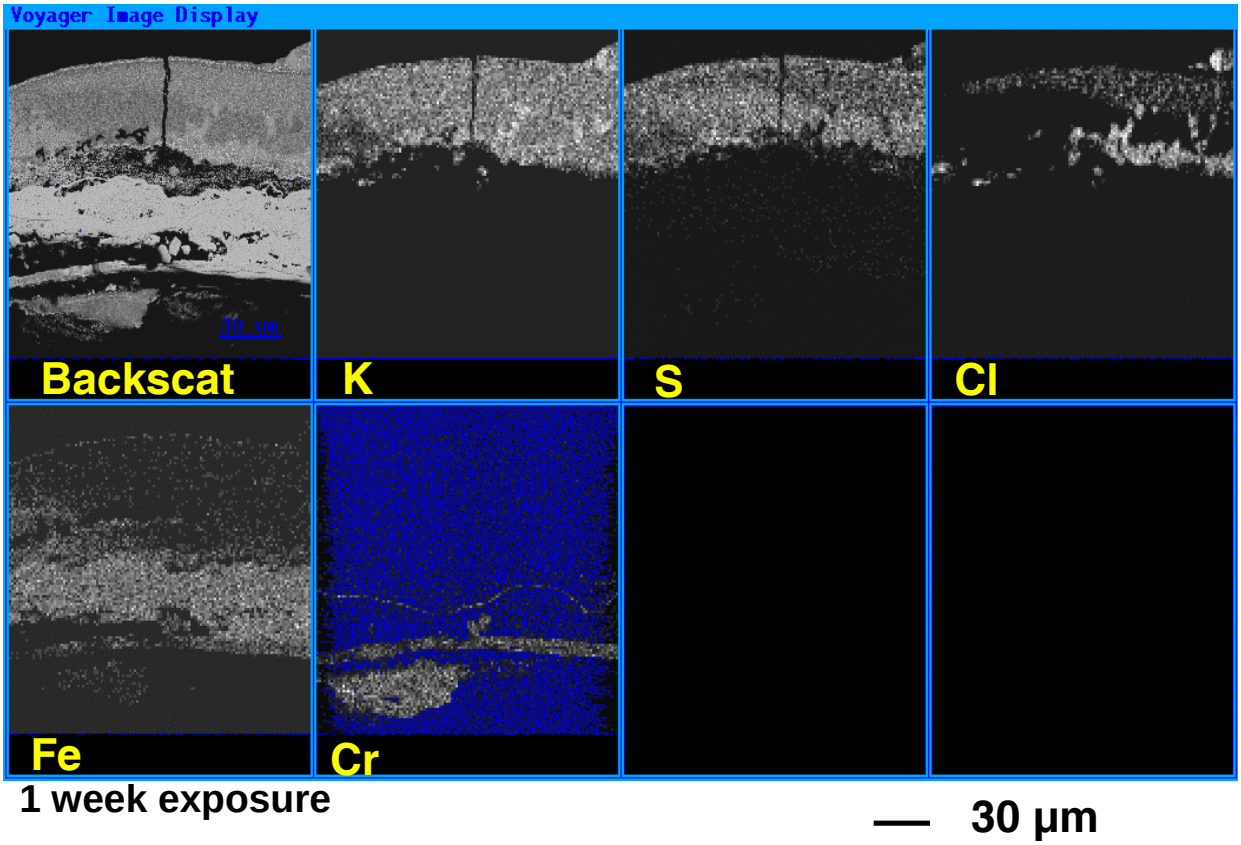

Figure 8: Elemental mapping of metal test elements covered by KCl, and exposed for one week in the CHEC corrosion test-rig. Source: [Nielsen, 1998].

In the samples exposed for one month or more, the mixed layer did not show any signs of Cl. After one week of exposure, the dense layer was similar to the ones formed during long exposure times but also contained minor amounts of KCl in designated areas, see Figure 8. The density and structure of the mixed layer indicate that it has been molten. In general, the threads of Fe_XO_Y were found only in combination with K_2SO_4 and the threads did not enter the KCl. This is illustrated in Figure 9, where threads of iron oxide in the K_2SO_4-layer are found between two KCl particles.

Individual particles consisting of KCl with a thin layer (0-10μm) of K_2SO_4 at the surface, were found on top of the mixed layer, indicating that the KCl-particles reacted to some extent with the SO_2 in the gas.

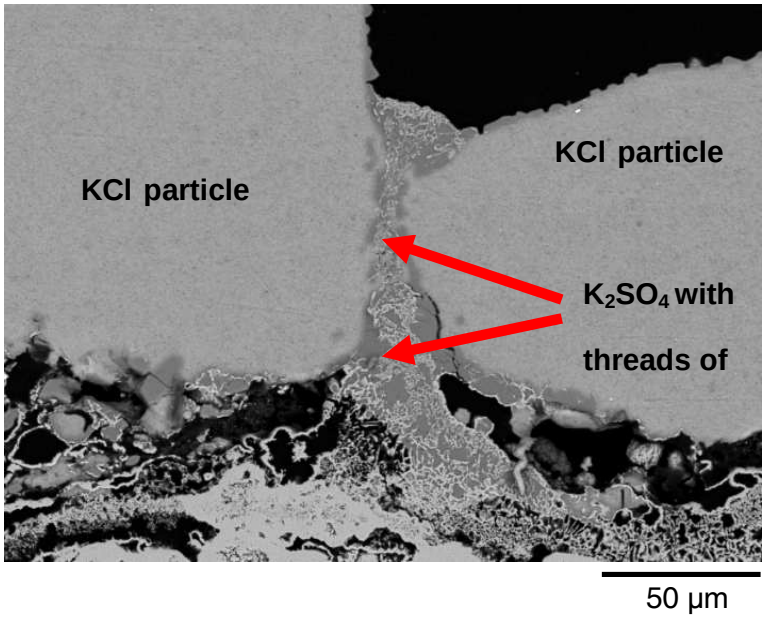

Figure 9: SEM micrograph of a mixed layer of K2SO4 and Fe oxide between two particles. Source: [Nielsen, 1998].

The samples covered either by KCl-K_2SO_4 or by the Rudkøbing real deposit, showed the same corrosion pattern as the ones covered by KCl. In contradiction, the samples covered with K_2SO_4 only showed a very thin layer of K_2SO_4 next to the metal oxide, but without the characteristic structure in the mixed layer was not found [Nielsen, 1998; Nielsen et al., 1999].

Figure 10 show the thickness of the oxide scale, as a function of exposure time, for the X20 metal test elements covered by KCl. A similar result was obtained for AISI 347. The data points are shown as the mean value of the measured thickness of the oxide layers, and the error bars represent one standard deviation. The corrosion depth increases with time, and the ferritic X20 was observed to suffer a greater corrosion attack than the austenitic AISI 347.

The thickness of the oxide scale from the metal test elements covered by different deposits is shown in Figure 11. It is seen, that the deposits containing KCl (KCl, Rudkøbing, KCl-K_2SO_4) causes thicker oxide scales than the pure K_2SO_4 deposit, and the absence of a

deposit. Furthermore, X20 showed thicker oxide scales for all the deposits, compared to AISI 347. The picture becomes more profound when the thickness of the mixed layer is added to the ones of the oxide layer [Nielsen et al., 1999].

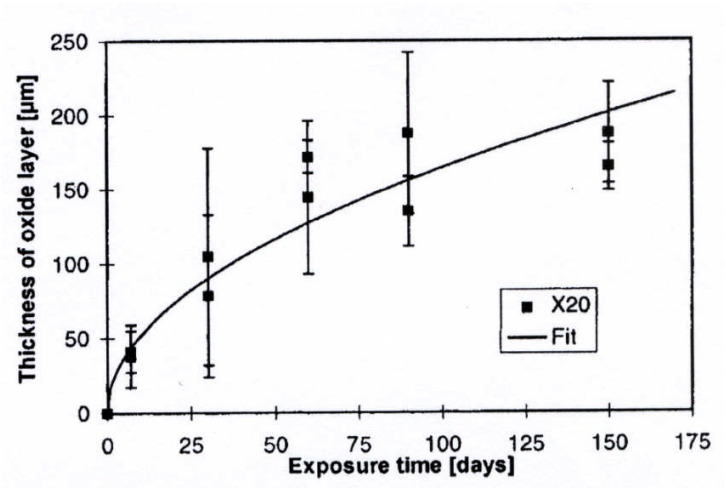

Figure 10: Thickness of oxide layer for X20 covered by KCl. Mean values. Error bars represent ± standard deviation. Source: [Nielsen, 1998].

A corrosion mechanism for the corrosion caused by Cl-containing deposits, including both the sulfation of KCl to K_2SO_4, and the essential presence of a molten phase based on lab-scale corrosion experiments, literature data from full-scale deposit and corrosion studies was proposed by [Nielsen et al., 1999].

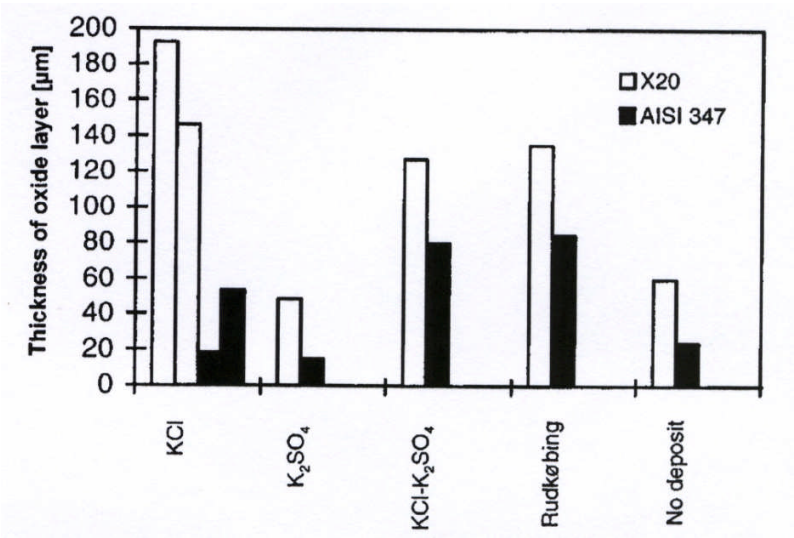

Figure 11: Thickness of oxide layer for metal test elements covered by different deposits.

Exposure time: 3 months.

Mean values shown.

Source: [Nielsen, 1998].

Potassium chloride, KCl, forms a melt with K_2SO_4 and different Fe-species (Fe_XO_Y, $FeCl_2$), adjacent to the oxide scale sulfation of KCl occurs rapidly in the melt, releasing HCl or Cl_2 close to the metal surface. The chlorine gas diffuses through the oxide scale, and reacts with Fe to form volatile iron chlorides ($FeCl_2$, $FeCl_3$). The iron chlorides are thermodynamically stable at the interface between the metal and the oxide scale where a very low partial pressure of oxygen exists. They diffuse out through the scale, and oxidize as they reach areas with higher partial pressures of oxygen. Thus, iron oxides will be formed either on top of the oxide scale or in the dense mixed layer on top of the oxide scale. This mechanism can explain the shift in corrosion behaviour with temperature which has been observed in full-scale corrosion tests [Larsen & Henriksen, 1996]. At low metal temperatures, the solid phase sulfation of KCl is slow and the corrosion is governed by general oxidation. When the metal temperature exceeds the lowest melting temperature in the KCl/K_2SO_4/iron species system, the sulfation reaction becomes much more rapid, generating a high partial pressure of Cl_2/HCl. This may cause accelerated oxidation and selective corrosion of the metal [Nielsen et al., 1999].

5. Corrosion when Co-Firing Coal and Straw in PF-Units

When co-firing coal and straw, in suspension-fired units, KCl, released from the straw, reacts with mineral inclusions in coal char particles in the flame, forming K-Al silicates and K_2SO_4, while chlorine is, in the presence of water, is released as HCl(g), according to the following reactions:

$$2\,KCl + Al_2O_3 + 6\,SiO_2 + H_2O \rightarrow K_2O \cdot Al_2O_3 \cdot 6\,SiO_2 + 2\,HCl \qquad (6)$$

$$2\,KCl + SO_2 + H_2O + ½\,O_2 \rightarrow K_2SO_4 + 2\,HCl \qquad (2)$$

The corrosion rates observed during co-firing of coal and straw are much lower than that seen in straw-fired power plants, and are closer to that in coal-fired power plants.

5.1. Corrosion Tests at MKS1

Elsam carried out on-site investigations at the Midtkraft-Studstrup Power Station, Unit 1, MKS1, in order to test the corrosive potential of coal-straw co-firing [Andersen, 1998; Montgomery and Larsen, 2002; Wieck-Hansen et al., 2000].

High-temperature corrosion was investigated by the use of [a)] air/water-cooled corrosion probes positioned close to the superheater, and, [b)] test sections welded into the existing superheater [Larsen et al. 1996; Montgomery and Larsen, 2002]. The positions of the test probes and sections in the platen and secondary superheater are shown in Figure 12. Corrosion investigations inside or close to the platen superheater were undertaken in order to investigate how a high flue gas temperature (1100 °C), and a relatively modest metal temperature (475 °C), influences the corrosion rate. Corrosion investigations were also conducted at the secondary superheater at a higher steam temperature, 540 °C, but also a lower flue gas temperature of 925 °C. An overview of the combination of experimental parameters is shown in Table 4. The chosen set temperature for the probes ranged from those actual in the plant to 580 °C [Montgomery and Larsen, 2002]. Test sections and probes were exposed to flue gas

derived from combustion of coal+10% straw, and, coal+20% straw, for approximately 3000 hours. Detailed specifications of the materials investigated in the MKS1 demo program are listed in Table 5.

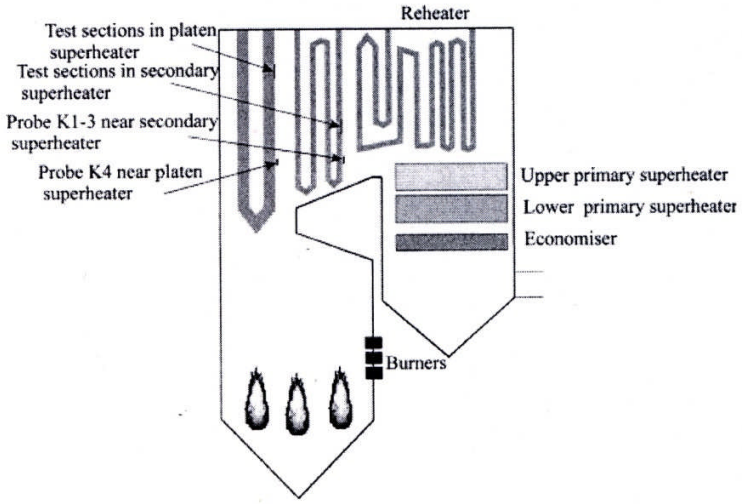

Figure 12: Schematic diagram of the Midtkraft- Studstrup Power Station, Unit 1, showing positioning of corrosion probes and test sections.

Source: [Montgomery and Larsen, 2002]

Sample type:	Corrosion probes:				Test tube sections:	
Position:	2nd SH	2nd SH	2nd SH	Plat SH	2nd SH	Plat SH
Flue gas temp, °C	925	925	925	1100	925	1100
Steam temp, °C	520	550	580	500-530	540	475
Metal temp, °C (10 % straw)	556	580	612	550	565	525
Metal temp, °C (20 % straw)	541	563	586	588	565	525
Exp. Time, hr (10 % straw)	2540	2770	2770	2770	300	3000
Exp. Time, hr (20 % straw)	2980	3012	3012	3012	3012	3012

Table 4: Overview of the experimental parameters investigated during the MKS1 demo program. Source: [Frandsen et al., 2006].

Material:	C:	Cr:	Ni:	Mo:	Si:	Mn:	Other:
13CrMo44	0.08 -0.18	0.70 – 1.10		0.40 – 0.60	0.10 – 0.35	0.40 – 1.00	
10CrMo910	0.07 – 0.15	2.0 – 2.5		0.9 – 1.1	0.20 – 0.50	0.40 – 0.70	Mn
X20CrMoV121	0.17 – 0.23	10.0 – 12.5	0.3 – 0.8	0.8 – 1.2	< 0.5	< 1	V
X8CrNiMoNb1616	0.04 – 0.10	15.5 – 17.5	15.5 – 17.5	1.6 – 2.0	0.30 – 0.60	< 1.50	Nb
TP321H	< 0.08	17.0 – 19.0	9.0 – 12.0		< 1.00	< 2.0	Ti
TP347H FG	0.04 – 0.10	17.0 – 20.0	9.0 – 13.0		< 1.00	< 2.00	Nb
Sanicro 31 HT	< 0.12	19.0 – 23.0	30.0 – 34.0		< 1.00	2.00	Al,Cu,Ti
HR3C	< 0.10	23.0 – 27.0	17.0 – 23.0		< 1.50	< 2.0	Nb,N
Castolin coating	?	30	Balance				B

Table 5: Specifications of the materials investigated in the MKS1 demo program.

Source: [Montgomery and Larsen, 2002].

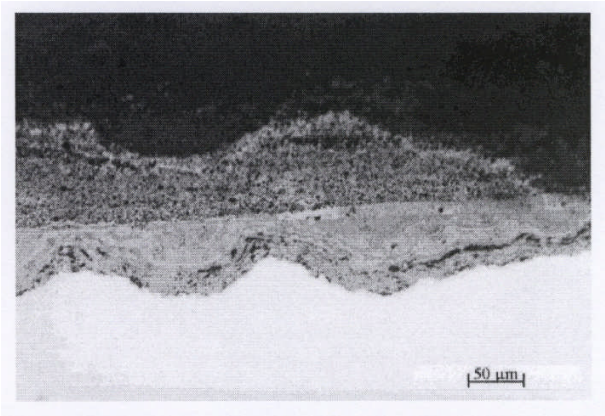

Figure 13: 2-layer oxide scale formed on top of X20CrMoV121 on corrosion probe 2 at a metal temperature of 563 °C, at 20 % straw co-fired. Source: [Montgomery and Larsen, 2002].

5.1.1. Feritic and Martensitic Materials

At both 10 % and 20% straw share, a thick 2-layer oxide scale was found for 13CrMo44, 10CrMo910 as well as X20CrMoV121, see e.g. Figure 13.

Some evidence of broad pits was also observed. The inner oxide scale was rich in Cr, while the outer scale was a Fe-oxide, with fly ash particles embedded along the outer surface. Sulfur was detected along the inner-outer scale interface and within the inner Cr-rich oxide scale, in concentrations up to about 3 – 4 %(w/w), but sometimes as high as 13 %(w/w) [Montgomery and Larsen, 2002].

5.1.2 Lower-Alloyed Austenitic Steels

For X8CrNiMoNb1616, an inner and an outer oxide scale was also observed, in which the inner scale was rich in Cr, while the outer scale was a Fe-oxide, see Figure 14, i.e. a structure similar to that observed for X20CrMoV121 [Montgomery and Larsen, 2002]. Sulfur was again present in the inner scale, and along the scale interface. Sulfur was also detected along grain boundaries along the corrosion front.

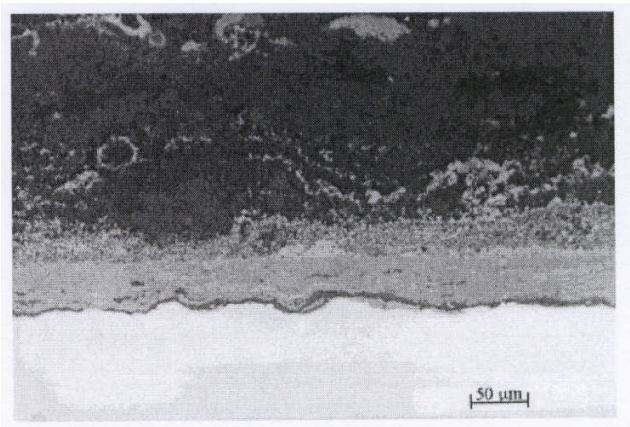

Figure 14: Oxide scale formed on top of X8CrNiMoNb1616 on corrosion probe 4 at a metal temperature of 588 °C, at 20 % straw co-fired. Source: [Montgomery and Larsen, 2002].

For TP 321 H, the oxide scale structure varied from a thick layer to broad pits. The oxide scale consisted again of two layers where the inner scale was a Cr-rich oxide, and the outer scale was a Fe-oxide. In addition, Ni was presented in the inner scale [Montgomery and Larsen, 2002].

For TP347H FG, broad pits were observed underneath a Cr-rich inner oxide scale, and an iron-rich outer oxide scale [Montgomery and Larsen, 2002]. Sulfur and Cr, presumably in the form of CrS_X, were found in the inner scale, close to the corrosion front, and there was Ni-enrichment in the metal adjacent to the corrosion front. The metal by the corrosion front was found to be porous, most likely due to excessive diffusion of Fe and Cr, leaving vacancies behind. The thin oxide consisted of a Cr-rich oxide with an outer layer of iron oxide [Montgomery and Larsen, 2002].

5.1.3. Higher-Alloyed Austenitic Steels

For HR3C, the oxide scale was found to be rather thin, although pits were also observed, especially when co-firing 20 % straw. At 20 % straw fired, the pits were found to be up to 150 μm deep at a metal temperature of 586 °C. The oxide scale formed within these pits was a Cr-rich Fe-Cr oxide, however S was also found in association with Cr, at the base of the pits [Montgomery and Larsen, 2002].

For Sanicro 31 HT, the oxide scale morphology varied for the different specimens, and even within the same specimen. A dark inner oxide scale was found to be rich in Cr, and in most cases had a higher S-content, indicating the presence of sulfides and sulfates [Montgomery and Larsen, 2002].

In all cases, the Castoline-coating had formed various oxide scales, rich in Fe, Ni and Cr. Sulfur was present in most of these scales. In addition, K was present adjacent to the oxide-metal interface [Montgomery and Larsen, 2002].

5.1.4. Summary of Corrosion at MKS1

Thus, to sum up, at MKS1, corrosion rates at 10 % straw share co-fired were similar to those reported for coal-firing. For both the secondary and the platen superheaters, the corrosion rate was highest for the low-alloy ferritic, steels like 13CrMo44 and 10CrMo910, and decreased with increasing alloying elements, giving HR3C and Sanicro 31 the lowest corrosion rates [Montgomery and Larsen, 2002]. There were less corrosion products on the specimens when soot blowing was applied, indicating that soot blowing had removed some of the oxide scale. It was also found that the corrosion rate was higher for the secondary superheater, i.e. a higher metal temperature had a more pronounced effect on the corrosion process, than an increased gas temperature [Montgomery and Larsen, 2002].

When co-firing 20 % straw, the corrosion rates were higher than at 10 % co-firing for all alloys in both the platen superheater, and the secondary superheater. For the ferritic steels, there was generally less corrosion products observed for the specimens with soot blowing than without. This trend was not observed for the austenitic steels [Montgomery and Larsen, 2002].

The effect of the gas temperature, under conditions of constant metal temperature can be investigated by comparing probe 1 and probe 3, see Figure 12, both having metal temperatures of 550 °C, while the gas temperature was 925 °C, respectively, 1100 °C. This comparison shows that the flue gas temperature does influence the corrosion, in that an increase of the gas temperature of 175 °C gives a significant increase in the corrosion rate [Montgomery and Larsen, 2002].

Analysis of the corrosion products from MKS1 also showed that S in the form of sulfates and sulfides were present within the corrosion products. It was suggested that at 10 % straw share, and at 20 % straw share at low temperatures, sulfidation and oxidation occur according to the reactions shown below, where the oxidants are supplied from K_2SO_4 present in the deposit [Montgomery and Larsen, 2002]:

$$2\,Fe + 1\tfrac{1}{2}\,O_2 \rightarrow Fe_2O_3 \qquad (7)$$

$$2\,Fe + S_2 \rightarrow 2\,FeS \qquad (8)$$

5.2. Corrosion Tests at SSV4

Since 2002, the Studstrup Power Station, Unit 4 (SSV4) has been co-firing approximately 10 % straw (on an energy base) with coal. Corrosion was investigated by exposing test sections in the actual superheaters 3 and 4 and the reheater loop. Sections were removed after 1 year (7231 hours), 2 years (17719 hours), and, 3 years (22597 hours).

Position	3rd SH			4th SH			Reheater		
Flue gas temp, °C	1220	1220	1220	1020	1020	1020	940	940	940
Steam temp, °C	465	465	465	575	575	575	560	560	560
Metal temp, °C	485	485	485	595	595	595	580	580	580
Straw share, %	7.5	9.8	9.3	7.5	9.8	9.3	7.5	9.8	9.3
Exposure time, hr	7231	17719	22567	7231	17719	22597	7231	17719	22597

Table 6: Overview of the experimental parameters investigated at SSV-4. Source: [Frandsen et al., 2006].

An overview of experimental parameters investigated at SSV4, is provided in Table 6. Superheater 3 at SSV4 had an outlet steam temperature of 550°C. The tube investigated was midway between the inlet and outlet, and the actual steam temperature was estimated to be 465°C. The flue gas temperature, before superheater 3, was 1220°C. Superheater 4 had an outlet steam temperature of 540°C. However, the actual outlet steam temperature of tube 18, where the test section was located was 575°C. Since the test section was close to the outlet, it was assumed that this has a similar steam temperature. The flue gas temperature, before superheater 4, was 1020°C. Finally, for the reheater tube investigated, the outlet steam temperature is 560°C and since the test section is close to the outlet, it is assumed

that it has a similar steam temperature. The flue gas temperature, before the reheater, is 940°C [Frandsen et al., 2006; Montgomery et al., 2008].

For all the samples investigated, the main elements detected in the deposits adjacent to the corrosion products were Al, Si, Ca, S, K and Fe. In some cases, especially in the reheater section, the thickness and the composition of the deposits were found to vary greatly with the flue gas direction, i.e. there were significant differences between the up- and downstream deposits. High concentrations of K were associated with high concentrations of S, indicating the presence of K_2SO_4. Chlorine was only detected in the fly ash at a few occasions [Frandsen et al., 2006].

On the X20CrMoV121 samples in superheater 3, a 2-layer oxide scale was formed. The inner oxide scale was rich in Cr, while the outer oxide scale was an almost pure Fe-oxide, Fe_XO_Y, in which fly ash particles were incorporated. At all exposure times, minor amounts of S were detected in the inner oxide scale, indicating the presence of sulphides or sulphates. Sulphur was also detected at the corrosion front but there was no evidence of significant internal corrosion attack [Frandsen et al., 2006].

On the austenitic TP347H FG tubes in superheater 3, 2-layer oxide scales were also formed. The inner oxide scale was again rich in Cr, while the outer oxide scale was a pure Fe-oxide, Fe_XO_Y, having fly ash particles incorporated. When compared to the X20CrMoV121 samples, both the inner and the outer oxide scale were much thinner when formed on TP347H FG. In some isolated areas, the inner oxide scale was only 2 – 3 µm thick, even after as much as 22597 hours of exposure. Sulphur was detected in the oxide scales, as well as along the corrosion front [Montgomery et al., 2008].

Only (the martensitic) X20CrMoV121 was exposed in superheater 4. All samples showed an inner and an outer oxide scale, where the inner oxide was rich in Cr, while the outer oxide scale was a Fe-oxide. At all exposure times, S, was detected in both the oxide scales as well as along the corrosion front. Severe internal corrosion attack in the form of sulphidation was observed at grain boundaries, down to a depth of 40 µm, already after 7231 hours of exposure. The depth of the internal corrosion attack remained constant over time, while the Cr-rich inner oxide layer grew in thickness [Montgomery et al., 2008].

The reheater samples showed a 2-layer oxide scale, after 7231 hours exposure. In addition, very thin oxide scales were occasionally found on the downstream side. On the upstream

side, internal grain boundary attacks, rich in S and metallic alloying elements, i.e. sulphides, were observed to a depth of approx. 25 µm. After 17719 hours of exposure, Cl appeared at the corrosion front, and the inner Cr-rich oxide scale was very thick in these areas [Montgomery et al., 2008].

Reheater samples after 7231 and 22597 hours exposure showed a similar oxide to superheater 4. The outer oxide was iron oxide with Al-silicate particles embedded. The inner oxide was Cr-rich, with S within the inner oxide layer. Internal sulfidation attack, particularly at grain boundaries was observed. After 2 years exposure, Cl appeared at the corrosion front in localized areas. The thickness of the inner Cr-rich oxide was greater here Cl was found compared to the other areas [Montgomery et al., 2008]. In some spots, traces of Cl were present with S, Cr and Ni at the oxide-metal interface, otherwise Fe and O were the main constituents. Although there was less than 1 % Ni in X29CrMoV121, Ni was present in these spots, probably as $NiCl_2$ [Montgomery et al., 2008].

6. Corrosion in Plants (Co)-Fired with Wood

Some previous projects made relevant attempts to investigate the basic mechanisms responsible for the behaviour of ash forming elements including ash deposition and corrosion in wood-fired combustion units.

6.1. Dedicated Wood-Firing on a Grate

One of these projects, carried out within FP5, was the project **BIOAEROSOLS** (ERK6-CT1999-00003), another one, the FP-6 project **BIOASH** (SES-CT2003-502679). One of the main objectives of **BIOAEROSOLS** was to characterise aerosols, fly ashes and deposits formed during fixed-bed combustion of wood fuels. Furthermore, parameters influencing aerosol formation as well as the melting behaviour of deposits were investigated. Within **BIOAEROSOLS**, a considerable step forward concerning a better understanding of particle and deposit formation during fixed-bed wood combustion was achieved. The main results of the project were [BIOAEROSOLS, 2003]:

- A collection of data on aerosol and fly ash shape, chemical composition, particle size distribution and concentration in the flue gas of fixed-bed combustion units with respect to the wood fuel used, and the operational conditions applied, during combustion.
- Three different mechanisms for aerosol formation during the combustion of chemically untreated wood chips, bark respectively waste wood were suggested.
- Data on deposit build-up rates and chemical compositions seen in relation to the chemical composition of the fuel used, and the operational mode of the combustion unit.

BIOAEROSOLS showed, that, in general, all relevant ash related problems in biomass combustion units depend on the operation mode of the furnace and the chemical composition of the fuel, but the release behaviour of ash forming compounds from the fuel, which is at the moment only insufficiently known, plays the most important role within these processes. Concerning particle emissions from biomass combustions it was concluded, that for small-scale biomass combustion systems, at present, no efficient and economically compatible technologies are available.

Based on these achievements of the **BIOAEROSOLS** project, the **BIOASH** aimed at the investigation of the release behaviour of ash forming compounds from biomass fuels in fixed-bed and in pulverised fuel combustion systems and on the determination of missing thermodynamic data, as a basis for investigations concerning aerosol and deposit formation.

In detail the objectives of the **BIOASH** project were [BIOASH, 2007]:

- To conduct investigations concerning the release of ash forming species from selected biomass fuels during fixed-bed and pulverised fuel combustion.
- Determination of basic thermodynamic data concerning the melting behaviour of ash mixtures containing Na, Zn, and Pb as well as the determination of the viscosity of molten ash deposits. Such data were identified as crucial within the **BIOAEROSOLS** project.
- To develop existing computer aided simulation tools regarding the formation of aerosols during biomass combustion further with special focus on elemental release from the fuel and the effects on transport properties caused by turbulence.
- Development of new codes for simulation of deposit build-up and deposit properties with relation to the combustion of different solid biomasses, mixtures of biomasses, and co-firing of biomass and coal.
- Investigation of the influence of the co-firing of biomass in coal combustion plants with special emphasis on aerosol and deposit formation as well as deposit melting behaviour.
- Development, test and optimization of a new, efficient and economically sound aerosol precipitation technology for reduction of aerosol emissions from small-scale biomass combustion units.
- Detailed study of deposit/chemistry, with special focus on the corrosive potential of deposits formed when firing different types of woody biomass on a grate.

The detailed investigations concerning these objectives were carried out in laboratory tests, test runs at pilot-scale, and at large-scale biomass combustion and co-firing plants. Woody biomass fuels (wood, bark, waste wood) as well as straw, sawdust and olive residue, was considered.

Within BIOASH, test runs took place at [BIOASH, 2007]:

- The MAWERA test-facility, Hard, Austria (wood-fired grate boiler), January 2005;
- The Dolna-Odra power station, Poland (co-firing of coal and sawdust in suspension), April 2005;

- The Esterwerda CHP-plant, Germany (waste wood-firing on a grate), August 2005, and;
- The Elean power station, UK (wheat straw firing on a grate), November 2005;

The following samples were taken and measurements were conducted at all the measuring campaigns; [1)] fuel sampling and subsequent analyses; [2)] aerosol and fly ash sampling with low-pressure cascade impactors, an electrical low-pressure impactor and a total dust sampling device in the flue gas downstream of the boiler; [3)] aerosol sampling in the hot furnace, applying a high-temperature impactor; [4)] deposit sampling with deposit probes at several locations in the furnace; [5)] long-term deposit sampling; [6)] flue gas measurements concerning CO, CO_2, O_2, SO_2, and HCl; [7)] Estimation of the furnace temperature with a suction pyrometer; [8)] sample taking from all relevant ash fractions (bottom ash, furnace fly ash, and ESP filter ash) and subsequent analyses, and [9)] recording of all relevant operating parameters (furnace temperatures, load, combustion air supply etc.). Thus, a very comprehensive set of data on which to address e.g. the corrosive potential of deposits formed when firing woody biomass fuels (wood, bark, waste wood), straw, sawdust and olive residue.

Deposit sampling within the **BIOASH** project, were carried out by Abo Academy University, Finland. Both long- and short-term deposits were collected on surface temperature regulated air-cooled probes equipped with detachable rings. The deposit sampling time varied between 2 hours (short-term) and 17-37 hours (long-term). Metal surface temperatures of 350, 450 respectively 550 °C were applied during the measurements. All samples were analysed for their elemental composition on the wind (upstream) side, lee (downstream) side and at a 50° angle from the wind side, since Cl, based on experience has been found to be highly enriched in the particular location of the probe. The elemental analyses were done by means of SEM/EDX analysis. The rings were further weighed before and after the tests and the rates of deposit build-up (RBU, g/m^2h) were determined [BIOASH, 2007].

Based on the specific data derived, for wood chips-firing on a grate, it was concluded that [BIOASH, 2007];

- The deposits are rich in K, Ca and S, low in Cl, and very low in Al and Si;
- [Cl] decreases with increasing probe temperature. No or only very low [cl] were found in deposits with a ring temperature of 550 °C;

- Cl was found only in the cyclone and the fly ashes, no Cl was found in the bottom ashes;
- All deposits were high in [K], to some degree [K] decreased with increasing temperature;
- Zn was found in all deposits, although mainly as ZnO in particles in the other deposit layer, never in the innermost deposit layers. No signs of association between Zn and Cl were found in the deposits;
- No Pb were found in the 450 respectively the 550 °C deposits, and low very low [Pb] was detected in the 350 °C deposits. Pb was found in all ashes;
- High [Fe] in association with Cr indicated corrosion of the probe rings, and;
- In the long-term experiments, 17 – 24 hours, Zn was only found on the cooler, 350 °C, probe. Again, mainly as ZnO-particles present in the outer deposit layer.

For bark-firing on a grate, it was concluded that [BIOASH, 2007];

- The deposits are rich in K, Ca and S, low in Cl, and very low in Al and Si;
- [Cl] decreases with increasing probe temperature;
- Max [Cl] was found to be 7 – 9 %(w/w) on the leeside of the 450 °C probe;
- All deposits were high in [K], to some degree [K] decreased with increasing temperature;
- Zn was found in all deposits, although mainly as ZnO in particles in the other deposit layer, never in the innermost deposit layers. No signs of association between Zn and Cl were found in the deposits;
- No or only very low [Pb] was detected in the deposits. No Pb was found in the ashes;
- Low [Cr] indicated lower corrosion of the probe rings than was the case for wood chips, and;
- In the long-term experiments, 37 hours at 450 °C, did not show any sign of corrosion and had very low [Cl].

Finally, in the case of waste wood, the BIOASH data lead to the following conclusions [BIOASH, 2007];

- The deposits are rich in K, Ca, S, and Zn, low in Cl, Al and Si;
- Significant variations in the deposit composition was detected as a function of surface temperature and exposure time;
- [Cl] ∈ [3 – 17 %(w/w)] on the leeside of the 450 °C probe;

- All deposits were high in [K], [K] ∈ [5 – 35 %(w/w)];
- Zn was found in all deposits, [Zn] ∈ [2 – 35 %(w/w)]. [Zn] higher on the leeside than on the wind side, indicating the presence of Zn in small particles, deposited via turbulence eddies on the downstream side of tubes;
- Pb only found on the 450 °C probe, with [Pb] ∈ [4-5 %(w/w)]. Pb was found in all ashes;
- Higher [Cr] than for wood chips, indicated lower corrosion of the probe rings than was the case for wood chips, and;
- In the long-term experiments, 17 hours at 450 °C, did not show any sign of corrosion and had very low [Cl] and [Zn]. Thus, the [Zn] decreases significantly with time.

To sum up the pilot- and full-scale experiences from firing wood in the BIOASH project, significantly lower corrosion was observed than what is usually reported for straw-fired system. Zinc was found in all deposits, but only played a major role in the inner deposit layer in connection to corrosion, when firing waste wood. Lead, does not take any active part in corrosion when firing woody fuels like wood chips, bark or waste wood, although theoretical considerations within the BIOASH framework indicated that Pb may decrease the temperature of the lowest melting phase in the system $(K,Na)(SO_4,Cl)$ by as much as 200 °C.

6.2. Co-Firing of Gas, Heavy Fuel Oil and Wood Pellets at AVV-2

The Avedøre 2 CHP-plant (AVV-2) was commissioned in 2001, and is located south of Copenhagen. It comprises three modules – a large USC (ultra super critical) plant, two paralle-powered gas turbines and a biomass plant. The steam pressure of the USC boiler is 300 bar and that of the reheater components is 80 bar. The main boiler in a once through tower boiler of the Benson-type with single reheat and is designed for USC steam data, i.e. 300 bar and 580/600 °C. It has a thermal input capacity of 800 MW [Jensen et al., 2005].

In superheater 3 at AVV-2, a test tube has been welded in with alternate sections of TP347H FG and Esshete 1250 in order to compare both steam- and fireside oxidation for these two steel types. During the first year of operation (3000 hours), the plant was fuelled alternately with natural gas (~ 1000 hours) and heavy fuel oil (~ 2000 hours). The outlet steam temperature of the test superheater section was 580 °C during gas firing and 540 °C during

oil firing. During the 2nd and 3rd years of operation (~ 8000 hours each year), the plant was fired simultaneously with heavy fuel oil [2,5 % S and max 120 ppmv V), gas and wood pellets, and the outlet steam temperature was 540 °C [Jensen et al., 2005].

Only very little deposit was detected after firing gas and heavy fuel oil during the first year, however thicker deposits were present after the 2nd and 3rd years, when wood pellets were co-fired with gas and heavy fuel oil. Soot blowing was used periodically during the 2nd and the 3rd year in order to remove the outer deposits, so only the innermost deposits were analysed after exposure [Jensen et al., 2005; Montgomery et al., 2008]. During the 1st year, the deposit formed was a Na_2SO_4-matrix with particles of mostly Fe-vanadate but also some Ni-vanadate, embedded. After the 3rd year, the chemistry of the matrix shifted from Na_2SO_4 to K_2SO_4-$CaSO_4$, at this time with less Fe vanadate particles present, anyhow now with FeXOY needles present in the sulphate-rich matrix [Montgomery et al., 2008].

The morphology of the fireside corrosion was similar for both the Esshete 1250 and the TP347H FG. The fireside oxide after the first year consisted of an inner Cr-rich oxide, covered by an Fe_XO_Y-layer. Investigation of the oxide layer after 2 years of exposure showed that adjacent to the oxide a matrix rich in K_2SO_4 and $CaSO_4$ was present. Needle-like precipitates of Fe_XO_Y was observed in the deposit matrix. Some precipitates of Fe-vanadates were observed close to the oxide surface, however not so many as after the 1st year [Jensen et al., 2005; Montgomery et al., 2008]. In the third year, similar types of deposit were observed as for the 2nd year. However, in addition to this, there were a few areas with grain boundary attack within the metal. Analysis of these grain boundaries revealed the presence of S, both for Esshete 1250 and TP347H FG. An increase in the [S] within the oxide at the oxide-metal interface was observed, from < 1 %(w/w) in the 1st year, to 8 %(w/w) in the 2nd year, and as high as 12 %(w/w) after the 3rd year, which could be responsible for the sulfur grain boundary attack, observed [Jensen et al., 2005; Montgomery et al., 2008].

Potassium chloride (KCl) in the gas phase was measured using an IACM-system (In-situ Alkali Continuous Monitoring system), based on differential optic absorbance spectroscopy. The data from the probe revealed that co-firing of wood pellets and gas caused higher KCl emissions, while the addition of oil removes KCl and shifts the K-chemistry toward formation of K2SO4. The ratio of oil-to-wood is very important, in order to keep the alkali chemistry in the boiler in balance. Therefore it was decided that wood pellets will only be used with at least 10 % heavy fuel oil containing 2 %(w/w) S. Introduction of heavy fuel oil introduced V, which may affect the SO_2/SO_3 oxidation chemistry, and thereby affect the stability of sulfates in the system, thereby causing the potential of hot temperature corrosion. In order to minimize this potential, coal fly ash, rich in Al-silicates was used as an additive to the AVV2 boiler for a period of 3 months. A probe developed by Vattenfall, where the temperature varies along the probe, allowing test of different alloys at different

temperatures in a single probe, was applied to test corrosion in the boiler under these operational conditions.

The alloys tested were: TP347H FG, Esshete 1250, X20CrMoV121 and 10CrMo910, at temperatures in the range 510 – 620 °C. The alloy showing the lowest corrosion rates is TP347H FG, where the corrosion rates show very little increase over a 100 °C metal temperature increase. Compared to this Esshete 1250, had a much higher corrosion rate, although this does not increase drastically with temperature either [Jensen et al., 2005; Montgomery et al., 2008]. X20CrMoV121 which has 12 % Cr showed a corrosion rate comparable to Esshete 1250, at lower temperatures (< 560 °C), but had a much higher corrosion rate at the higher temperatures. 10CrMo910 had a higher corrosion rate than X20CrMoV121 and TP347H FG at the lower temperatures [Montgomery et al., 2008].

Concerning the experiences from AVV 2, with respect to corrosion, the correct combination of heavy fuel oil and wood pellets removes KCl from the deposit, which is to prefer compared to the high-KCl highly corrosive deposits formed in straw-fired boilers. Anyhow, the presence of vanadate and K_2SO_4 may also lead to corrosion, since vanadate and K_2O forms low-melting eutectics, which may cause type 1 corrosion [Montgomery et al., 2008]. Iron oxide may react with sulphate to form ferric sulfates. This can result in a eutectic with K_2SO_4 and lead to type 2 corrosion.

The TP347H FG steel gave best corrosion resistance indicating that a Cr-rich oxide is required to act as barrier against S-penetration. In general, it is the higher Cr-alloyed elements than can better withstand sulfidation and sulfation which are the two dominant corrosion mechanisms. However, if the temperature is too high, NiS_X forms a liquid phase eutectic Ni-Ni_3S_2, which can destroy the protective Cr-oxide layer [Jensen et al., 2005; Montgomery et al., 2008].

7. Summary on Corrosion in Biomass-(Co-)Fired Plants

A serious amount of work has been conducted in order to address problems in relation to corrosion in systems fired fully or partly (i.e. co-fired) with straw, both in the laboratory, under rather well-controlled conditions, but also in full-scale boilers, applying either cooled deposition/corrosion probes or cutting out sections of real tubes or test sections of superheaters.

[Nielsen et al., 1999] showed in a lab-scale study that metal samples covered by KCl-crystals, and exposed, isothermally, at 550 °C, to an SO_2-laden gas, after 1 month had a thin layer (5 – 20 µm) of K_2SO_4 with iron threads included, formed close to the oxide scale. This layer resembled the structure of the inner layer found in mature deposits from the Masnedø CHP-boiler. For samples having been exposed only 1 week in the oven, the formation of the characteristic K_2SO_4-layer had barely started, and at this point, small KCl-inclusions were still present in the layer [Nielsen, 1998].

The following mechanism for the formation of a K_2SO_4-layer in the inner deposit was proposed by [Nielsen, 1998]:

1. Initially, KCl deposits on the superheater surface, e.g. by inverse sublimation of gaseous KCl, $KCl(g) \rightarrow KCl(s)$. The evidence of such a layer has been reported e.g. at the Maribo-Sakskøbing straw-fired CHP-boiler.

2. KCl reacts with Fe_xO_y, $FeCl_2$, or K_2SO_4, to form a molten phase. This reaction is likely to happen as KCl forms eutectic mixtures with $FeCl_2$ (at 355 °C), with K_2SO_4 (at 690 °C), and possibly also with Fe_xO_y, even though the latter has not been verified.

3. The molten KCl reacts with gaseous SO_3, and forms K_2SO_4. Gaseous SO_3 may be present, since Fe_xO_y is known for catalysing the oxidation of SO_2 to SO_3 [Harlow, 1944, 1949; Reid, 1971].

Potassium chloride, KCl, forms a melt with K_2SO_4, and different iron components (Fe_XO_Y, $FeCl_2$), adjacent to the oxide scale. The sulfation reaction occurs rapidly in the melt, releasing HCl, or Cl_2, close to the metal surface. The chlorine gas has the ability to diffuse through the oxide scale and reacts with Fe to form volatile iron chlorides ($FeCl_2$, $FeCl_3$). The iron chlorides are thermodynamically stable at the interface between metal and metal oxide where a very low partial pressure of oxygen exist. They then diffuse out through the scale, and oxidize as they reach areas with higher partial pressures of oxygen. Thus, iron oxides will be formed either on top of the metal oxide layer or in the dense mixed layer.

By this mechanism, optimal conditions for the sulfation of KCl are present, close to the Fe-rich oxide scale, which may increase the rate of SO_3-formation catalytically. The hypothesis is consistent with the compact structure of the K_2SO_4-layer, as compared to the porous KCl-layer located just on top of it. It is also consistent with the presence of Fe-oxides in the K_2SO_4-layer: The iron oxide threads reach to the very outer edge of the K_2SO_4-layer, while no iron oxide threads are seen, traversing through the KCl, at any point in the mature deposits. This strongly indicates that the K_2SO_4-formation is related to the presence of, and close contact with, Fe_xO_y.

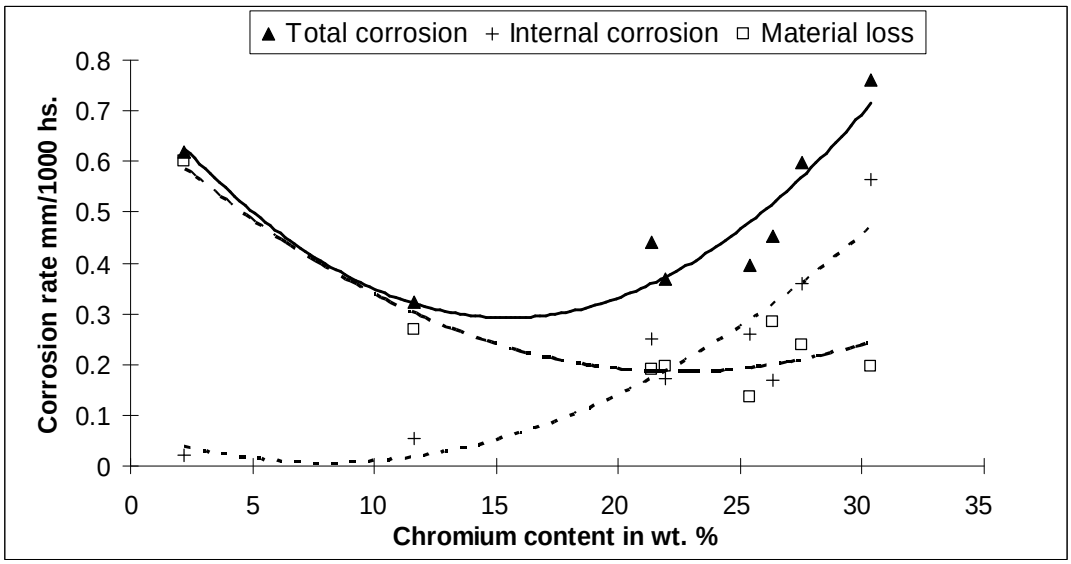

Figure 15: Corrosion rate with various chromium contents in the alloys at approx. 580°C. Source: [Montgomery and Larsen, 2002].

This mechanism can explain the shift in corrosion behaviour with temperature which has been observed in full-scale corrosion tests [Larsen & Henriksen, 1996].

The natural question arising is;

what parameters are important/controlling for the corrosion ?

Among the more obvious answers to that question is; the choice of material will influence the corrosion, the metal surface temperature will also affect the corrosion, and, last, but certainly not least, the chemistry of the deposit will affect the corrosion. The latter is being addressed at present in the actual PSO-5820 R&D-project on Cl-Induced Corrosion in Biomass-Fired boilers.

7.1. Effect of Alloy Composition (Cr-Content)

In conventional coal-firing, alloys with high Cr-content causes lower corrosion rates, however the contrary is the case for straw-firing plants. Results from three separate investigations at straw-fired plants [Larsen and Henriksen, 1996; Henriksen et al., 1995; Montgomery et al., 2000a] testing a variety of steels, revealed that at high temperatures, high-Cr steels were rapidly attacked. Figure 15 shows data on total corrosion rate, as a function of the Cr-content in the metal, for a range of alloys from a 2½% Cr, to a 30% Cr steel [Montgomery et al., 2000a]. The low-Cr steels exhibit a high material loss whereas the high-Cr steels are characterised by severe internal attack, in the form of chromium depletion. These results indicate a minimum the in total corrosion rate of steels, at an intermediate Cr-content of 12-18% Cr [Montgomery and Karlsson, 1999].

7.2. Effect of Metal Surface Temperature

Selective removal of Cr and Fe from an alloy, causes a porous metal structure, and often also grain boundary attack. For austenitic steels, grain-boundary corrosion is a precursor to corrosion within the grains. The corrosion products formed are Cr oxide [Cr_2O_3] and Fe oxides [Fe_2O_3, Fe_3O_4]; being present at the surface of the specimen. In many cases, Ni is also present in the outer corrosion product, as non-reacted nickel.

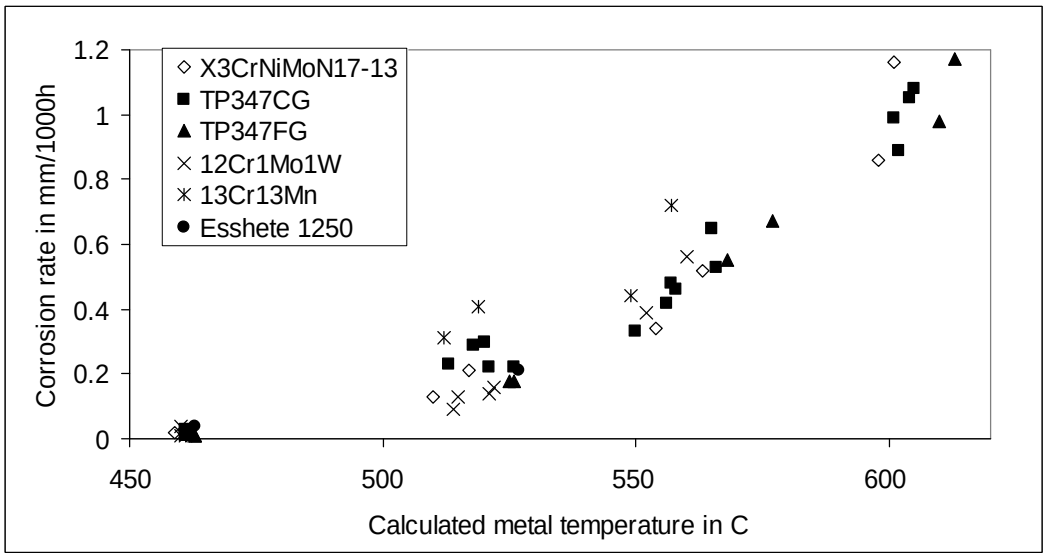

Figure 16: Corrosion rate of specimens in one investigation at the Masnedø straw-fired CHP-plant relating metal temperature to corrosion rate. Source: [Montgomery and Larsen, 2002a,b].

In Figure 16, the corrosion rate of 12-18% Cr steels is plotted against temperature [Montgomery et al., 2002a,b]. It is clearly visible that the rate of corrosion is increasing with increasing temperature of the metal surface.

For the austenitic alloys investigated, a gradual change in the corrosion morphology, as a function of temperature was observed. Corrosion rates were modest at 460°C, where a protective Cr-rich Fe oxide scale was formed. With increasing temperatures of up to 525°C, the corrosion rates become more linear with respect to temperature. At around 500-520°C, both grain boundary attack and protective oxide scales has been observed for the same specimen. Above this temperature, Cr-depletion and grain boundary attack are always observed [Montgomery et al., 2002a,b].

7.3. Why Corrosion Rates are Lower in Co-Fired Systems

Co-firing of coal and straw, in a suspension-fired boiler, at straw shares of 10-20 % on a thermal base, removes the danger of catastrophic Cl-induced corrosion, as was observed at

MKS1. The corrosion rates observed in co-firing systems are much lower than those having been observed in straw-fired units, and are closer to the corrosion rates observed in coal-fired power plants. For comparative purposes, the corrosion rates for TP347H FG have been plottet in an Arrhenius-type plot, see Figure 17, assuming a parabolic corrosion kinetics [Montgomery and Larsen, 2002]:

$$x^2 = 2 \cdot k_p \cdot t$$

where x is the thickness of the corroded material, and, t is the duration of time of exposure.

Parabolic kinetics is assumed for all three types of corrosion, although it is apparent from previous work that linear kinetics is more applicable for corrosion in 100 % straw-fired boilers at high temperatures [Montgomery and Karlsson, 1999]. It is clear from Figure 17, that the corrosion is significantly lower in co-fired plants as when compared to 'pure' straw-firing.

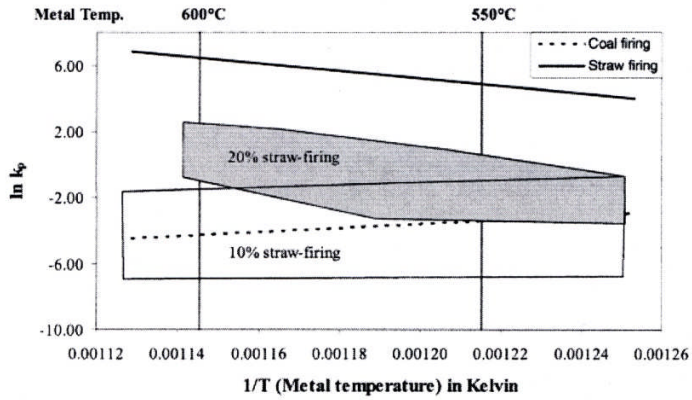

Figure 17: Arrhenius plot showing that corrosion of TP347H FG in co-firing compared to pure coal- respec-tively straw-firing. Source: [Montgomery and Larsen, 2002].

The most important outcome of the MKS1 corrosion investigation was that there was no sign of chlorine found in the deposits, within the corrosion products, or, at the metal-oxide scale interface. This shows that KCl released from the straw, reacts with Al and Si in the coal ash, forming non-corrosive K-Al silicates and HCl in the gas phase [Andersen, 1998]:

$$2\,KCl + Al_2O_3 + 6\,SiO_2 + H_2O \rightarrow K_2O \cdot Al_2O_3 \cdot 6\,SiO_2 + 2\,HCl \qquad (6)$$

$$2\,KCl + SO_2 + H_2O + ½\,O_2 \rightarrow K_2SO_4 + 2\,HCl \qquad (2)$$

Formation of HCl gas does not pose nearly as great a corrosive potential as deposition of KCl, followed by subsequent sulfation at the metal-oxide scale surface. An increase in the straw

fraction fired from 10 % to 20 % on a thermal base, caused a higher local concentration of KCl in the combustion chamber which is converted to more K_2SO_4 (eqn. (2), above), causing the HCl emissions from the stack to increase [Wieck-Hansen et al., 2000].

At SSV4, for both X20CrMoV121 and TP347H FG samples in superheater 3 (steam temperature 465 °C), double-layered oxides were formed where the inner oxide layer was rich in Cr, while the outer oxide layer was an iron oxide, with fly ash particles embedded in it. As to be expected, the oxide on X20CrMoV121 was thicker. For all exposure times, minor amounts of S were detected in the inner oxide indicating the presence of sulfides or sulfates. Sulfur was also detected at the corrosion front; a slight internal attack was observed for TP347H FG. In superheater 4, where only X20CrMoV121 was tested, all investigated samples reveled an inner oxide rich in Cr, and an outer oxide rich in Fe, and with fly ash particles embedded in it. Significant internal corrosion attack in the form of sulfidation was observed at grain boundaries to a depth of 40 μm already after 7231 hours of exposure. The depth of the internal corrosion attack remained constant over time, while the Cr-rich inner oxide layer grew in thickness. SEM/EDX spot analyses on samples exposed for 17719 hours revealed [S] ∈ [35; 45 %(w/w)] [Frandsen et al., 2006; Montgomery et al., 2008]

The intensive corrosion investigations conducted co-fired plants, show that the corrosion caused by co-firing of 10 % straw is low in general, and that it is not, or only slightly, increased compared to coal-firing;

- <u>When co-firing of 10 % straw</u>, the corrosion seems to be parabolic, and the corrosion rate for 10CrMo910 are at the same low level, as normally observed in coal-fired plants, i.e. up to 2 mm/100.000 hours of operation, at normal steam temperatures. The corrosion rate was decreasing at higher alloyed metals [Wieck-Hansen et al., 2000].
- <u>By co-firing 20 % straw</u>, the corrosion rate increased by a factor 2-3, at moderate metal temperatures. This corrosion rate is equal to the upper corrosion limit for low-corrosive coals. At elevated metal temperatures and especially at simultaneously higher flue gas temperature, a significant increase in the corrosion rate was observed, corresponding to the level of medium-corrosive coals.

The corrosion may, though, be dependent on the coal type. Especially, coal types with a considerable content of water soluble alkali, may provide a higher risk of increased

corrosion rates than observed in the tests at MKS1. Based on the corrosion studies carried out at MKS1 and SSV4, it was concluded that there are no corrosion problems related to Cl, when co-firing 10 % straw (thermal base), in a recent boiler, with a standard steam temperature of 540 °C. Furthermore, the results do not show any considerable corrosion risks caused by introduction of co-firing of 10 % straw at plants with elevated steam temperatures – up to 580 °C. Anyhow, the data from SSV4 indicated that over longer exposure times at elevated temperatures, there is a significant risk of corrosion caused by the presence of S (i.e. sulfidation or sulfation) to occur [Frandsen et al., 2006; Montgomery et al., 2008].

7.4. Remedial Measures to Minimize Corrosion

Remedial measures involve reducing the temperature of the flue gas before the entry into the final superheater, and assuring turbulent conditions in the gas stream, in order to maximize the sulfation reaction of the alkali chlorides in the gas stream, before contacting the hot tube surfaces. When these changes cannot be accomplished through modification to the operation of the boiler, design changes are required, such as installing a sufficiently large evaporator section before the final superheater [Wright and Krause, 1996].

In case it is not possible to install new heating surface to act as screen tubes for the existing finale superheater, it may be possible in some boilers to reroute the steam/water flow in the superheater section so that the coolest tubes contact the hottest gas. An example of this principle was the conversion of the original final superheater into an evaporator section, and to subdivide the original primary superheater to become the final superheater, as well as the primary superheater, in a German combustor [Schirmer, 1984]. This change resulted in a reduction in flue gas temperature from 760 to 600 °C as it passed through the new evaporator, compared to 760 to 675 ° when the evaporator was connected as the final superheater. The tube wall temperature of the new evaporator was 270 to 275 °C, compared to 300 to 435 °C as the final superheater; the new final superheater had a wall temperature of 325 to 435 °C while the flue gas temperature at this location was 450 to 600 °C [Wright and Krause, 1996].

Another approach is to install tubes of corrosion-resistant alloy in those locations prone to attack. A number of boilers in the U.S. have several rows of superheater tubing made from Alloy 825. Corrosion in the convection zone may be aggravated by erosion from soot blowing, particularly when steam is the cleaning medium [Wright and Krause, 1996]. Sootblowing is thought to remove the exixting scale/deposit, thus stripping the tube of a potential barrier to the corrosive reaction and exposing fresh metal to attack at higher rate. Tubes adjacent to soot blower lanes have been protected by shields, as in coal-fired utility boilers. Half shields, which cover only one face of the tube, have been used as well as full shields which completely encase the tubes. In many cases, these shields have been made from Type 309 stainless steel, but trials have been made with other alloys as well, including Alloy 625 and 825 [Wright and Krause, 1996].

In summary, the remedial measures credited with reducing corrosion of the superheater and other convection pass tubes in WtE boilers, include those that [Wright and Krause, 1996];

- Minimize particle carry over from the combustion zone;
- Reduce the temperature of the flue gas entering the convection tube banks to a maximum of 760 °C. If this cannot be achieved because of furnace size limitations, the use of several rows of screen tubes (evaporator tubes) ahead of the superheater may be effective;
- Reduce the metal/steam temperature of the leading tubes in the first rows that contact the flue gas;
- Protect the first 2 – 4 rows of the final superheater, using devices such as metallic shields or ceramic protective tubes, although these require extensive maintenance to maintain attachment and alignment;
- Replace upstream rows of superheater tubes with a more resistant alloy, such as Alloy 825;
- Protect areas where directional changes in the flue gas flow occur, usually by shields or refractory coverings;
- Protect tubes adjacent to soot blower lanes predominately using shields;
- Replace soot blowers with mechanical rappers or sonic horns.

8. Experimental Set-Up Applied in FORSKEL-5820

The experimental set-up applied for the lab-scale corrosion investigation in this project, consists of the following components, see Figure 18 [van Lith et al., 2009]:

- A gas mixing panel, where gases such as N_2, O_2, CO_2, HCl, and SO_2 can be mixed. The mixture of N_2, O_2, and CO_2 can be led through a water column (which is kept at room temperature) to saturate the gas mixture with H_2O before mixing it with the gas mixture of HCl and SO_2. The tube leading the mixed gas to the reactors is heated to 140 °C to prevent condensation.
- An electrically-heated horizontal tube furnace, containing five horizontal quartz tube reactors.
- A gas cleaning system, consisting of a scrubber containing 1M NaOH and a drying column containing silica gel behind each reactor, to remove the acid gases (HCl and SO_2) and water from the exit gas.
- A ball flow meter behind each reactor and cleaning system, to regulate the gas flow in each reactor.

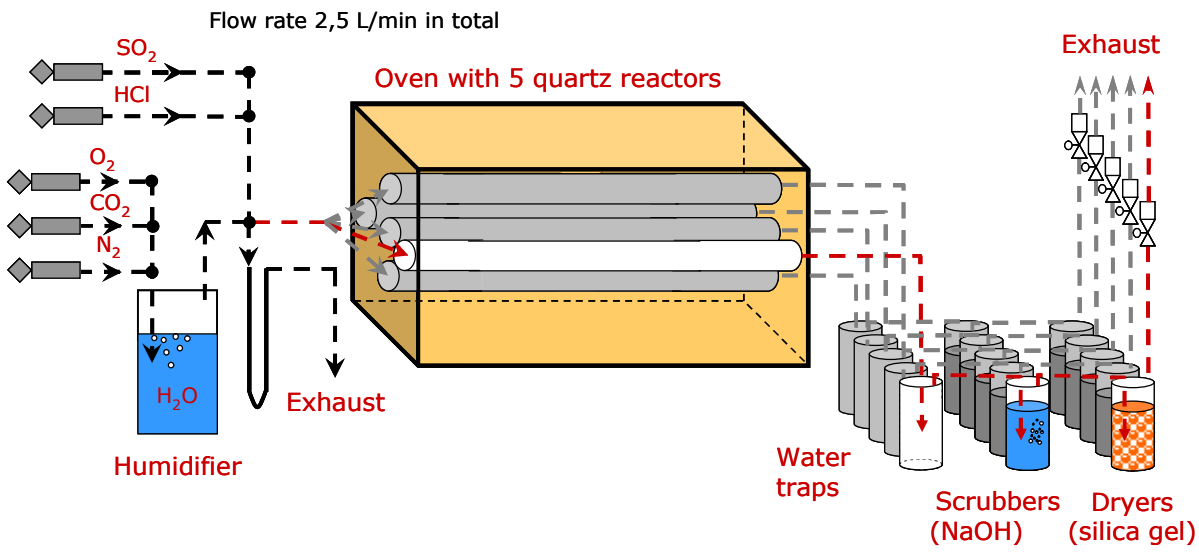

Figure 18: Experimental set-up to investigate the corrosion of superheater tubes under well-controlled conditions.

This set-up was based on the experimental set-up used in the Ph.D. project of Hanne Philbert Nielsen at the CHEC Research Centre during 1996 [Nielsen, 1998]. The difference is that in the current set-up, five quartz reactors are placed in parallel in a single horizontal tube furnace, so that the exposure tests can be performed in a more efficient way.

8.1. Metal Specimens

Metal test elements were cut out of unexposed superheater tube material TP 347H FG (composition given in Table 7), resulting in arc-shaped specimens. The geometry of the specimens and the approximate dimensions are presented in Figure 19.

C	Si	Mn	P	S	Cr	Ni	Nb + Ta	Fe
0.06-0.10	<0.75	<2.00	<0.040	0.0030	17.0-20.0	9.00-13.00	0.481.0	bal.

Table 7: Composition of TP 347H FG (wt %)

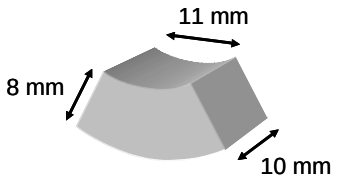

Figure 19: Approximate specimen geometry and dimensions.

8.2. Deposits

Synthetic deposits were used, consisting of a simple salt (KCl), or, a mixture of a simple salt (KCl) and a simple oxide (SiO_2 or CaO). The salt and the oxides were in powder form. KCl was obtained from Fluka (purum p.a., ≥99.0%). A SEM-investigation of the KCl revealed

that the particle size was approximately 300 μm. For one experiment, a size fraction of 32-50 μm was used, which was obtained by crushing the original KCl in a mortar, and sieving it. SiO_2 was used in three different size ranges. Size ranges of 14-50 μm, and, 50-90 μm, were obtained by sieving Fluka Quartz BCR certified reference material, which originally had a particle size range of 14-90 μm. A 0.5-10 μm fraction was obtained from Sigma-Aldrich (naturally occurring microcrystalline silica, which has been finely ground). Approximately 80% of this powder is between 1 and 5 μm. CaO obtained from Merck, as small lumps from marble, was crushed in a mortar, and sieved to a size range of 32-50 μm. To ensure that the deposits had the desired concentration of salt, each mixture was prepared separately. On average, the amount of deposit on each test element was about 0.110 g.

8.3. Procedure

The synthetic deposits were placed (as uniform layers) on top of the metal test elements (on the inner arc), after which these were placed onto alumina sledges, and, inserted into the quartz reactors in the horizontal tube furnace. Some metal specimens without deposit were placed in the oven as well, as reference materials.

During the tests, the furnace was kept at a constant temperature, and a constant gas flow rate was applied. The temperature was chosen to resemble the metal temperatures in current and projected straw-fired boilers: 560 °C is the superheater metal temperature of the Maribo Sakskøbing straw-fired boiler, and, the expected superheater metal temperature of the straw-fired boiler at Fyn Power Station Unit 8 (scheduled for commissioning in 2009). A superheater metal temperature of 560 °C generally corresponds to a steam temperature of 540 °C. The tests were assumed to be isothermal, that is, the metal temperature was assumed to be the same as the gas temperature. The metal test elements were not oxidized prior to exposure. The samples were exposed to a synthetic flue gas, simulating the flue gas during straw-firing, or, co-firing of coal and straw. The gases N_2, H_2O, O_2, CO_2, HCl, and SO_2 were mixed, in order to simulate the desired flue gas composition. The tests are similar to the tests performed by [Nielsen et al., 1999] except that they performed the tests at 550 °C, and exposed the samples between 1 week and 1, 2, 3, and 5 months, in order to obtain corrosion rate laws [van Lith et al., 2009].

After exposure, the samples were removed from the reactor, and, subsequently cooled to room temperature and mounted in epoxy under vacuum. After this, the embedded samples were cut through the middle (lengthwise) with a hacksaw (without using lubricants), and

remounted in epoxy. Then, the cut surface was ground, and polished, using water-free lubricants (sunflower oil and ultra pure ethanol), in order to ensure that water-soluble compounds such as chlorides, at the metal surface, remained in the sample. After that, the thickness, chemistry, and morphology of the corrosion products, and the reacted deposit were studied in a scanning electron microscope (SEM), equipped with an energy-dispersive X-ray (EDX) detector. For the measurement of the selective corrosion, the metal-(inner-) oxide interface was taken as zero level. The grain boundary attack was measured under the selective corrosion (if present).

flue gas composition	straw-firing					**straw-firing, no HCl**	**cofiring**	**cofiring, low SO_2**
KCl particle size (µm)	~300			32-50	~300	~300		
deposit oxide	SiO_2				CaO	SiO_2		
deposit oxide particle size (µm)	14-50	0.5-10	50-90	14-50	32-50	14-50		
experiment No.	1	2	3	4	5	6	7	8

Table 8: Experimental Conditions for the Corrosion Tests

8.4. Experimental Matrix

Table 8 gives an overview of the 3-day exposure tests performed at 560 °C. The experimental matrix was designed, in order to systematically investigate, the effect of different parameters on sulfation and corrosion behavior.

The gases N_2, H_2O, O_2, CO_2, HCl, and SO_2 were mixed in the concentrations given in Table 9. The composition called "straw-firing" corresponds to the measured flue gas composition in a Danish grate-fired boiler firing 100% wheat straw [Nielsen et al., 1999] whereas the composition called "co-firing" corresponds to the (in situ) measured flue gas composition in a Danish PF-fired boiler (Studstrup Power Station), co-firing coal and wheat straw (10% wheat straw on an energy basis) [Hansen, 1977; Hansen et al., 1998]. Besides

the comparison between the straw-firing gas composition (experiments 1-5) and the cofiring gas composition (experiment 7), also the effects of leaving out HCl from the flue gas in the straw-firing case (experiment 6), and using a lower SO_2 concentration for the cofiring case (experiment 8), were investigated.

The synthetic deposits consisted of pure KCl, or a mixture of KCl (25 wt %) and SiO_2 (75 wt %). KCl is a major constituent of deposits formed in straw-fired boilers, and presumably also in co-fired boilers with a high biomass percent, and its presence in deposits is believed to play a major role in the corrosion observed in biomass-fired boilers [Nielsen et al., 1999]. SiO_2 is also a common constituent in deposits formed in biomass-fired and co-fired boilers, but it was used here, mainly to dilute the KCl concentration in the deposit, as it was expected to be inert during exposure at 560 °C. For the KCl-SiO_2 mixture, the value of 25 wt % of KCl was chosen, because preliminary results had indicated that little or no chlorine-induced corrosion could be observed when exposing specimens covered with mixtures containing lower amounts of KCl (≤15 wt %) for 1 week, to the straw-firing gas composition, at 560 °C [van Lith et al., 2009].

	O_2	CO_2	SO_2	HCl	N_2	H_2O
	% (v/v) dry	% (v/v) dry	ppmv dry	ppmv dry	% (v/v) dry	% (v/v)
straw-firing	6	12	60	400	82	2–3
straw-firing, no HCl	6	12	60	0	82	2–3
cofiring	6	13	500	75	81	2–3
cofiring, low SO_2	6	13	200	75	81	2–3

Table 9: Gas Compositions

As mentioned previously, the effect of SiO_2-particle size on the sulfation behavior was studied by using three different particle size ranges (14-50 μm (experiment 1), 0.5-10 μm (experiment 2), and 50-90 μm (experiment 3)) for SiO_2 in the 25 wt % KCl deposits, exposed to the straw-firing gas composition.

The effect of KCl particle size on the sulfation behavior and corrosion attack was investigated by using a smaller size fraction (32-50 μm) in experiment 4 (for both the 100% KCl and the 25 wt % KCl deposits).

In experiment 5, CaO was used, instead of SiO_2, in the 25 wt % KCl deposit, in order to investigate the effect of deposit oxide composition. CaO was chosen, because Ca is also commonly found as a major element in deposits formed in boilers firing straw or other types of biomass.

9. PSO-5820: Cl-Induced High Temperature Corrosion

9.1. Effect of KCl Concentration in the Deposits

In the first experiment, specimens covered with 100% KCl, a mixture of 25 wt % KCl - 75 wt % SiO_2 (particle size 14-50 μm), and specimens without deposit were exposed to the straw-firing gas composition, at 560 °C, for 3 days. SEM micrographs of selected areas of the cross sections of the 100% KCl and 25 wt % KCl samples, as well as a comparison of the results of the internal attack, oxide thickness, and mixed layer thickness measurements for the 100% KCl sample and the 25 wt % KCl sample after exposure, are presented in Figure 20 [van Lith et al., 2009].

The sample covered with 100% KCl, showed a rather uniform corrosion attack: a band of selective corrosion of ~5 μm thickness, followed by a ~10 μm thick oxide scale, and, a ~30 μm thick mixed layer (see Figure 20a). The fact that small amounts of Cl (~1-4 wt %) were detected at the corrosion front, and a Ni-rich skeleton was left behind, suggests that the Cr and Fe were removed by selective Cl-corrosion. Similar findings of severe selective corrosion, where Cr, and, to a lesser extent, Fe were removed from the alloy, leaving a degraded metal phase enriched in Ni, have been reported for corrosion probes with metal temperatures exceeding 500 °C, exposed in a straw-fired boiler [Larsen et al., 1996; Michelsen et al., 1998]. Montgomery and co-workers [Montgomery and Karlsson, 1999; Montgomery et al., 2002a,b] also observed selective corrosion of Cr for austenitic steels exposed as probes (metal temperatures of 525 and 613 °C), and, in a test superheater (metal temperatures in the range of 450-620 °C) in a straw-fired boiler (Masnedø CHP).

The oxide scale was detached from the metal surface, during cooling of the sample. The mixed layer on top of the oxide scale consisted of iron oxide threads in a layer of K_2SO_4, and had a molten appearance. Locally, some Cl was detected in the mixed layer. The corrosion morphology was very similar to the findings of [Nielsen et al., 1999] for test elements covered with a KCl deposit, and exposed to a straw-firing gas composition, at 550 °C. Furthermore, the mixed layer is similar in morphology and chemistry, to the mixed layer observed on superheater tubes with a steam temperature of 520 °C, at the Masnedø straw-fired boiler, and on test tubes of various ferritic steels and TP 347H (metal temperatures of 490 °C), exposed at the Ensted straw-fired boiler [Montgomery, 2002b].

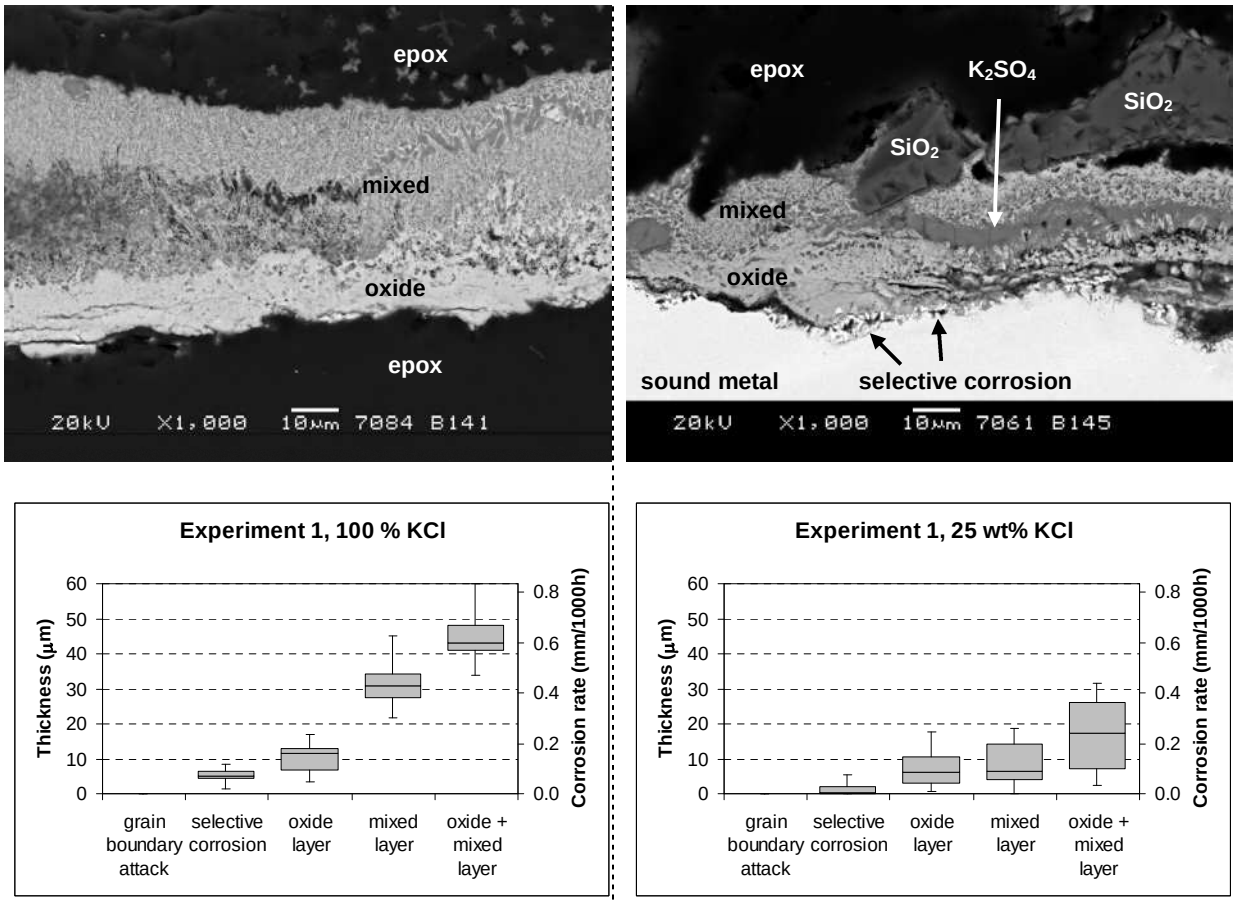

a) 100% KCl b) 25 wt % KCl

Figure 20: Effect of percentage of KCl in the deposit on corrosion attack, for specimens initially covered with 100% KCl (a) and 25 wt % KCl~ 75 wt % SiO_2 (b), exposed to the straw-firing gas composition at 560 °C (1040 °F), for 3 days. SEM micrograph in panel a shows only the spalled oxide and mixed layer. Indicated in the graphs are the first and third quartile (the lower and upper lines of the gray boxes), the median value (the lines inside the gray boxes), and the minimum and maximum values (the ends of the vertical lines), based on 2~040 measurements. The corrosion rates were calculated assuming linear corrosion kinetics.

[Nielsen et al., 1999] argue that the mixed layer of iron oxide threads in K_2SO_4 observed in the lab-scale exposure tests may be due to the formation of a melt containing KCl, K_2SO_4, Fe_xO_y, and possibly $FeCl_2$. When KCl is present in the molten phase, it readily sulfates to form more K_2SO_4, at the same time releasing gaseous chlorine. The composition of the melt

thus changes continuously, until, at some point, solid K_2SO_4 and Fe_xO_y become the thermodynamic stable species and precipitate out, forming a solid phase with a pin-striped eutectic structure. The same mechanism may apply for the formation of the mixed layer observed in the Masnedø straw-fired boiler [Hansen et al., 2000] and for the mixed layer observed in our lab-scale study.

For the sample covered by 25 wt % KCl - 75 wt % SiO_2, a much thinner mixed layer (~9 μm on average) of iron threads in K_2SO_4 was found on top of the oxide scale. The reason for this could be the lower amount of KCl in the sample (providing a lower amount of melt), and/or the presence of the SiO_2-particles (as will be discussed later). At some locations in the sample, a thin layer (<8 μm) of pure K_2SO_4 was present between the oxide and the mixed layer (see SEM micrograph of Figure 20b). In general, a rather thin oxide scale (~8 μm on average) was formed, which is comparable to the sample with a 100% KCl deposit (see Figure 20). In contrast to the sample with a 100% KCl deposit, selective Cl-corrosion occurred only locally, and the maximum depth was 5 μm. Only traces of Cl (<1 wt %) were found at the corrosion front [van Lith et al., 2009].

The reference sample (without deposit), showed a thin (<5 μm) and rather discontinuous oxide scale, consisting of Fe and Cr oxides. At a few places, minor internal attack was observed (<3 μm). Traces of S (<2 wt %), and Cl (<1 wt %), were found at the corrosion front.

SEM-EDX investigations of the synthetic deposits after exposure, showed partial sulfation of the KCl particles, for both the test element initially covered with 100% KCl and that covered with 25 wt % KCl - 75 wt % SiO_2. In the case of the 100% KCl deposit, the sulfation product was mainly visible as rims of dense K_2SO_4, around the KCl-particles in the outermost layer of the deposit (top and sides), and, as small K_2SO_4 crystallite grains (<5 μm) around the KCl particles in the middle of the deposit. In the 25 wt % KCl case, the K_2SO_4 crystallite grains were attached to the surface of the SiO_2-particles. This result combined with the thinner mixed layer observed, suggests that K_2SO_4 produced by the sulfation of KCl is present on to the SiO_2-particles, so that less K_2SO_4 is formed on the oxide or mixed layer [van Lith et al., 2009].

ICP-OES analyses of the deposits showed that, for experiment 1, the degree of sulfation is much higher (about 10 times) in the 25 wt % KCl deposit compared to the 100% KCl deposit. The same trend was observed for all other experiments, as can be seen in Figure 21. A higher SO_2/KCl molar ratio in the 25 wt % KCl deposits could explain the higher degree of sulfation, but not by a factor 10. Other possibilities could be that the SO_2 is captured in

between the SiO_2 particles, thereby increasing the possibility for reaction between KCl and SO_2, or that the presence of SiO_2 has a catalyzing effect on the sulfation process.

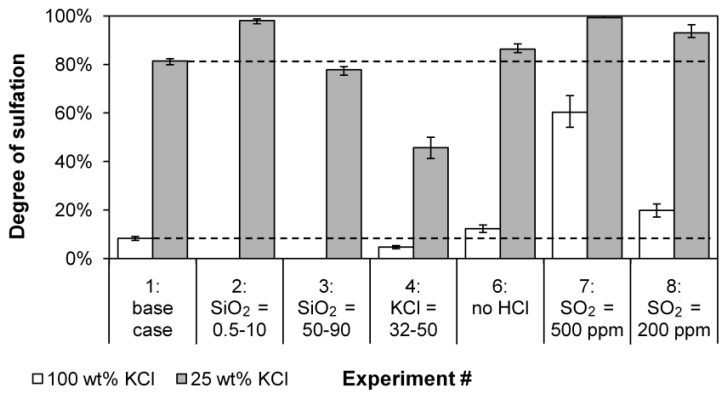

Figure 21: Degree of sulfation in the deposit after exposure, for the different experiments. White bars indicate experiments with an initially 100% KCl deposit, whereas gray bars indicate tests with an initially 25 wt % KCl - 75 wt % SiO_2 deposit. In experiment 1 (the "base case"), the samples were exposed to the straw-firing gas composition (60 ppm SO_2; 400 ppm HCl) at 560 °C, for 3 days, whereby the particle size of KCl was ~300 μm and that of SiO_2 14-50 μm.

[Jørgensen et al., 2007] studied the effects of quartz wool; crushed, nonporous alumina; and chips of steel (type 316) on the oxidation of SO_2 to SO_3 in a fixed-bed quartz reactor, in the temperature range of 750-1050 °C. They found no effect of quartz wool, but little catalytic effect of the alumina particles, and a strong catalytic effect of the steel chips. The sulfation of solid KCl is known to be slow in the presence of SO_2, but orders of magnitudes faster in the presence of SO_3 [Halck, 2008; Gudzinska, 2007; Ozawa et al., 2003]. [Dennis and Hayhurst, 1988] investigated the effect of silica sand bed material (particles of 425-500 μm) on the oxidation of SO_2 in a fluidized bed reactor, made of 321 stainless steel, in the temperature range of 700-950 °C, and measured SO_2 oxidation rates of approximately 100 times faster than expected for gas-phase oxidation. They concluded that the SO_3 was mainly produced on the surface of the quartz sand, and proposed a model in which O_2 and SO_2 competitively chemisorb on the sand, with the rate controlled by SO_2(g) reacting with adsorbed O-atoms. The effect of the stainless steel reactor wall was, however, not thoroughly investigated. It therefore remains unclear if the enhanced sulfation of KCl

observed in our tests with SiO_2 particles can be attributed to a catalytic effect of SiO_2 particle surfaces on the oxidation of SO_2 to SO_3.

Knowing the initial amount of KCl in the deposits, and the degree of sulfation after exposure, the amount of HCl formed according to reaction (1) can be calculated for each sample. It was found that 36% more HCl was formed in the case of the 25 wt % KCl sample compared to the 100% KCl sample. The lower amount of selective corrosion, and thinner oxide and mixed layers, observed in the 25 wt % KCl deposit case may indicate that less HCl reaches the metal surface, than in the case of the 100% KCl deposit. This could be explained by the fact that there are more KCl-particles present close to the metal surface in the case of the 100% KCl deposit, compared to the 25 wt % KCl deposit, causing a higher probability of HCl to reach the metal surface, instead of being removed with the flue gas.

The results of experiment 1 indicate that the presence of a KCl-containing deposit strongly enhances the corrosion attack in a straw-firing atmosphere, in good agreement with the findings of [Nielsen, 1998] and that an increase of the percentage of KCl in the deposit results in a more uniform, and deeper, internal attack, and a thicker oxide scale and mixed layer. The presence of SiO_2 particles may influence the sulfation behavior, and mixed layer thickness, by providing surfaces for K_2SO_4 to stick to, so that less K_2SO_4 is deposited on the oxide scale, and a thinner mixed layer is formed. The corrosion rate is probably more dependent on the amount of KCl-particles close to the metal surface, than on the total amount of HCl formed by sulfation of KCl in the deposit [van Lith et al., 2009].

9.2. Effect of SiO_2-Particle Size

In experiments 1-3, the effect of the size of the SiO_2-particle was investigated for deposits containing 25 wt % KCl. A comparison of the results concerning the oxide thickness and the mixed layer thickness measurements is presented in Figure 22. Minor internal attack (<5 μm) was observed in all three samples.

The sample containing 0.5-10 μm SiO_2 particles (experiment 2), showed a rather different sulfation and corrosion behavior compared to the sample containing 14-50 μm SiO_2 particles (experiment 1), as described above. SEM-EDX analysis showed that most of the K_2SO_4 in the sample was found on the surfaces of the SiO_2 particles closest to the original KCl particles, and only a small amount of K_2SO_4 seemed to have deposited on the oxide scale, as the mixed layer was relatively thin (~4 μm). The thickness of the oxide scale (~7

μm), on the other hand, did not differ that much from the sample with the 14-50 μm SiO_2 particles.

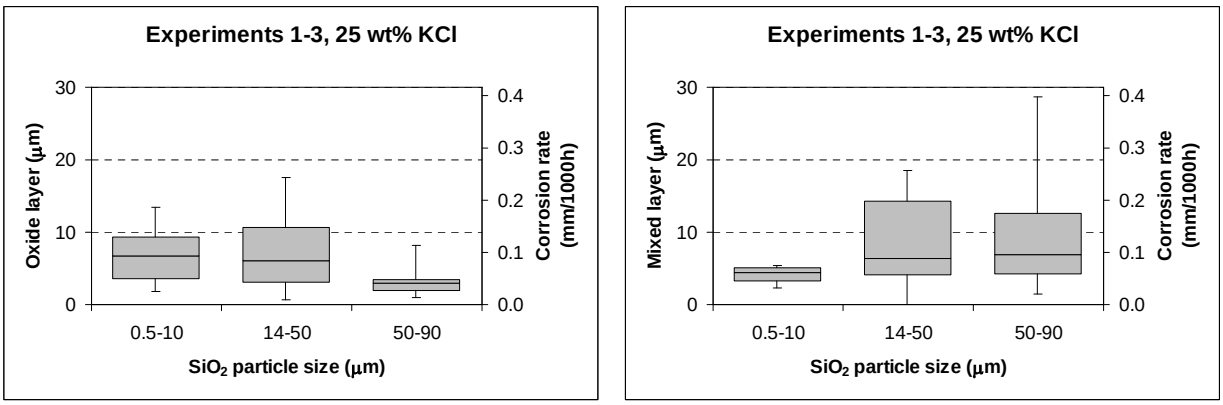

a) Oxide layer thickness b) Mixed layer thickness

Figure 22: Effect of SiO_2 particle size on the thickness of the corrosion products, for specimens covered with a 25 wt % KCl deposit, exposed to the straw-firing gas composition at 560 °C, for 3 days. See Figure 20 for graph explanation.

For the sample with the 50-90 μm SiO_2 particles (experiment 3) it was observed that a relatively small amount of K_2SO_4 was deposited on the SiO_2-particles. The mixed layer was found to be somewhat thicker on average, compared to the 14-50 μm sample, and very thick (up to ~30 μm), at places close to (partly converted) KCl particles. The oxide scale was ~3 μm thick on average, which is considerably thinner than the oxide scale in the 14-50 μm sample (see Figure 22) [van Lith et al., 2009].

The ICP-OES analyses showed that the KCl in the deposit with the smallest SiO_2 particle size range (experiment 2), was almost completely sulfated, whereas the degree of sulfation in the deposits is around 80%, in the deposits with the larger SiO_2 size fractions (experiments 1 and 3) (see Figure 21). This result supports the possible catalytic effect of the SiO_2 surface on the SO_2 oxidation, and thereby on the sulfation reaction.

9.3. Effect of KCl-Particle Size

An experiment similar to experiment 1 (i.e., specimens covered with 100% KCl respectively 25 wt % KCl - 75 wt % SiO_2, exposed to the straw-firing gas composition) was performed, applying a smaller KCl particle size (32-50 μm instead of ~300 μm) (experiment 4), in order to study the effect of KCl particle size, on the sulfation and corrosion behavior [van Lith et al., 2009].

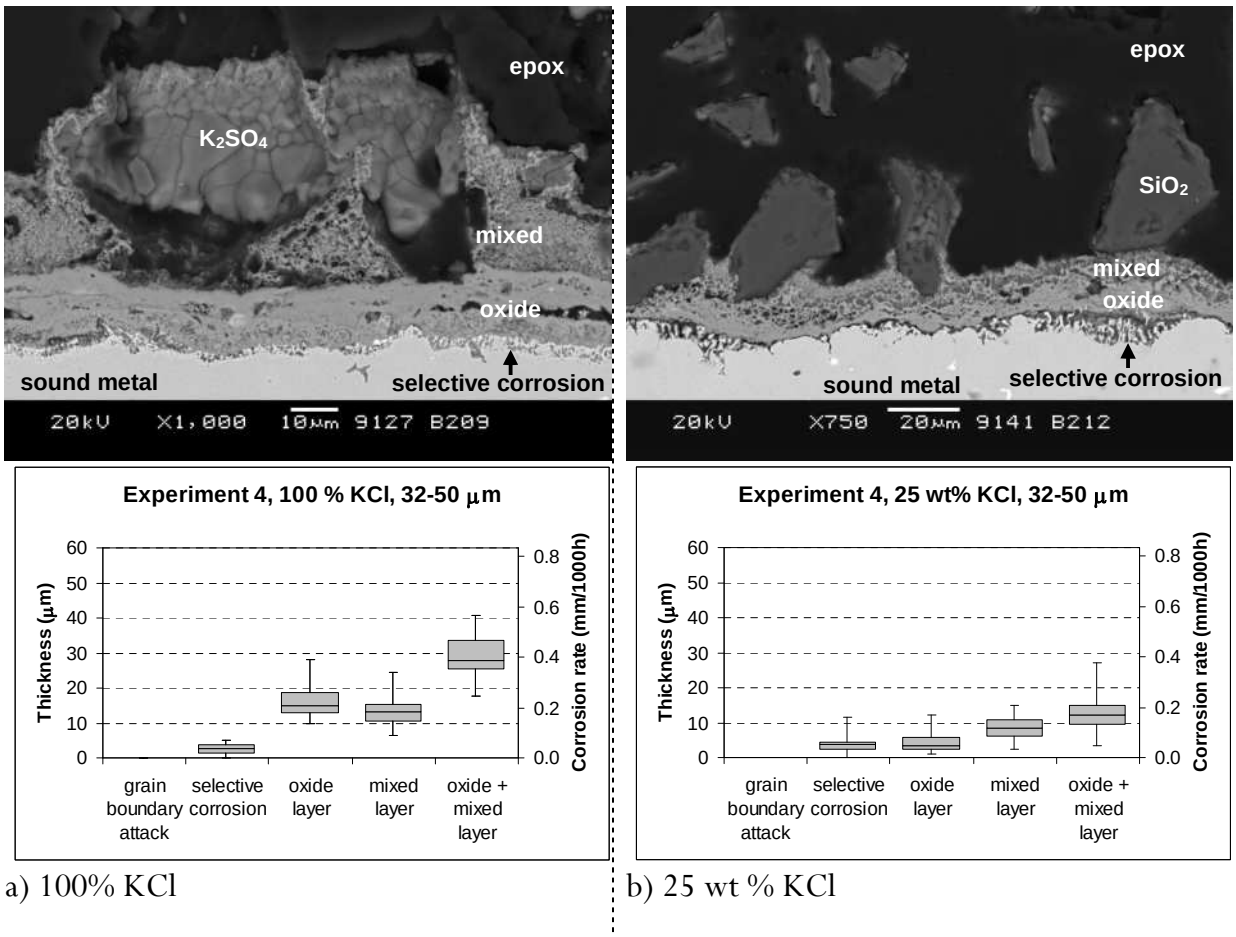

a) 100% KCl b) 25 wt % KCl

Figure 23: Corrosion attack for samples initially containing 100% KCl (a) and 25 wt % KCl - 75 wt % SiO_2 (b) exposed to the straw-firing gas composition at 560 °C, for 3 days, whereby the KCl particle size range was 32-50 μm. Compare with Figure 20 (experiments performed under similar conditions, but using a KCl particle size of ~300 μm) to see the effect of KCl particle size.

For the 100% KCl deposit, the SEM analyses show a relatively uniform corrosion attack (see Figure 23a), consisting of a more-or-less continuous band of selective corrosion (~2 to 5 μm thick), an oxide scale of ~15 μm, and a somewhat thinner mixed layer of iron oxide and K_2SO_4. This uniform corrosion attack was also observed in experiment 1 (see Figure 20a), but the oxide scale is somewhat thicker, and the mixed layer considerably thinner, for the specimens covered with the smaller KCl particles. In both cases, the oxide consists of an inner layer rich in Cr, and an outer layer rich in Fe. The mixed layer looks similar to that of the samples of experiment 1, but no KCl was detected inside this layer [van Lith et al., 2009].

The effect of the KCl particle size on the degree of sulfation in the deposit, can be seen in Figure 21 (experiment 4). For both the 100% KCl and the 25 wt % KCl deposit, it is seen that using a smaller KCl-particle size results in a lower degree of sulfation in the whole deposit. Now, since smaller KCl-particles have a larger specific surface area available for reaction with SO_2, a higher degree of sulfation would be expected. Other parameters, such as the packing density or bed porosity, may therefore play a more important role in the sulfation of a KCl-containing deposit. The deposits containing the smaller KCl particles may be more densely packed, resulting in a lower bed porosity and a higher resistance to the gas flow, which could explain the lower degree of sulfation.

9.4. Effect of Deposit Oxide Composition

In experiment 5, CaO-particles were used instead of SiO_2-particles, in the 25 wt % KCl deposit, exposed to the straw-firing gas composition. The corrosion attack was found to be very different from the corrosion attack observed for the specimen covered by the KCl-SiO_2 deposit (experiment 1). Most apparent is the ~10 times thicker oxide layer formed in the KCl-CaO deposit (see Figure 24). The two SEM pictures in Figure 24 show the outer oxide layer, and the inner oxide layer, which are separated by a large gap. The outer oxide consists of a Cr-rich layer in the bottom, and a Fe-rich layer on top of this. The inner oxide layer is rich in Cr and Ni. Point and area analyses and X-ray mappings of the sample indicate that large quantities of Ca (up to 9 wt %) and Cl (up to 18 wt %) are present in both the inner and outer oxide layer. Smaller quantities of Cl (up to 6 wt %) were detected in the mixed layer. Furthermore, the mixed layer contains little or no K, but instead Ca was found together with S, probably as $CaSO_4$ [van Lith et al., 2009].

The fact that Ca is present close to the corrosion front means that it must have formed a melt together with other compounds, such as chlorides of Fe and Cr. To be able to form this melt at 560 °C, Ca has probably been present in the form of $CaCl_2$. This could be the result of a reaction of the CaO in the deposit, with the HCl from the flue gas. In fact, SEM-EDX analyses of the exposed sample indicate that $CaCl_2$ is present in the deposit, as well as in large areas in the inner oxide layer, close to the corrosion front. Thus, unlike SiO_2, CaO is not inert in the deposit but plays a very important role in the corrosion attack. Interesting to note is that in the case of the CaO deposit, grain boundary attack is seen in addition to selective corrosion (see Figure 24).

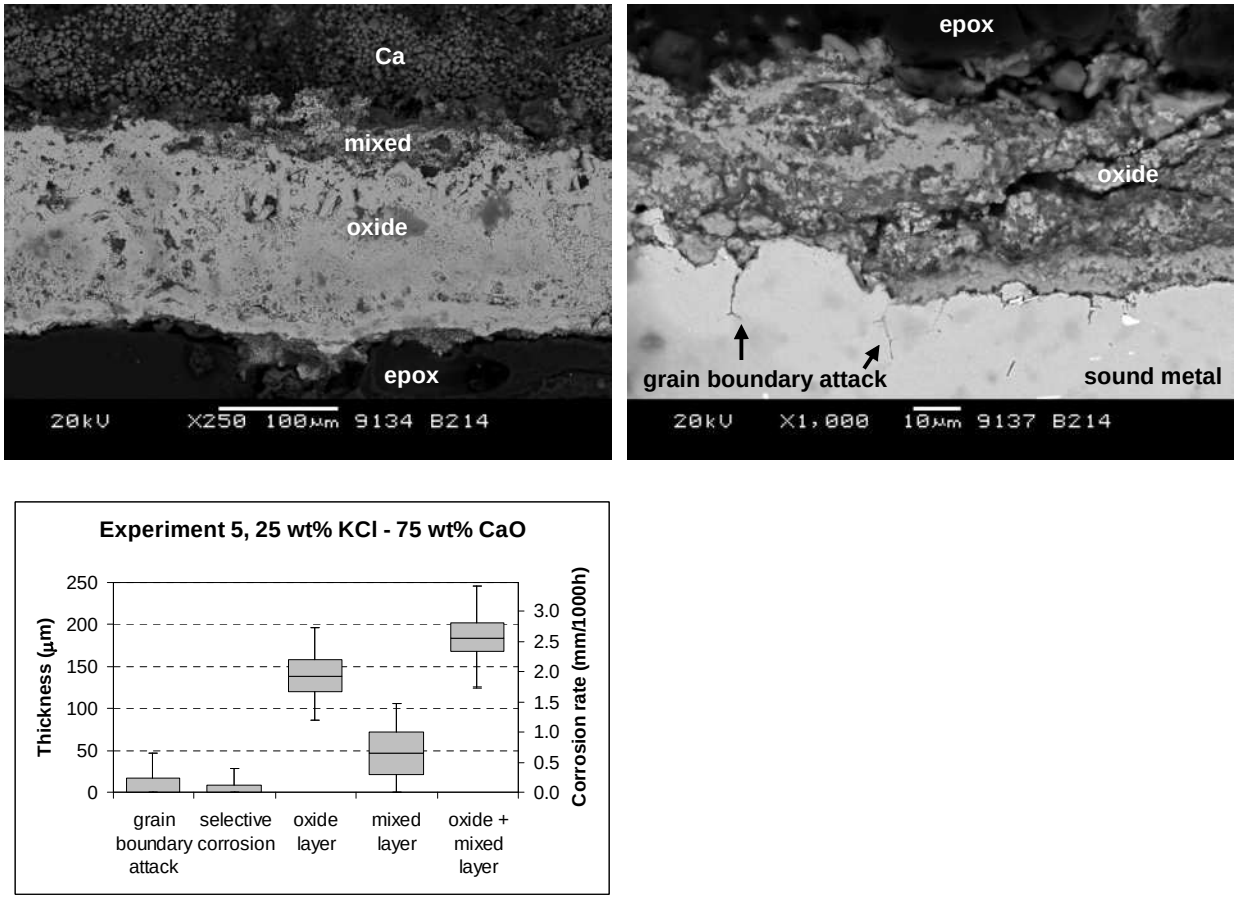

Figure 24: Corrosion attack for specimens initially covered with 25 wt % KCl - 75 wt % CaO, exposed to the straw-firing gas composition at 560 °C, for 3 days. Compare with Figure 20 (experiments performed under similar conditions, but using a SiO_2 instead of CaO) to see the effect of deposit oxide composition.

The degree of sulfation of KCl in the CaO-deposit remains unclear from the ICP-OES analysis, because Cl and S are also present in relation to Ca in the deposit. However, as KCl was detected in the deposit by SEM-EDX, this at least indicates that the sulfation has not been complete.

9.5. Effect of the Presence of HCl in the Flue Gas

The effect of the presence of HCl, in the gas flow, was studied for samples exposed to the straw-firing gas composition (experiment 6). The results of the measurements of internal attack and oxide scale, respectively mixed layer thickness, are presented in Figure 25.

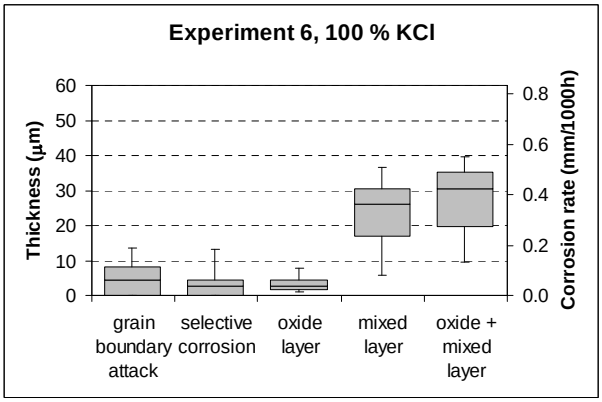

Figure 25: Corrosion attack for specimens covered with a 100% KCl deposit, exposed to the straw-firing gas composition without HCl, at 560 °C, for 3 days. Compare with Figure 20a (experiment performed under similar conditions, but exposed to the normal straw-firing gas composition) to see the effect of HCl in the gas flow.

For the specimen covered by 100% KCl, and exposed to the straw-firing conditions, without HCl, grain boundary attack and local selective corrosion were observed, with small amounts of Cl (~1-2 wt %) present at the corrosion front. These observations indicate, that HCl in the bulk gas phase is not essential for chlorine-induced corrosion to occur, when a deposit containing KCl is present. However, the average values of the thickness of the oxide scale and mixed layer were found to be lower than for the normal straw-firing case (experiment 1, see Figure 20a), which suggests that presence of HCl in the flue gas enhances

the corrosion rate. Furthermore, it was observed that the mixed layer was less uniform in thickness [van Lith et al., 2009].

ICP-OES analyses of the deposits after exposure showed that the presence of HCl in the straw-firing gas flow has little or no effect on the degree of sulfation of the KCl in the deposits (see Figure 21, experiment 6).

9.6. Effect of SO_2 Concentration in the Flue Gas

Information about the effect of the SO_2 concentration in the flue gas was obtained by comparing the results of experiments 1 (straw-firing gas composition, i.e., containing 60 ppm SO_2), 7 (cofiring gas composition, i.e., 500 ppm), and 8 (cofiring gas composition with reduced SO_2 concentration, i.e., 200 ppm), emphasizing that the straw-firing gas composition contained a higher concentration of HCl (400 ppm) than the cofiring gas composition (75 ppm). The results of the comparison of the oxide scale and mixed layer thickness measurements are presented in Figure 26.

For samples exposed to the cofiring gas composition, the degree of sulfation in the deposits, was found to be considerably higher than that observed for the samples exposed to the straw-firing gas composition. For example, for specimens covered with a 25 wt % KCl deposit, the KCl-particles in the sample exposed to straw-firing gas composition are only partly sulfated, whereas the deposit is completely sulfated in the case of the sample exposed to the cofiring gas composition (see Figure 27 and Figure 21, experiment 7). The higher degree of sulfation can be explained by the higher concentration of SO_2 in the co-firing flue gas. The SEM study of the deposits after exposure shows that the sulfation of the KCl proceeds according to the "unreacted shrinking core model" [van Lith et al., 2009].

The corrosion attack was found to be quite different for samples exposed to the straw-firing gas composition compared to the cofiring gas composition. As can be seen for specimens covered with a 100% KCl deposit, the sample exposed to the straw-firing gas composition shows an almost continuous layer of internal attack, followed by a rather uniform oxide and mixed layer (see Figure 28a), whereas the sample exposed to the co-firing gas composition shows very irregular and localized internal attack and non-uniform thicknesses of the oxide scale and mixed layer (see Figure 28b). Furthermore, very little (≤1 wt %) or no Cl was detected at the corrosion front in the samples exposed to the co-firing gas composition,

whereas ~1-4 wt % Cl was detected at the corrosion front, in the samples exposed to the straw-firing gas composition [van Lith et al., 2009].

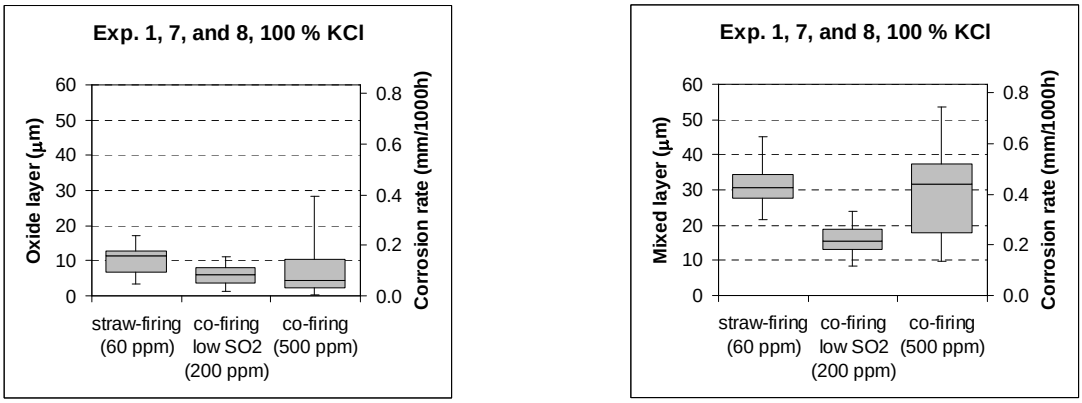

a) Oxide layer thickness b) Mixed layer thickness

Figure 26: Effect of the SO_2 concentration in the gas flow (given in brackets) on the corrosion attack, for specimens covered with a 100% KCl deposit, exposed at 560 °C, for 3 days. See Figure 20 for graph explanation.

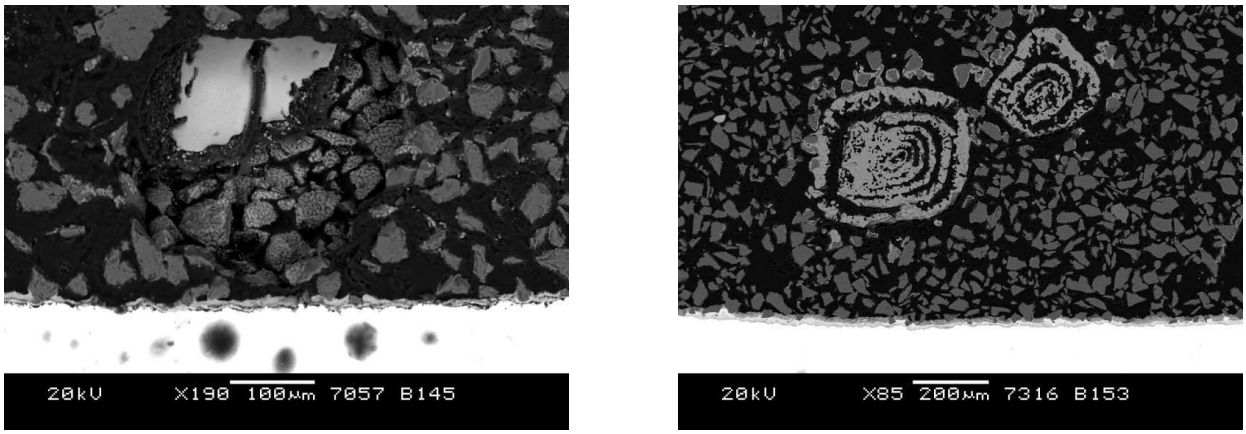

a) Gas composition: straw-firing b) Gas composition: cofiring

Large bright area: KCl; smaller grey particles: SiO_2; small light grey spots: K_2SO_4

Small grey particles: SiO_2; Light grey areas / rims: K_2SO_4

Figure 27: SEM micrographs of cross sections of the top of initially 100% KCl deposits, after exposure at 560 °C, for 3 days. The metal surface is visible in the bottom of the pictures.

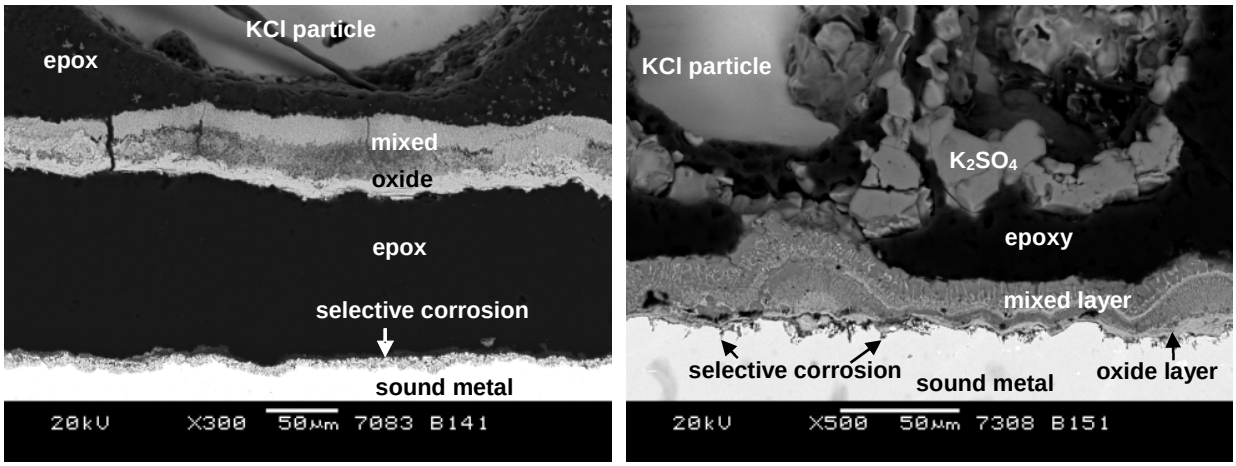

a) Gas composition: straw-firing b) Gas composition: cofiring

Figure 28: SEM micrographs of cross sections of the corrosion products of specimens covered with a 100% KCl deposit, after exposure at 560 °C (1040 °F), for 3 days. Note: Pictures have different scales.

Samples exposed to the cofiring gas composition with a reduced SO_2 concentration (see Table 2) clearly showed a lower degree of sulfation of KCl in the deposit. For example, for the specimens covered with a 100% KCl deposit, it can be seen that the top particles of the deposit are completely sulfated when exposed to the cofiring gas composition (gray areas in Figure 29a), whereas only rims of the top particles are sulfated when exposed to the cofiring gas composition with a reduced SO_2 concentration (gray rims in Figure 29b), resulting in an overall degree of sulfation of around 20% according to the ICP-OES analysis (see Figure 21, experiment 8). For the samples with a 25 wt % KCl deposit, complete sulfation was observed when exposed to the cofiring gas composition, while some KCl was left in the deposits of the samples exposed to the cofiring gas composition with reduced SO_2 concentration (around 93% sulfation according to the ICP-OES analysis).

The thickness of the oxide scale of the sample exposed to the co-firing gas composition, with reduced SO_2 concentration, was smaller than for the sample exposed to the straw-firing gas compositions, but was on average, higher than the sample exposed to co-firing gas composition. However, the mixed layer was noticeably thinner than for the samples exposed to the straw-firing and cofiring conditions (see Figure 29), indicating that there is no clear relationship between the thickness of the mixed layer and the SO_2 concentration in the flue gas, and that the concentration of HCl in the flue gas possibly also plays a role.

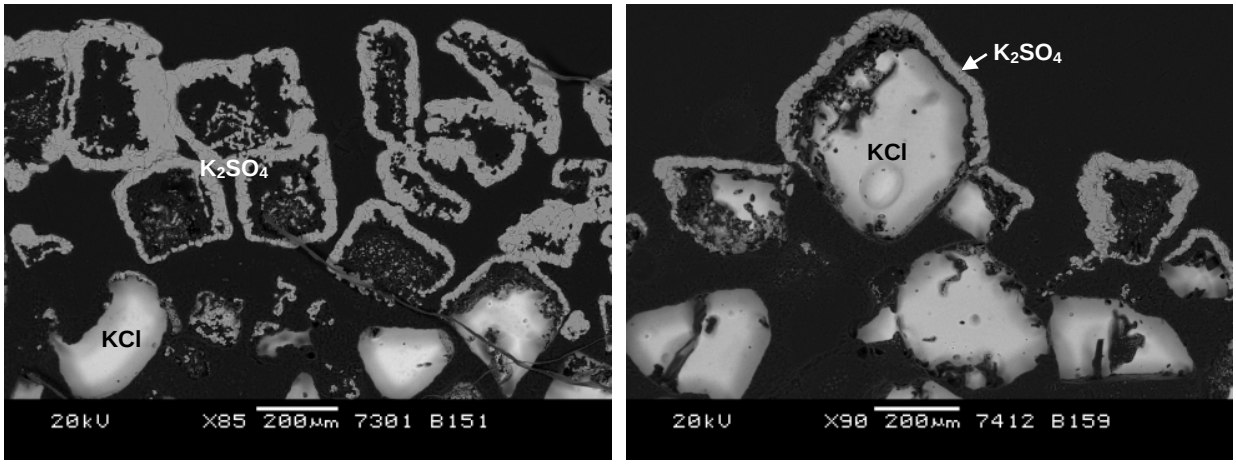

a) Gas composition: cofiring b) Gas composition: cofiring, low SO_2

Figure 29: SEM micrographs of cross sections of the top of initially 100% KCl deposits, after exposure at 560 °C, for 3 days.

9.7. Effect of temperature (560 °C vs. 600 °C vs. 640 °C)

Straw-firing conditions. The effect of temperature for straw-firing conditions was investigated by comparing the results of experiment 1, performed at 560 °C, and experiment 4, which was performed at 600 °C. An overview of the corrosion attack for each experiment is shown in Figure 30. The figure shows that increasing the temperature from 560 °C to 600 °C has a very pronounced effect on the corrosion attack, both for the sample containing a pure KCl deposit, and for the sample containing a 25 wt% KCl –75 wt% SiO_2 deposit.

As described above, for the specimen covered with a 100 % KCl deposit exposed at 560 °C, a rather uniform corrosion attack was observed, consisting of a band of selective corrosion of ~5 µm thick, followed by a ~10 µm thick oxide layer, and a ~30 µm thick mixed layer (see Figure 30a). SEM-EDX analysis of the specimen covered with a 100 % KCl deposit and exposed at 600 °C also showed a continuous band of selective chlorine corrosion, but this band was much thicker on average (~40 µm), and the thickness varied more within the cross-section of the sample. Mainly Cr was removed by this mechanism, leaving a skeleton rich in Fe and Ni behind. Small amounts of Cl (1–3 wt%) were detected within the band of selective corrosion. The SEM-investigation indicated that entire grains had been attacked, so the band of selective corrosion possibly also includes grain boundary attack.

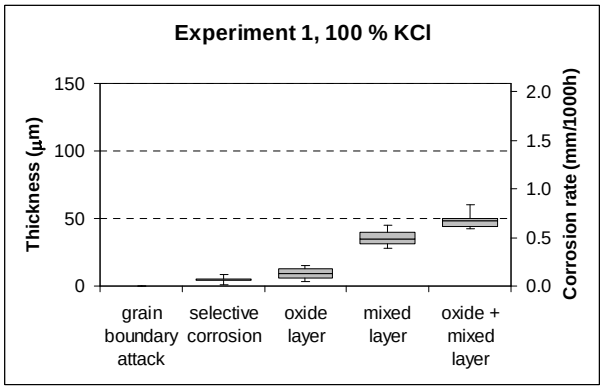

a) 100 % KCl, 560 °C

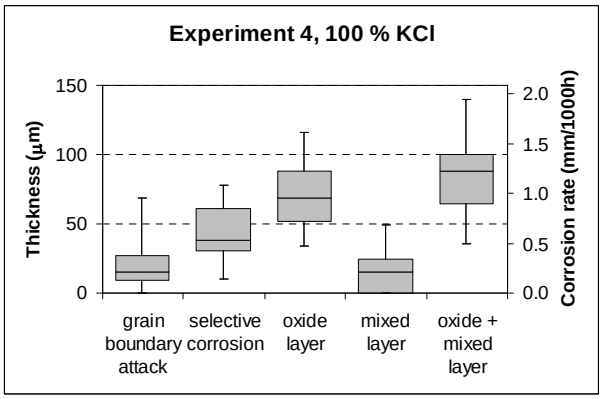

b) 100 % KCl, 600 °C

N.B.: Grain boundary attack was measured only in an area of ~350 µm wide, and underneath the selective corrosion

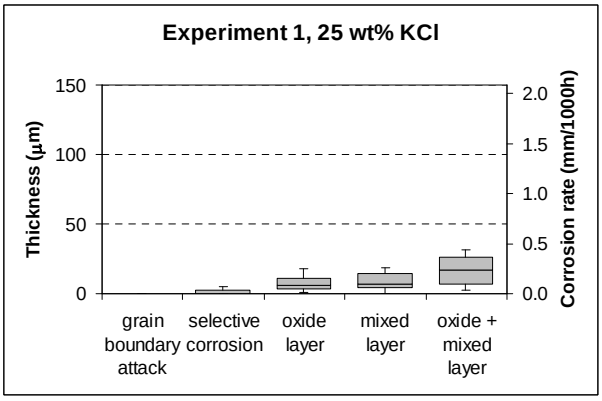

c) 25 wt% KCl , 560 °C

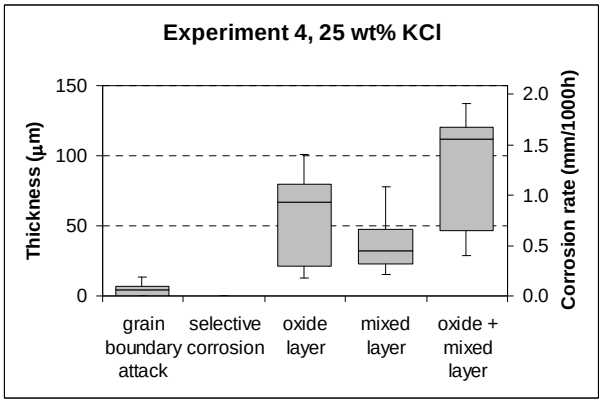

d) 25 wt% KCl, 600 °C

Figure 30: Effect of temperature on the corrosion attack, for specimens exposed to the straw-firing gas composition for 3 days. See Figure 20 for graph explanation.

At most places, no grain boundary attack was observed under the band of selective corrosion. However, in an area of about 350 µm wide, grain boundary attack was abundant, having a depth of ~20 µm on average, and locally up to ~70 µm (see Figure 31a). Only the measurements of grain boundary attack in this area have been included in Figure 30b. The oxide layer was almost entirely detached from the metal surface, and was divided into a dense, Cr-rich inner layer and a rather porous, Fe-rich outer layer. This phenomena has also been observed in full-scale corrosion studies in straw-fired boilers [Montgomery et al.,

2002] and can be explained by the higher volatility of $FeCl_2$ compared to $CrCl_2$, resulting in the oxidation of iron oxide, at higher oxygen partial pressure than chromium oxide. Both the inner and the outer oxide contained traces of Cl (<1 wt%), but no S. The total oxide layer was ~70 μm thick on average, which is much thicker than the oxide layer formed during exposure at 560 °C (see Figure 30). The mixed layer of iron threads in K_2SO_4 was, on the other hand, much thinner (~15 μm on average) [van Lith et al., 2009].

Increasing corrosion attack with increasing temperature has also been observed in full-scale straw-fired boilers. [Montgomery et al., 2002] reported that the corrosion rate of TP 347H FG exposed in the test superheater at the straw-fired boiler Masnedø was approximately doubled at a metal temperature of 613 °C compared to at a metal temperature of 567 °C. At the higher metal temperature, selective removal of Cr and grain boundary attack was seen to a greater extent than at the lower temperature.

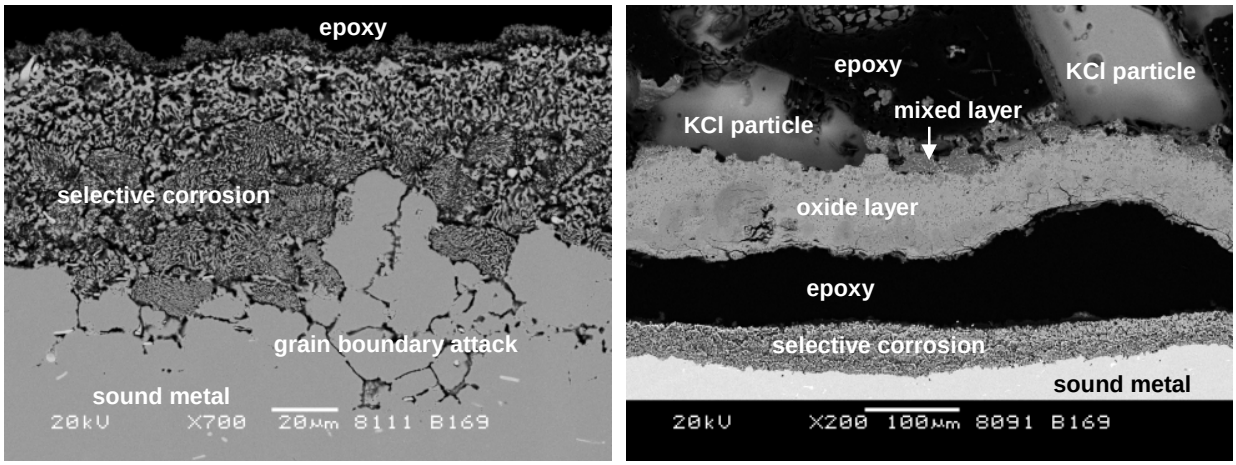

a) Internal corrosion attack b) Corrosion products and part of deposit

Figure 31: SEM micrographs of a cross-section of a specimen covered with a 100 % KCl deposit after exposure to the straw-firing gas composition at 600 °C, for 3 days.

The effect of temperature on the degree of sulfation of KCl in the deposit is presented in Figure 32. The results show that the degree of sulfation is somewhat lower at 600 °C than at 560 °C. This corresponds to the lower equilibrium conversion of SO_2 to SO_3 at 600 °C compared to at 560 °C [Gudzinkas, 2007]. Because the corrosion attack is clearly enhanced at the higher temperature, the corrosion attack does not seem to be directly related to the degree of sulfation in the deposit. Probably, a higher amount of molten phase formed, and a

faster diffusion of oxygen and chlorine, at the higher temperature are more important for an enhanced corrosion attack [van Lith et al., 2009].

[Pedersen, 2009] conducted a series of measurements on test elements covered by 100 % KCl, 75 % KCl:25 % SiO2, 100 % NaCl, and 80 % NaCl:20 % SiO2 at 640 °C. The conclusions from her data was that test elements covered by a pure alkali chloride salt (100 KCl respectively 100 % NaCl) were significantly more corroded than those test elements covered by 75 % KCl respectively 80 % NaCl, i.e. the diluted systems. Furthermore, she concluded that KCl causes more significant corrosion than NaCl, at 640 °C.

Co-firing conditions. The specimen covered with a pure KCl deposit, and exposed to the co-firing gas composition as 600 °C, showed very different corrosion morphologies within the sample, as well as compared to the sample exposed to 560 °C. In most areas of the sample, a rather uniform corrosion attack was seen, in the form of a ~5 μm thick band of grain boundary attack, with a ~25 μm thick oxide layer, and a ~55 μm thick mixed layer, on top (see Figure 33b and Figure 34a). In contrast to the sample exposed to the straw-firing gas composition at 600 °C, the grain boundary attack was most likely the result of sulphidation, as some S (~2–8 wt%) but no Cl, was detected at the grain boundaries. The oxide is divided into two parts (detached from each other in most areas); the inner layer being rich in Fe and Ni, whereas the outer layer was found to be rich in Cr, and in addition contained some Ni. The mixed layer consisted mainly of Fe, K, and S, but also contained some Cr. Some areas in the mixed layer, close to the oxide layer, were depleted in K and S, but contained some Cl (dark area in the middle of Figure 34a). At some of these locations, the mixed layer was detached from the oxide layer. The average oxide and mixed layer are thicker than observed for the sample exposed at 560 °C. At a few locations in the sample, selective corrosion of Fe was seen instead of the grain boundary attack. Some S (~1–6 wt%) and traces of Cl (<1 wt%) were detected in these areas.

[Montgomery and Larsen, 2002] observed a dramatic increase in the corrosion rate at a metal temperature of 586 °C, compared to a metal temperature of 550 °C, during in-situ exposure tests at the Studstrup Power Plant, when co-firing coal and 20 % wheat straw (on energy basis). However, the corrosion attack at the higher temperature consisted of pitting attack, caused by low temperature hot corrosion. At 10 % co-firing, and at the lower metal temperature during the 20 % co-firing tests, the corrosion was caused by sulphidation attack. Virtually no Cl was found in the deposits or corrosion products. Instead, a matrix of K_2SO_4 with iron oxide threads was observed, similar to the mixed layer in our lab-scale study [van Lith et al., 2009].

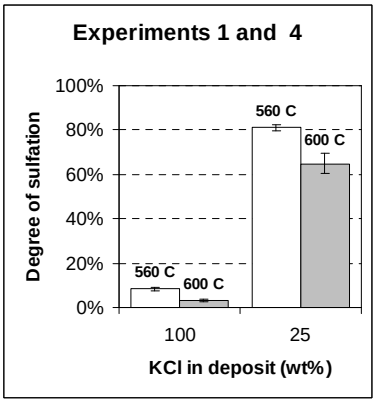

Figure 32: Effect of the temperature on the degree of sulfation of KCl in the deposit, for samples initially containing 100 % KCl and 25 wt% KCl – 75 wt% SiO_2 exposed to the straw-firing gas composition for 3 days. See Figure 21 for graph explanation.

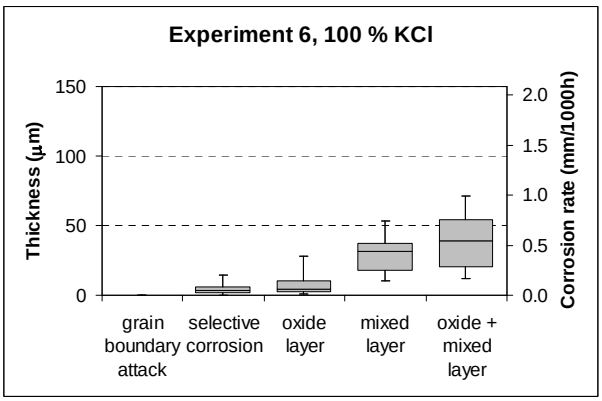

a) 100 % KCl, 560 °C

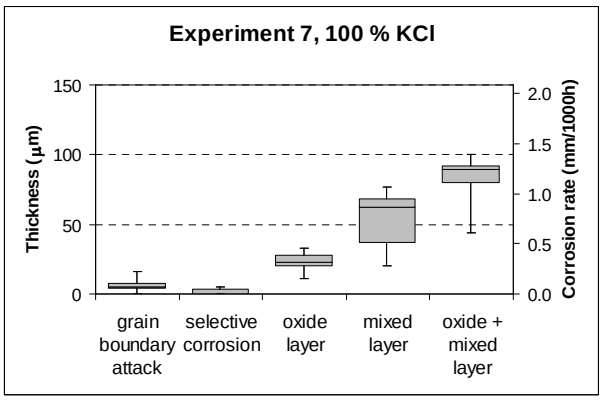

b) 100 % KCl, 600 °C

N.B.: Selective corrosion was observed only locally, instead of grain boundary attack. The grain boundary attack occurred by sulphidation.

Figure 33: Effect of temperature on the corrosion attack for specimens exposed to the co-firing gas composition for 3 days. See Figure 30 for graph explanation.

The effect of temperature on the degree of sulfation, for the co-firing gas composition, is shown in Figure 35. The results indicate a lower degree of sulfation at 600 °C than at 560 °C, similar to what was seen for the samples exposed to the straw-firing gas composition.

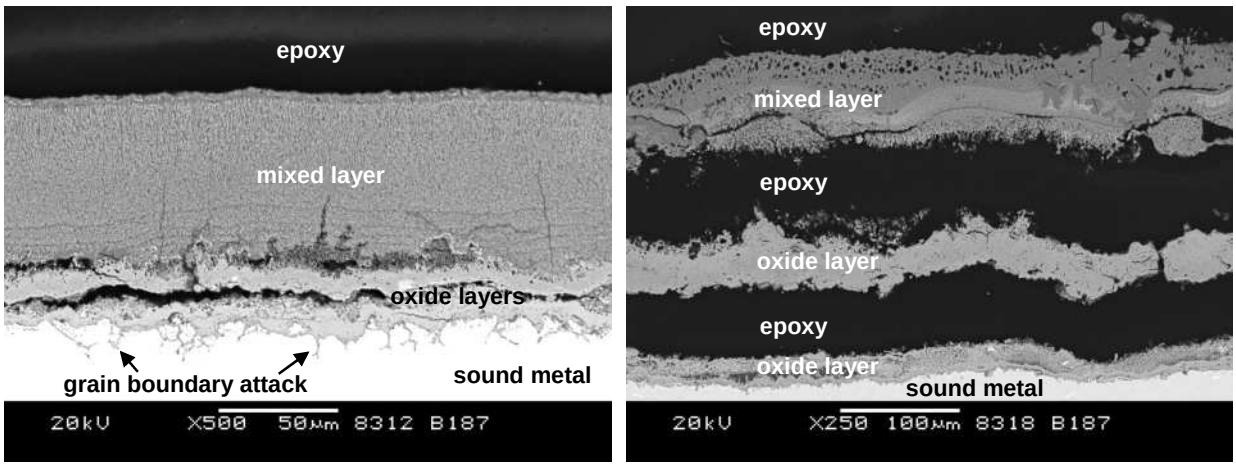

a) b)

Figure 34: SEM micrographs of a cross-section of a specimen covered with a 100 % KCl deposit after exposure to the co-firing gas composition at 600 °C, for 3 days.

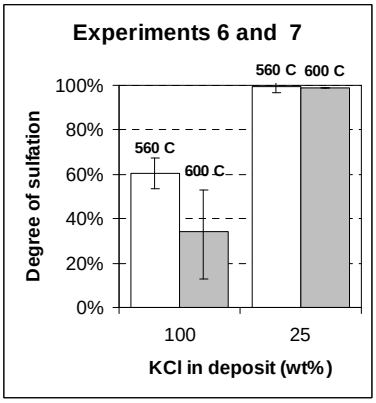

Figure 35: Effect of temperature on the degree of sulfation of KCl in the deposit, for samples initially containing 100 % KCl and 25 wt% KCl – 75 wt% SiO_2 exposed to the co-firing gas composition for 3 days.

9.8. Effect of Cat-Ion Mobility (KCl vs. NaCl, 600 °C)

Straw-firing conditions. Figure 36 shows the effects of salt composition (pure KCl vs. pure NaCl) on the corrosion attack for specimens exposed to straw-firing conditions at 600 °C. Large differences in the both the internal attack and the thickness of the oxide and mixed layer can be seen.

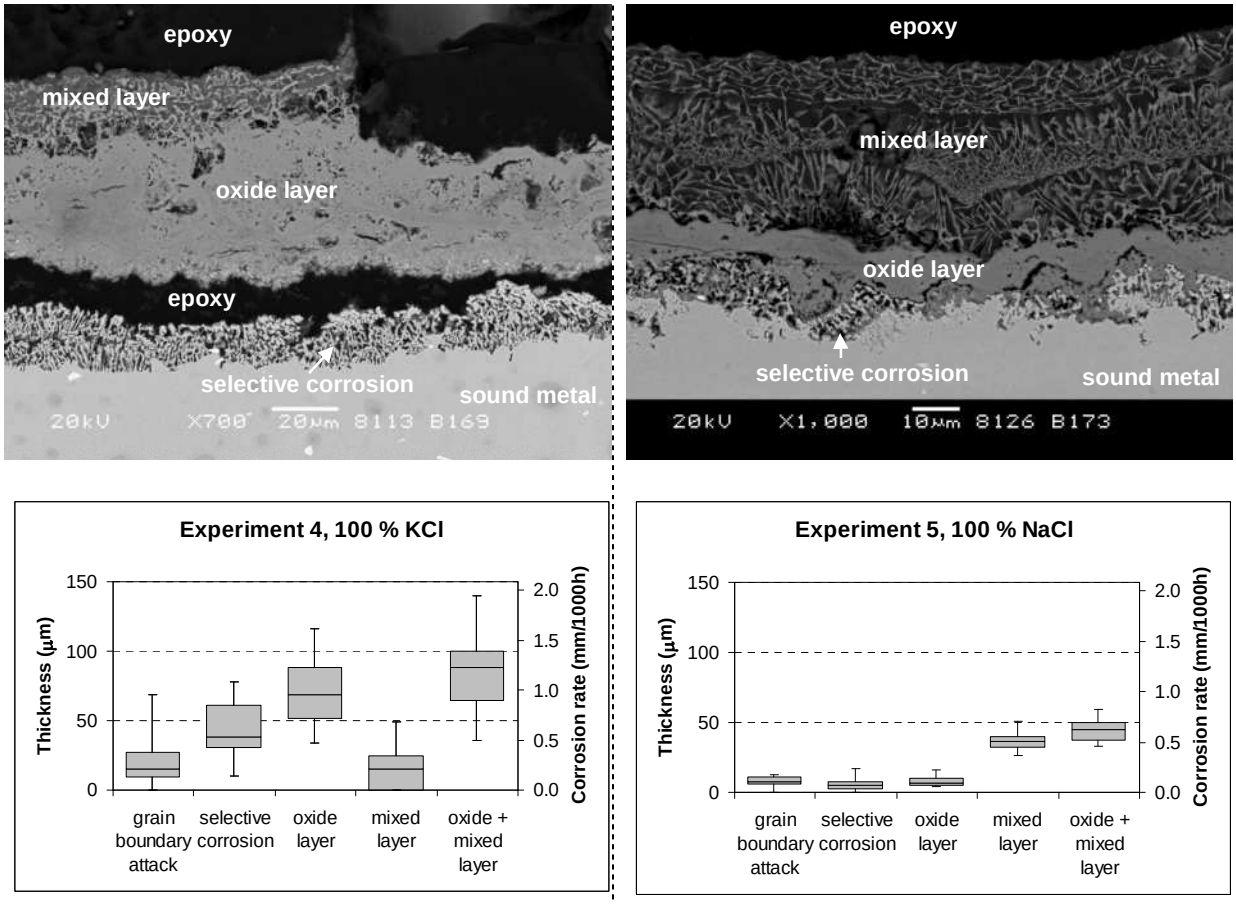

a) 100 % KCl

b) 100 % NaCl

Figure 36: Effect of salt composition on the corrosion attack, for specimens exposed to the straw-firing conditions at 600 °C for 3 days. See Figure 20 for graph explanation.

First of all, the selective corrosion is less deep, and, more localized, for the specimen covered by NaCl. In the sample with NaCl, the areas of selected corrosion contained minor amounts of Cl and S (~1–3 wt%), whereas in the sample with KCl only Cl was detected . As for the sample with KCl, the sample with NaCl shows grain boundary attack, instead of selective corrosion, in some areas of the sample, but the depth of attack is much less, and S was found at the grain boundaries [van Lith et al., 2009].

The oxide layer was much thinner, and showed less variation in the thickness, for the sample with NaCl compared to the sample with KCl. Whereas the oxide layer of the sample with KCl was divided into a Cr-rich inner layer and a Fe-rich outer layer, both layers containing traces of Cl (<1 wt%) but no S, there did not seem to be a divided oxide for the sample with NaCl, but locally high mounts of S (up to ~10 wt%) were present together with high amounts of Cr.

The mixed layer, on the other hand, was much thicker and of more uniform thickness for the sample covered with NaCl. The general morphology and chemistry of the mixed layer were found to be very similar for samples with KCl and NaCl: threads of mainly iron oxide in a matrix of potassium or sodium sulfate. However, in the case of NaCl, the iron oxide threads seem more straight and organized, and the mixed layer seems to be composed of various layers on top of each other [van Lith et al., 2009].

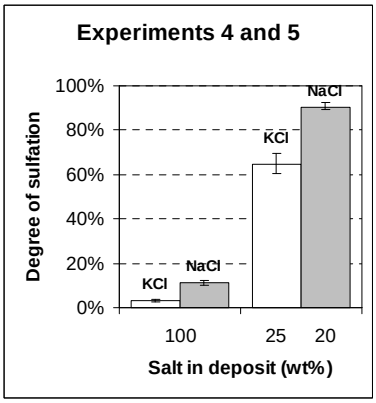

Figure 37: Effect of salt composition on the degree of sulfation of KCl in the deposit, for samples initially containing 100 % KCl / NaCl and 25 wt% KCl / 20 wt% NaCl (the remainder being SiO_2) exposed to the straw-firing gas composition at 600 °C for 3 days.

From Figure 37 it can be seen that the NaCl deposits were more sulfated than the KCl deposits exposed to the straw-firing gas composition at 600 °C. [Ozawa et al., 2003] observed higher sulfation rates for solid NaCl than for solid KCl, at both 450 °C and 650 °C, for particles with a mean diameter of 75–125 μm and a gas flow consisting of 0.9 % (v/v) SO_2, 5 % (v/v) H_2O, 10 % (v/v) O_2, and N_2 as balance. After 2 h of exposure to this gas composition at 650 °C, about 20 % of NaCl was sulfated, compared to about 10 % of KCl. The degree of sulfation was determined from the rate of HCl emission. Reasons for the much higher sulfation rates observed by [Ozawa et al., 2003] compared to this study are most likely the smaller particle size range, and the higher concentration of SO_2 in the gas flow [van Lith et al., 2009].

Co-firing conditions. Large differences in the corrosion behavior were also seen between the samples covered by KCl and samples covered by NaCl, when exposed to the co-firing gas composition at 600 °C (see Figure 38). The sample with NaCl showed minor internal attack (maximum ~8 μm deep), but it was difficult to determine whether this was due to selective corrosion or grain boundary attack. Some S (~5 wt%) and traces of Cl (<1 wt%) were found at the corrosion front. The sample with KCl mainly showed grain boundary attack with only S present at the grain boundaries.

A very thin oxide layer (~3 μm) was observed for the sample with NaCl compared to the sample with KCl (~40 μm on average). The oxide layer was rich in Fe, but in some locations, an inner layer rich in Cr and S was also observed.

When comparing Figure 39 with Figure 37, it can be seen that the degree of sulfation of NaCl (similar to KCl) is higher when exposed to the co-firing gas composition compared to the straw-firing gas composition, most likely as a result of the higher SO_2 concentration. The degree of sulfation is higher for NaCl than for KCl in the co-firing case, as was also observed for the straw-firing case. SEM-EDX analysis of the deposits after exposure showed that NaCl (similar to KCl) is sulfated according to the "unreacted shrinking core model".

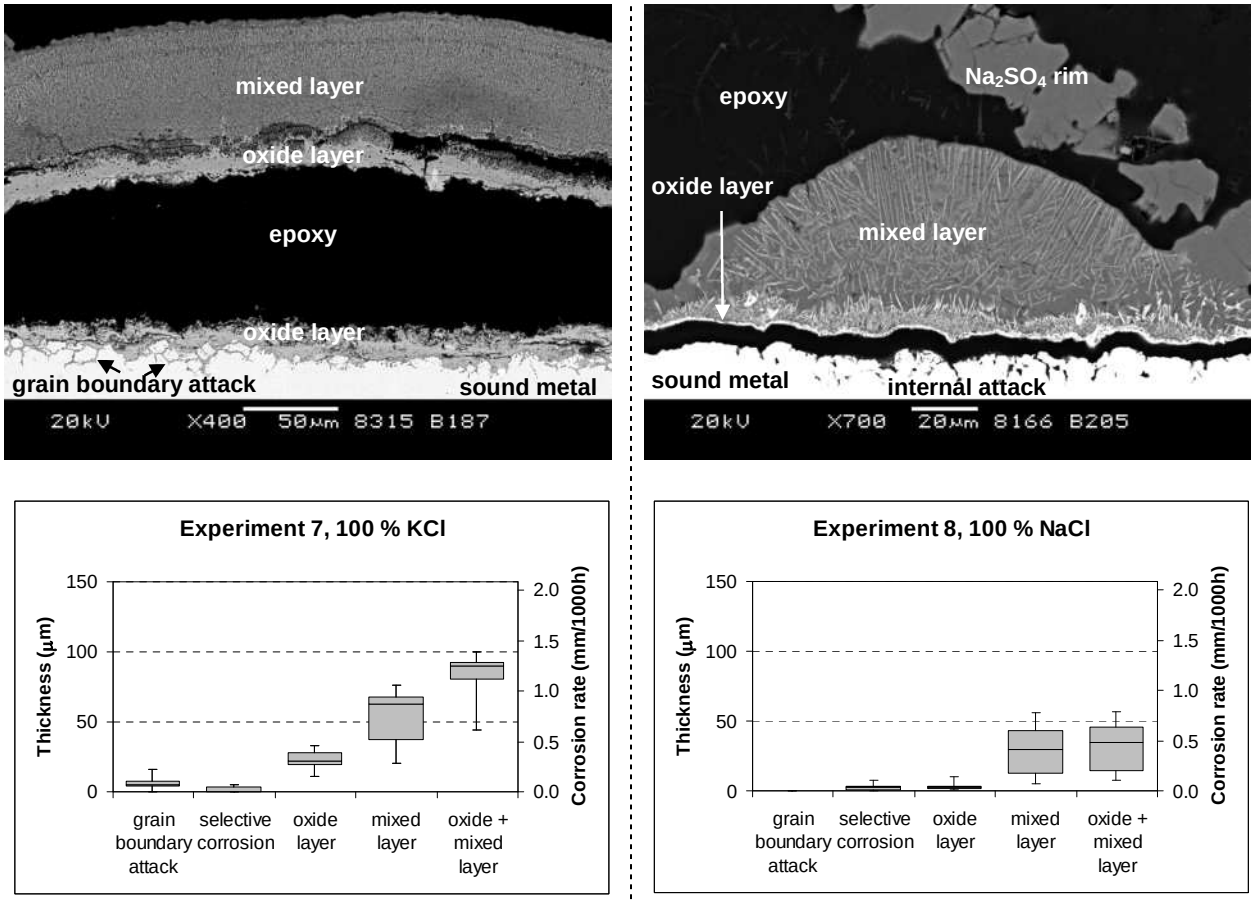

a) 100 % KCl

b) 100 % NaCl

Figure 38: Effect of salt composition on the corrosion attack, for specimens exposed to the co-firing gas composition at 600 °C for 3 days. See Figure 20 for graph explanation. N.B.: SEM micrographs have different scales.

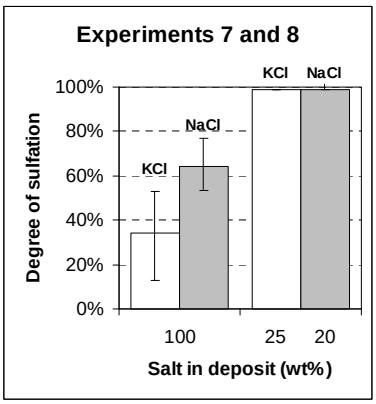

Figure 39: Effect of salt composition on the degree of sulfation of KCl in the deposit, for samples initially containing 100 % KCl / NaCl and 25 wt% KCl / 20 wt% NaCl (the remainder being SiO_2) exposed to the co-firing gas composition at 600 °C for 3 days.

10. Summary and Suggestions to Further work

We aimed at investigating the critical level of Cl to cause corrosion in biomass-fired boilers, and had to make some assumptions while planning the experiments for this. First we decided to consider a model system of a deposit, when calculating the deposit composition. A sketch of the model system is shown in Figure 40.

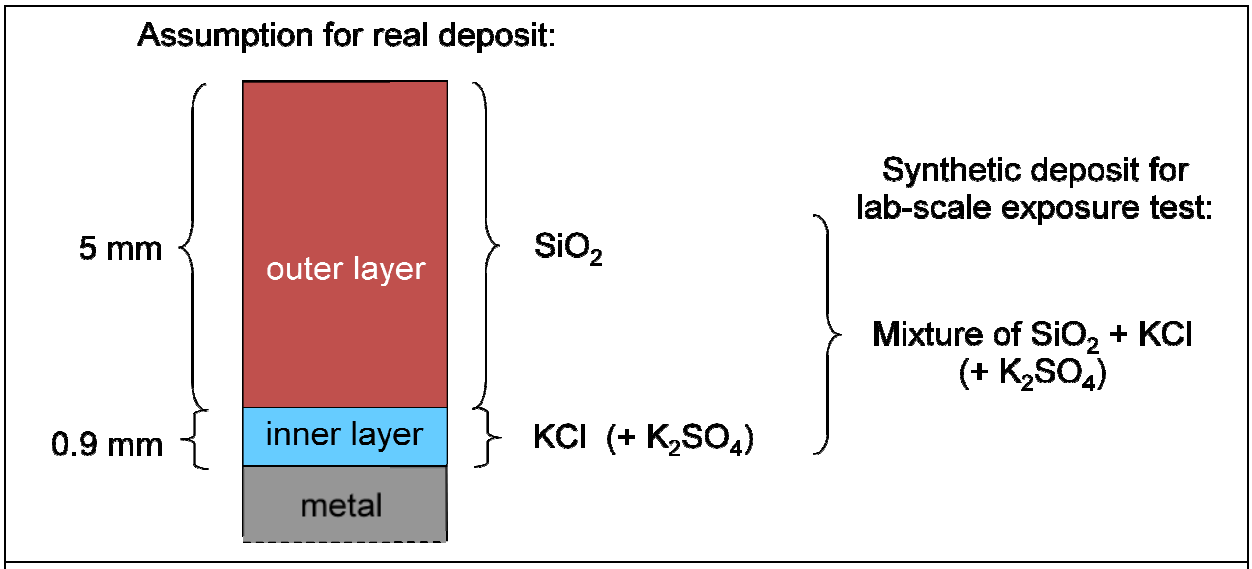

Figure 40: Model system considered for calculation of the [Cl] to be used in the experiments conducted in order to find the critical level of Cl to cause corrosion.

The model system is based on a deposit, formed on a probe in the Masnedø CHP.

Measurements have been conducted on the systems, i.e. compositions or deposit layer thicknesses shown in Table 10, at 560 °C, and with the same flue gas composition as provided in Table 9.

Deposit Type	I	II	III	IV
Composition in inner deposit layer (0,9 mm): %(w/w)				
KCl	100	84,1	67,7	52,6
K2SO4	0	15,9	32,3	47,4
[Cl] in inner layer (%(w/w))	47,6	40,0	32,2	25,0
Thickness of total deposit (mm)	5,9	5,9	5,9	5,9
[Cl] in total deposit (%(w/w))	7,3	6,3	5,2	4,1
Composition of synthetic mixtures for corrosion tests: % (w/w)				
KCl	15,4	13,2	10,8	8,6
K2SO4	0	2,5	5,2	7,7
SiO2	84,6	84,3	84,0	83,7
Deposit Type	V	VI	VII	VIII
Composition in inner deposit layer (0,9 mm): %(w/w)				
KCl	100	100	100	100
K2SO4	0	0	0	0
[Cl] in inner layer (%(w/w))	47,6	47,6	47,6	47,6
Thickness of total deposit (mm)	1,8	2,7	3,6	4,5
[Cl] in total deposit (%(w/w))	23,9	16,0	12,0	9,6
Composition of synthetic mixtures for corrosion tests: % (w/w)				
KCl	50,3	33,6	25,3	20,2
K2SO4	0	0	0	0
SiO2	49,7	66,4	74,8	79,8

Table 10: Composition of synthetic deposit coatings tested in order to detect the critical limit of [Cl] causing corrosion.

For each experiment, the corrosion loss was determined and plotted, as shown in Figure 41, in which it is seen that the data for machined samples shows a very significant scattering, but also, interesting enough that there seems to be a linear dependence between the metal loss as quantified here and the [Cl] in the deposit. Based on the data, it seems as if a chlorine concentration lower than 6-8 % will cause a rather low corrosion, while a higher [Cl] will cause increased corrosion.

These experiments are based on a model system with a given structure, introduced to define the compositions to work with, in the corrosion tests. The limit found may be hard to apply in real boilers, since the [Cl] in deposits in boilers are not a controlled parameter, and we

still do not know the exact correlation between the feedstock composition fed to a boiler and the composition of the deposits formed in that boiler.

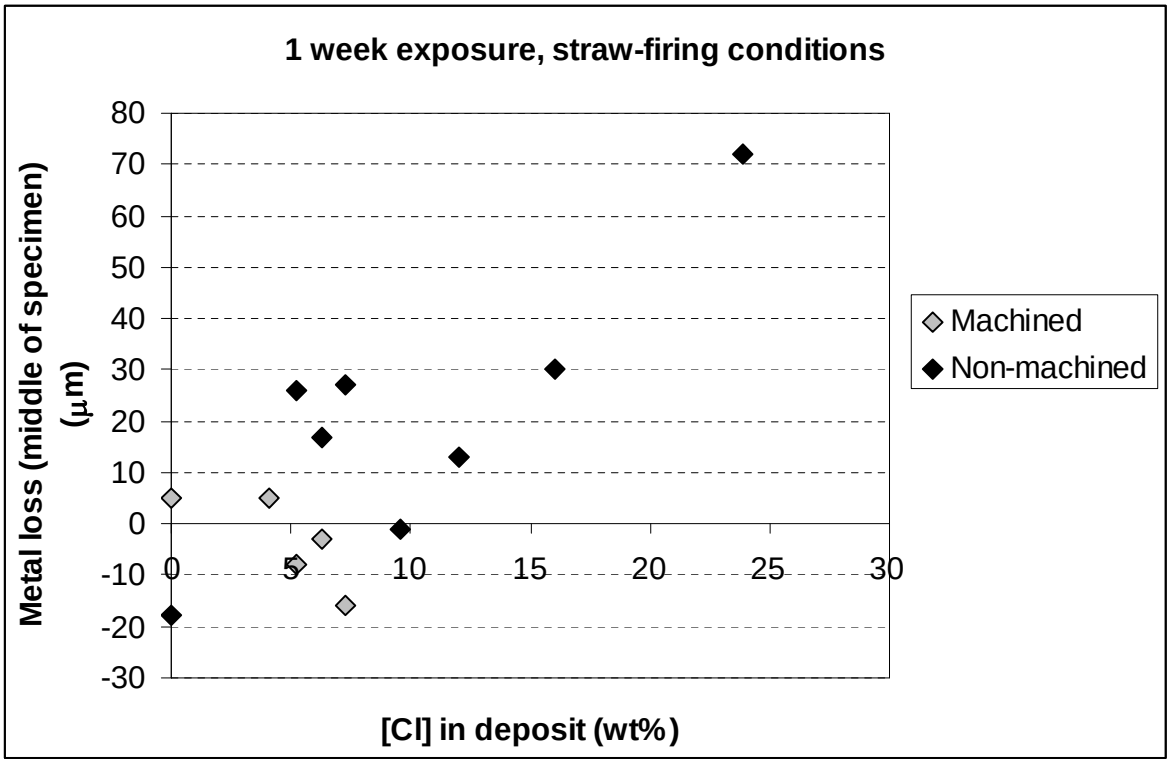

Figure 41: Metal loss by corrosion, as measured at the middle of the specimen vs. [Cl] in the deposit.

The lab-scale corrosion tests reported here have been performed under well-controlled conditions, simulating the conditions in straw-fired boilers and boilers co-firing coal and straw. For example, the choice of metal composition, metal surface temperature, and gas compositions was based on knowledge and experience from full-scale biomass- and co-fired boilers in Denmark, defined in close dialogue with the advisory group following the project, see section 1. Other conditions, such as the chemical and physical characteristics of the deposit, and the gas temperature, and, flow around the deposit, are very complex and variable in full-scale boilers and therefore had to be simplified in the lab-scale tests.

Based on the outline of the work carried out within the frame of FORSKEL Project 5820, as briefly outlined above, the following conclusions can be drawn [van Lith et al., 2009];

- It was confirmed that the presence of a KCl-containing deposit strongly enhances the corrosion attack. In addition, it was found that an increase of the percentage of KCl in the deposit results in a more uniform and deeper internal attack.
- A characteristic mixed layer of iron oxide threads in alkali sulfate matrix was formed under all investigated conditions. However, the thickness of this layer was strongly dependent on the experimental conditions. In the case of a 25 wt % KCl - 75 wt % SiO_2 deposit, a thinner mixed layer was formed rather than for a pure KCl deposit. This is probably due to both the lower KCl content in the deposit and to the presence of SiO_2 particles providing surfaces for the K_2SO_4 grains (formed by the sulfation of KCl) to stick to. The smaller the SiO_2 particles, the more surface area is available and the less K_2SO_4 is formed on the oxide scale, resulting in a thinner mixed layer. The iron oxide threads of the mixed layers do not occur inside unreacted KCl particles or (parts of) particles converted to K_2SO_4 by reaction of KCl with SO_2 in the flue gas.
- A deposit with small KCl particles sulfates to a lower degree than a deposit with large KCl particles, possibly because of a denser packing and lower bed porosity. Despite the significant influence on the degree of sulfation, the KCl particle size has minor effect on the corrosion attack.
- Whereas SiO_2 particles are chemically inert with respect to the flue gas and the corrosion attack, CaO particles react with HCl from the flue gas to form $CaCl_2$, which plays an important role in the corrosion mechanism. As a result, the corrosion rate is strongly enhanced when CaO is present in the deposit, instead of SiO_2.
- Samples exposed to a straw-firing gas composition, with and without HCl, showed that the presence of HCl in the flue gas is not essential for chlorine-induced corrosion to occur when a deposit containing KCl is present, but it enhances the corrosion rate.
- A higher concentration of SO_2 in the flue gas causes a higher degree of sulfation of KCl particles in the deposit. The sulfation of the KCl particles proceeds according to the "unreacted shrinking core model".
- No simple relation was observed between the degree of sulfation in the deposit and the depth of internal attack or the thickness of the oxide scale or mixed layer. Although the sulfation reaction has shown to be important for the formation of Cl close to the metal surface, and initiating the active oxidation process, there is no evidence that a higher degree of sulfation in the deposit results in an enhanced corrosion attack.
- Increasing the temperature from 560 °C to 600 °C results in local grain boundary attack for both straw-firing and co-firing conditions. In the case of co-firing

conditions, the main mechanism for this type of attack is most likely sulphidation. In the case of straw-firing conditions, the selective corrosion is strongly enhanced at the higher temperature. For both straw-firing and co-firing conditions a much thicker oxide layer is formed at 600 °C.

- NaCl has a considerably lower corrosion potential than KCl, at all temperatures considered i.e. 560, 600 and 640 °C. For both straw-firing and co-firing conditions, the internal attack is much less severe, and the oxide and mixed layers are much thinner in the presence of a NaCl deposit, as when compared to a KCl deposit.

The experimental work presented in this report has caused some ideas and suggestions to further work to be done on this issue [van Lith et al., 2009]:

1. The effects of oxide composition (e.g., using Al_2O_3 or CaO instead of SiO_2) on the sulfation and corrosion behavior, needs further attention. Tests with fly ashes from straw-fired and co-fired boilers instead of the synthetic deposits should be carefully done.
2. The effect of shift in the temperature – both the gas temperature in the reactor, which is here assumed to be the same as the metal temperature, but also differences between gas and metal temperatures, and/or dynamic changes in the gas composition – e.g. changes in [SO_2] or [HCl] vs. time - as experienced in real plants, is another factor that needs further attention, via systematic measurements.
3. The effect of different materials does also need further investigation. Here we have picked a common superheater material, based on experience from e.g. SSV4 and AVV2, but there may be other relevant material, including probably also coatings.
4. It may also be worth studying the contact between the synthetic deposits and the test elements further. In this study we have applied powdery deposits, but deposits formed by evaporation of water from an aqueous solution of the relevant salts or a salt melt may provide a tighter contact, and thereby probably a changed corrosion pattern.
5. Further attention on other cat-ions, like Zn^{2+}, and, Pb^{+} and Pb^{2+} is definitely needed in order to extrapolate the results obtained here to eg. waste incinerators.

As a result, the effects of individual parameters on the corrosion and sulfation behavior became clear, as was the main objective of this work, but the extrapolation of the results to full-scale boiler conditions has to be done with care. The composition, structure, and build-up with time of a deposit on a superheater tube in a full-scale boiler are dependent on many factors, such as the boiler type and design, the temperature profile within the boiler, and the composition of the fuel feedstock. Both short-term probe deposits and mature deposits on superheater tubes have been studied in grate-fired boilers utilizing 100% straw [Nielsen,

1998; Jensen et al., 2004]. The probe deposits from Rudkøbing CHP contained large amounts of K and Cl (the sum being 40-80 wt % of the deposit), and to a lesser extent Si, Ca, and S. SEM-EDX analysis revealed that the deposits consisted of a layer of almost pure KCl close to the metal surface, followed by a very porous KCl-rich layer, and an outer layer consisting of fly ash particles rich in Si and Ca, being glued together by KCl [Nielsen, 1998]. The KCl-rich inner layer was found to be thicker and denser on the probe with a metal temperature of 550 °C, compared to the 460 °C probe. Mature deposits on corrosion probes (exposed for 450-3000 h) also consisted mainly of KCl and fly ash particles, but in some cases a layer of K_2SO_4 was also present, either next to the metal oxide, on top of a KCl-Fe_xO_y layer, or in between two KCl-Fe_xO_y layers. Studies at Masnedø CHP showed that deposits formed on probes at metal temperatures of 540-620 °C, exposed for 6 h, consisted mainly of KCl with iron oxide threads, see [Nielsen, 1998], whereas mature deposits consisted of various layers, with the inner layer being rich in K_2SO_4 and iron oxide and the outer layers being rich in KCl.

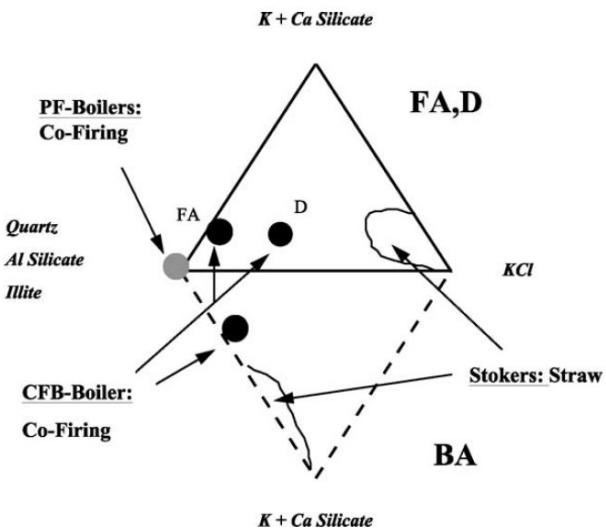

Figure 40: CCSEM compositional data for bottom and fly ashes, and probe deposits from wheat straw-fired grate boilers, a coal-straw cofired CFB boiler, and a coal-straw cofired PF-boiler., illustrated in a triangular diagram consisting of: (1) quartz, Al-silicates, and illite; (2) K+Ca silicate; and (3) KCl. The top triangle provides the composition of fly ashes (FA) and probe deposits (D) and the bottom triangle contains the same information for the bottom ashes (BA). Source: [Frandsen et al., 1997].

The inner layer of mature superheater deposits formed at Ensted CHP contained a high percentage of K_2SO_4 and iron oxide, and very little chlorine [Montgomery et al., 2000a,b;

Jensen et al., 2004]. The formation of K_2SO_4 in the inner layer of mature deposits may be due to the sulfation of solid phase KCl. [Montgomery et al., 2000a,b] found that, despite these variations in the deposit compositions, the corrosion morphology was similar for the straw-firing boilers at Rudkøbing, Masnedø, and Ensted.

Figure 40 shows a comparison of the compositions of probe compositions from wheat straw-fired grate boilers, a coal-straw fired CFB-boiler, and a coal-straw cofired PF-boiler, based on computer controlled scanning electron microscopy (CCSEM) analysis [Frandsen et al, 1997]. It can be seen that the probe deposits from the coal-straw cofired PF-boiler are rich in aluminosilicates (often mixed with small amounts of Ca and K). Further analysis showed the presence of K_2SO_4 in the deposits. Similarly, [Montgomery and Larsen, 2002] found that the superheater deposit in the Studstrup coal-straw cofired PF-boiler consisted of particles rich in Al, Si, and K, in a matrix of K_2SO_4.

No KCl was observed in the deposits, but this may be due to the low Cl content of the coal. It seems that the K from the straw is captured by the coal ash. This phenomenon was also observed in the Grenaa CFB-boiler, although in this case the probe deposits in the Grenaa boiler were enriched in Cl. The presence of KCl in a CFB boiler deposit may be due to the fact that the combustion takes places at a lower temperature (~850 °C) compared to a PF-boiler (~1400-1700 °C) [Montgomery and Larsen, 2002]. Mature deposits, on the other hand, contained very little KCl (<0.5 wt %), indicating a sulfation of the KCl in the deposit with time [Hansen et al., 1998]. The addition of limestone or lime to the bed in a CFB boiler (for sulfur capture) can result in an increased amount of Ca-particles in CFB deposits [Miles et al., 1996].

The compositions of superheater deposits are thus strongly dependent on boiler conditions, but are also changing over time. Simplifying the deposit compositions in the lab-scale tests to pure KCl or mixtures of KCl-SiO_2 or KCl-CaO, and exposure for only 3 days, will most likely result in higher corrosion rates compared to what will occur in full-scale boilers.

Another limitation of the lab-scale corrosion tests is that the tests were performed under isothermal conditions. In a full-scale boiler, the flue gas temperature is higher than the metal temperature of the superheater tube, so that a temperature gradient exists within the deposit. Lab-scale studies have been reported whereby a temperature gradient within the deposit was taken into account by exposing the specimens in a furnace in which the metal was air cooled [Montgomery, 1998; Kawahara et al., 2002]. These studies indicate that the presence of a temperature gradient results in a 2-10 times higher corrosion rate, depending on the environment. The lack of a temperature gradient in the present work thus makes it difficult to extrapolate the measured corrosion rates to long-term boiler data.

References:

P.A. Alexander; *Laboratory Studies of the Effects of Sulphates and Chlorides on the Oxidation of Superheater Alloys*; **The Mechanism of Corrosion by Fuel Impurities, Eds. R. Johnson and D. J. Littler, Butterworths, 1963, pp 571-582.**

K.H. Andersen; *Deposit Formation during Coal-Straw Co-Combustion in a Utility PF-Boiler*; **Ph.D.-Thesis, Department of Chemical Engineering, Technical University of Denmark, ISBN-87-90142-43-8, 1998.**

L. Boonsongsup, K. Iisa, W. J. Frederick; *Kinetics of the Sulfation of NaCl at Combustion Conditions*; **Ind. Eng. Chem. Res.; 36; pp 4212-4216, 1997.**

BIOAEROSOLS, **Final Report, EU DGXII Contract No. ERK6-CT1999-00003, 2003.**

BIOASH, **Final Report, EU DGXII Contract No. SES-CT2003-502679, 2007.**

J.L. Crolet; *Mechanisms of uniform corrosion under corrosion deposits*; **J. Mat. Sci., 28, pp. 2589-2606, 1993a**.

J.L. Crolet; *The eltrochemistry of corrosion beneath corrosion deposits*; **J. Mat. Sci., 28, pp. 2577- 2588, 1993b**.

J.S. Dennis, A.N. Hayhurst; *The formation of SO_3 in a fluidized bed*; **Combust. Flame 1988, 72, 241–258.**

W.L. Fielder, C. A. Stearns, F. J. Kohl; *Reactions of NaCl with Gaswous SO_3, SO_2, and O_2*; **J. Electrochem. Soc., Solid-State Science and Technology; pp 2414-2417; 1984.**

F.J. Frandsen, H.P. Nielsen, P.A. Jensen, L.A. Hansen, H. Livbjerg, K. Dam-Johansen, P.F.B. Hansen, K.H. Andersen, H.S. Sørensen, O.H. Larsen, B. Sander, N. Henriksen, P. Simonsen; *Deposition and Corrosion in Straw- and Coal-Straw Co-Fired Utility Boilers, Danish Experiences*; **Proc. United Eng. Found. Conf. on Impact of Mineral Impurities in Solid Fuel Combustion, Kona, Hawaii, November 2-7, pp 271-283, 1997.**

R.B. Frandsen, M. Montgomery, O.H. Larsen; *Field test corrosion experiences when co-firing straw and coal: Ten years status within Elsam*; **4th International Workshop "Materials Issues Governing the Performance of Advanced 21st Century Energy Systems" held in Wellington, New Zealand, February 2006.**

H. Fujikawa, N. Maruyama; *Corrosion Behavior of Austenitic Stainless Steels in High Chloride-Containing Environment*; **Materials Science and Engineering; A120; pp 201-306; 1986.**

H.J. Grabke, E. Reese, M. Spiegel; *The effects of chlorides, hydrogen chloride, and sulfur dioxide in the oxidation of steels below deposits.* **Corros. Sci. 1995, *37* (7), 1023–1043.**

A. Gudzinkas; *Sulphation of Solid KCl (Report 07-02)*; **M.Sc. Thesis, Åbo Akademi: Åbo, Finland, 2007.**

C.S. Halck; *Solid Phase Sulphation of Potassium Chloride to Potassium Sulphate*; **M.Sc. Thesis, Technical University of Denmark: Lyngby, Denmark, 2008.**

L.A. Hansen, H.P. Nielsen, F.J. Frandsen, K. Dam-Johansen, S. Hørlyck, A. Karlsson; *Influence of deposit formation on corrosion at a straw-fired boiler*; **Fuel Processing Technology; 64; pp 189-209; 2000.**

P.F.B. Hansen; *MKS1 Demonstration Programme. Mass balances and flue gas emissions*; **Confidential Internal Report, I/S MIDTKRAFT and ELSAM, July 1997.**

P.F.B. Hansen, K.H. Andersen, K. Wieck-Hansen, P. Overgaard, I. Rasmussen, F.J. Frandsen, L.A. Hansen, K. Dam-Johansen; *Co-firing straw and coal in a 150-MW_e utility boiler: in situ measurements*; **Fuel Processing Technology; 54; pp 207-225; 1998.**

W.F. Harlow; *Causes of High Dewpoint Temperatures in Boiler Flue Gases*. **Proc. Inst. Mech. Engrs., 151: 293, 1944.**

W.F. Harlow; *Causes of Flue Gas Deposits and Corrosion in Modern Power Plants*; **Proc. Inst. Mech. Engrs., 160: 359, 1949.**

N. Henriksen, O.H. Larsen, R. Blum, S. Inselman; *High-temperature Corrosion when Co-Firing Coal and Straw in Pulverized Coal Boilers and Circulating Fluidized Bed Boilers; VGB Conference*; **Corrosion and Corrosion Protection in Power Plants, Essen, November 29 and 30, pp 6.1-6.23, 1995.**

N. Henriksen and O.H. Larsen; *Corrosion in ultra supercritical boilers for straw combustion*; **Materials at High Temperatures, 14 (3) pp. 227-236, 1997.**

N. Hiramutsu, Y. Uematsu, T. Tanaka, M. Kinugasa; Effect of Alloying Elements on NaCl-Induced Hot Corrosion of Stainless Steels; Materials Science and Engineering, A120, 319-330, 1989.

K. Iisa, Y. Lu, K. Salmenoja; *Sulfation of Potassium Chloride at Combustion Conditions*; **Energy & Fuels 13(6), 1184 - 1190, 1999.**

J.P. Jensen, K. Nielsen, M. Montgomery, C. Andersen; *Ash Chemistry, Corrosion and Heavy Metal Emissions from a 800 MW Wood Pellet + Oil + Natural Gas Fired Power Plant*; **Proc. 14th Eur. Biomass Conf., Paris, France, October 17-21, 2005.**

P.A. Jensen, F.J. Frandsen, J. Hansen, K. Dam-Johansen, N. Henriksen, S. Hörlyck; *SEM Investigation of Superheater Deposits from Biomass-Fired Boilers*; **Energy & Fuels; 18, pp 378-384, 2004.**

T.L. Jørgensen, H. Livbjerg, P. Glarborg; *Homogeneous and heterogeneously catalyzed oxidation of SO_2*, **Chem. Eng. Sci. 2007, *62*, 4496–4499.**

Y. Kawahara; *High Temperature Corrosion Mechanisms and Effect of Alloying Elements for Materials Used in Waste Incineration Environment*; **Corrosion Science 2002, 44, 223–245.**

H.H. Krause; *Corrosion by Chlorine in Waste-Fuelled Boilers*; **In: R.W. Bryers (Ed.), Incinerating Municipal and Industrial Waste, Hemisphere Publishing Corporation, 1989.**

O.H. Larsen and N. Henriksen; *Ash Deposition and High Temperature Corrosion at Combustion of Aggressive Fuels*; **Proc. Power Plant Technology, Kolding 4-6 Sept. pp 7.1-7.18., 1996.**

O.H. Larsen, N. Henriksen, S. Inselmann, R. Blum; *The Influence of Boiler Design and Process Conditions on Fouling and Corrosion in Straw and Coal/Straw-Fired Ultra Supercritical Power Plants*; **Proc. 9th European Bioenergy Conference: Copenhagen, Denmark, 1996.**

P. Mayer, H.J. Westwood, A.V. Manolescu; *Corrosion Related Problems in Fossil Fired Boilers*; **J. Materials for Energy Systems, 2, pp. 55-64, 1980**.

H.P. Michelsen, F.J. Frandsen, K. Dam-Johansen, O.H. Larsen; *Deposition and high temperature corrosion in a 10 MW straw fired boiler*; **Fuel Processing Technology; 54; pp 95-108, 1998.**

P.D. Miller, H.H. Krause, J. Zupan, Walter K. Boyd; *Corrosive Effects of Various Salt Mixtures Under Combustion Gas Atmospheres*; **Corrosion-NACE, 28(6), pp. 222-225, 1972**.

P.D. Miller, H.H. Krause, D.A. Vaughan, W.K. Boyd; *The Mechanism in High Temperature Corrosion in Municipal Incinerators*; **Corrosion-NACE, 28(7), pp. 274-281, 1972**.

M. Montgomery, A. Karlsson; *In situ Corrosion Investigation at Masnedø CHP Plant*; **Materials and Corrosion, 50 579-584, 1999.**

M. Montgomery, F.J. Frandsen, A. Karlson, O.H. Larsen; *Corrosion Investigation in Straw-fired Power Plants in Denmark*; **Proc. United Eng. Found. Conf. on Effects of Coal Quality on Power Plant Performance: Ash Problems, Management and Solutions, Park City, UT, USA, May 9-13, 2000a.**

M. Montgomery, F.J. Frandsen, O.H. Larsen; *The Effect of Co-Firing with Straw and Coal on High Temperature Corrosion.* **Proc. United Eng. Found. Int. Conf. on 'Effects of Coal Quality on Power Plant Management: Ash Problems, Management and Solutions', Park City, Utah, May 8-11, 2000b.**

M. Montgomery, A. Karlsson, O.H. Larsen; *Field test corrosion experiments in Denmark with biomass fuels Part I: Straw firing*; **Materials and Corrosion 53 pp. 121-131, 2002a.**

M. Montgomery, O. Biede and O.H. Larsen; *High Temperature Corrosion in straw fired power plants: Influence of steam/metal temperature on corrosion rates for TP347H*; **Materials for Advanced Power Engineering 2002 Part II pp 957-966, 2002b.**

M. Montgomery, T. Vilhelmsen, S.A. Jensen; *Potential High Temperature Corrosion Problems due to Co-Firing of Biomass and Fossil Fuels*; **Materials and Corrosion, 59(10), 783 – 793, 2008.**

H.P. Nielsen; *Deposition and High-Temperature Corrosion in Biomass-Fired Boilers*; **Ph.D.-Thesis, Department of Chemical Engineering, Technical University of Denmark, ISBN-87-90142-47-0, 1998.**

H.P. Nielsen, F.J. Frandsen, K. Dam-Johansen; *Lab-Scale Investigations of High-Temperature Corrosion Phenomena in Straw-Fired Boilers*; **Energy & Fuels; 13(6), pp 1114-1121, 1999.**

N. Otsuka, T. Kudo; *High-Temperature Corrosion of Advanced Materials and Coatings*; **In: Y. Saito, N. Onay, T. Maruyama (Eds.), Elsevier Science Publishers, B.V. 1992.**

S. Ozawa, K. Naruse, K. Ito, Y. Kojima, H. Matsuda, S. Mishima, M. Endo, T. Yanase; *Evolution of HCl from KCl, $CaCl_2$ and NaCl in an SO_2-O_2-H_2O atmosphere under a simulated condition of municipal waste incineration*; **J. Chem. Eng. Japan, 2003, *36* (7), 867-873.**

J.S. Pedersen; Belægningsinitieret korrosion i biomassefyrede kedler, B.Sc.-projekt, DTU Kemiteknik, Januar 2009.

W.T. Reid; *External Corrosion and Deposits - Boilers and Gas Turbines*; **American Elsevier, New York, 1971.**

Y. Shinata, Y. Nishi; *NaCl-Induced Accelerated Oxidation of Chromium*; **Oxidation of Metals, 26, pp 201-212, 1986.**

Y. Shinata, F. Takahashi, K. Hashiura; *NaCl-Induced Hot Corrosion of Stainless Steels*; **Materials Science and Engineering; 87; pp 399-405; 1987.**

M. Spiegel, H.J. Grabke; *High Temperature Corrosion of Low and High Alloy Steels in Simulated Waste Incineration Atmospheres*; ***Incinerating Municipal and Industrial Waste. Fireside Problems and Prospects for Improvement* edited by R. W. Bryers, Hemisphere Publishing Corporation, pp 758-764, 1991.**

S.C. van Lith, F.J. Frandsen, M. Montgomery, T. Vilhelmsen, S.A. Jensen; *Lab-Scale Investigation of Deposit Induced Chlorine Corrosion of Superheater Materials under Simulated Biomass-Firing Conditions*; **Proc. Int. Conf. *EUROCORR 2008*, Edinburgh, UK, September 7-11, 2008**

S.C. van Lith, F.J. Frandsen, M. Montgomery, T- Wilhelmsen, S.A. Jensen; *Lab-Scale Investigation of Deposit-Induced Chlorine Corrosion of Superherater Materials under Simulated Biomass-Firing Conditions. Part 1; Exposure at 560 °C*; **Energy and Fuels, 23, 3457-3468, 2009**

S.C. van Lith, F.J. Frandsen, M. Montgomery, T. Vilhelmsen, S.A. Jensen; *Lab-Scale Investigation of Deposit-Induced Chlorine Corrosion of Superheater Materials under Simulated Biomass-Firing Conditions*; **Proc. Int. Conf. *Impacts of Fuel Quality on Power Production and the Environment*, Banff, Alberta, Canada, September 29 – October 3, 2008.**

D.A. Vaughan, H.H. Krause, W.K. Boyd; **Batelle Interim Report to US EPA, June 1974.**

D. A. Vaughan, H.H. Krause, W.D. Boyd; *Chloride Corrosion and Its Inhibition in Refuse Firing*; **Proceedings of the International Conference on Ash Deposits and Corrosion From Impurities in Combustion Gases, Henniker, New Hampshire, June 26-July 1, pp 473-493, 1977.**

K. Wieck-Hansen, P. Overgaard, O.H. Larsen; *Co-firing coal and straw in a 150 MWe power boiler experiences*; **Biomass & Bioenergy, 19, 395-409, 2000.**

I Wright, H.H. Krause; *Assessment of Factors Affecting Boiler Tube Lifetime in Waste-Fired Steam Generators: New Opportunities for Research and Technology Development*; **National Renewable Energy Laboratory, Golden, Colorado, Rep. No. NREL/TP-430-21480, 1996.**